FUNCTIONAL VALIDATION OF ALZHEIMER'S DISEASE RISK GENES USING ESTABLISHED AND PLURIPOTENT HUMAN CELL CULTURE MODELS

Dissertation

zur Erlangung des akademischen Grades des
Doktors der Naturwissenschaften (Dr. rer. nat.)

eingereicht im Fachbereich Biologie, Chemie, Pharmazie
der Freien Universität Berlin

vorgelegt von
Ina-Maria Rudolph

Berlin
2018

Die Arbeit wurde von 02/2014 bis 04/2018 unter der Anleitung von Prof. Dr. Thomas E. Willnow am Max Delbrück Centrum für Molekulare Medizin in Berlin durchgeführt.

1. Gutachter: Herr Prof. Dr. Thomas E. Willnow
Max Delbrück Centrum Berlin

2. Gutachterin: Frau Prof. Dr. Silke Sperling
Freie Universität Berlin
Charité - Universitätsmedizin Berlin

Tag der Disputation: 25.02.2019

SUMMARY

Alzheimer's disease is a neurodegenerative disorder that leads to the progressive loss of neurons and affects millions of patients worldwide. The risk of Alzheimer's disease is mainly conferred through genetic risk factors, some of which are still not identified. The recent advances in sequencing technologies have uncovered many previously unknown and potentially pathogenic single-nucleotide polymorphisms (SNPs) in Alzheimer's disease patients. Given the large number of these Alzheimer's disease-associated SNPs, the functional characterization and proof of their relevance for this disease is urgently needed.

Here, I functionally analyzed the relevance of coding and non-coding risk SNPs in the *SORL1* and *SORT1* gene that encode for the VPS10P domain receptors SORLA and sortilin. VPS10P domain receptors are a unique class of neuronal sorting receptors that direct intracellular transport of target proteins between *trans*-Golgi network (TGN), cell surface and endosomes.

Sortilin acts as a neuronal clearance receptor for both APOE (apolipoprotein E), the major genetic risk factor for late-onset Alzheimer's disease, and progranulin, a protective factor for frontotemporal lobar degeneration. A risk locus of several genetically linked SNPs upstream of the *SORT1* gene was associated with *SORT1* expression levels in the liver. To test whether this risk locus is indeed a regulator of *SORT1* expression in the liver and possibly in the brain, I differentiated human iPSCs carrying minor or major variants of these SNPs into hepatocytes and cortical neurons. I also used genome-editing techniques to specifically exchange the proposed functional SNP rs12740374 from major to minor variant in order to verify the functionality of this SNP in isogenic cell lines. My data demonstrated that the *SORT1* risk locus predicts *SORT1* expression in iPSC-derived hepatocytes, but not in iPSC-derived neurons, which may be explained by lower expression levels of the transcription factor C/EBPα in neurons. Analysis of isogenic iPSC lines suggested that the proposed functional SNP rs12740374 indeed determines *SORT1* expression in hepatocytes.

SORLA is a trafficking receptor for both the Aβ peptide as well as its precursor protein (APP) and thus affects Aβ accumulation in the brain, one of

the hallmarks of Alzheimer's disease. Recently, potentially pathogenic coding *SORL1* mutations were identified in early-onset Alzheimer's disease (EOAD) patients. I functionally characterized the EOAD-associated *SORL1* mutations by overexpressing mutant receptor variants in an established neuronal cell line (SH-SY5Y). Out of the three analyzed EOAD-associated *SORL1* mutations, the N1358S mutation demonstrated an increase in extracellular Aβ levels compared to the wildtype condition. Neither impaired binding of APP nor affected lysosomal targeting of Aβ could explain the increase in Aβ levels in the mutant $SORLA^{N1358S}$ cells. However, the subcellular trafficking of both SORLA and APP was altered in the $SORLA^{N1358S}$ overexpressing cell line, with more SORLA and APP localizing to endosomal instead of Golgi compartments when compared to the $SORLA^{WT}$ overexpressing cell line. I performed an unbiased interactome screen of $SORLA^{WT}$ and $SORLA^{N1358S}$ and identified several interaction partners of SORLA related to endosomal trafficking that may be affected by the N1358S mutation. Furthermore, the interactome screen revealed the exosomal protein MFG-E8 as a previously unknown interaction partner of SORLA, suggesting a novel role of SORLA in sorting MFG-E8, and potentially Aβ, for exosome secretion.

Taken together, my data elucidate the cell type specific transcriptional regulation of *SORT1* and the pathological mechanism of the EOAD-associated N1358S mutation in *SORL1*. They also highlight the importance of validating disease-associated genetic variants and substantiate iPSC-derived neurons and hepatocytes for modeling VPS10P domain receptor function.

ZUSAMMENFASSUNG

Die Alzheimer-Krankheit ist eine neurodegenerative Erkrankung, die zum fortschreitenden Verlust von Neuronen führt und weltweit Millionen von Patienten betrifft. Das Risiko an Alzheimer zu erkranken wird zum großen Teil durch genetische Faktoren bedingt, von denen einige noch nicht identifiziert wurden. Die jüngsten Fortschritte in Sequenzierungstechnologien haben zu der Identifizierung vieler bisher unbekannter und potenziell pathogener Sequenzvariationen ("single-nucleotide polymorphisms", SNPs) bei Alzheimer-Patienten geführt. Angesichts der großen Anzahl dieser Alzheimer-assoziierten SNPs ist die funktionelle Charakterisierung und der Nachweis ihrer Relevanz für diese Erkrankung dringend erforderlich.

In meiner Doktorarbeit habe ich die funktionale Relevanz von intronischen und exonischen Risiko-SNPs in den *SORL1*- und *SORT1*-Genen analysiert, die für die VPS10P-Domäne Rezeptoren SORLA und sortilin kodieren. VPS10P-Domäne Rezeptoren gehören zu einer Familie von neuronalen Transmembran-Rezeptoren, die den intrazellulären Transport von Zielproteinen zwischen dem *trans*-Golgi Netzwerk (TGN), der Plasmamembran und Endosomen regulieren.

Sortilin fungiert als neuronaler Abbau-Rezeptor sowohl für APOE (Apolipoprotein E), den wichtigsten genetischen Risikofaktor für die spät auftretende Alzheimer-Krankheit, als auch für Progranulin, einen protektiven Faktor für die frontotemporale Demenz. Ein Risiko-Lokus mehrerer genetisch gekoppelter SNPs nahe dem *SORT1*-Gen wurde mit *SORT1*-Expressionsleveln in der Leber assoziiert. Um zu testen, ob dieser Risiko-Lokus tatsächlich ein Regulator der *SORT1*-Expression in der Leber und möglicherweise im Gehirn ist, differenzierte ich humane iPSCs, die minore oder majore Varianten dieser SNPs trugen, in Hepatozyten und kortikale Neuronen. Ich nutzte außerdem Genom-Editierungs-Techniken, um die majore Variante von rs12740374, der als möglicher funktionaler SNP vorgeschlagen wurde, gegen die minore Vairante auszutauschen und so die Funktionalität dieses SNPs in isogenen Zelllinien zu verifizieren. Meine Daten zeigten, dass der *SORT1*-Risiko-Lokus die *SORT1*-Expression in iPSC-abgeleiteten Hepatozyten, aber nicht in iPSC-abgeleiteten Neuronen bestimmte, was durch niedrigere Expressionslevel des Transkriptionsfaktors

C/EBPα in Neuronen erklärt werden kann. Die Analyse von isogenen iPSC-Linien legte nahe, dass der vorgeschlagene funktionelle SNP rs12740374 tatsächlich die *SORT1*-Expression in Hepatozyten bestimmt.

SORLA ist ein Trafficking-Rezeptor sowohl für das Aβ-Peptid als auch für sein Vorläuferprotein (APP) und beeinflusst somit die Akkumulation von Aβ im Gehirn, eines der zentralen Kennzeichen der Alzheimer-Krankheit. Kürzlich wurden potentiell pathogene kodierende *SORL1*-Mutationen bei Patienten mit früh beginnender Alzheimer-Krankheit (EOAD) gefunden. Ich charakterisierte die EOAD-assoziierten *SORL1*-Mutationen funktionell, indem ich mutierte Rezeptorvarianten in einer etablierten neuronalen Zelllinie (SH-SY5Y) überexprimierte. Von den drei analysierten EOAD-assoziierten *SORL1*-Mutationen zeigte die N1358S-Mutation einen Anstieg der extrazellulären Aß-Level im Vergleich zur Wildtyp-Kondition. Weder eine beeinträchtigte Bindung von APP noch ein beeinflusster lysosomaler Abbau von Aβ konnte die erhöhten Aβ-Level in den $SORLA^{N1358S}$-Zellen erklären. Der subzelluläre Transport von SORLA und APP war jedoch in der $SORLA^{N1358S}$-überexprimierenden Zelllinie verändert, wobei SORLA und APP verstärkt in endosomalen anstelle von Golgi-Kompartimenten lokalisiert waren, verglichen mit der $SORLA^{WT}$-überexprimierenden Zelllinie. Ich führte einen vergleichenden Interaktom-Screen von $SORLA^{WT}$ und $SORLA^{N1358S}$ durch und identifizierte mehrere Interaktionspartner von SORLA, die mit dem endosomalen Transport zusammenhängen und von der N1358S-Mutation betroffen sein könnten. Darüber hinaus identifizierte ich durch den Interaktom-Screen das exosomale Protein MFG-E8 als einen bisher unbekannten Interaktionspartner von SORLA, was auf eine möglich neue Rolle von SORLA in der Regulation von Exosom-Sekretion hinweist.

Zusammengefasst zeigen meine Daten die Zelltyp-spezifische Transkriptionsregulation von *SORT1* und den pathologischen Mechanismus der EOAD-assoziierten N1358S-Mutation in *SORL1* auf. Sie betonen außerdem die Wichtigkeit der Validierung Krankheits-assoziierter genetischer Varianten und bestätigen iPSC-abgeleitete Neuronen und Hepatozyten als Modellsysteme für die Untersuchung von VPS10P-Domäne Rezeptoren.

TABLE OF CONTENT

LIST OF FIGURES

LIST OF TABLES

LIST OF ABBREVIATIONS

°C	degrees celsius
AD	Alzheimer's disease
ADAM	'a disintegrin and metalloprotease'
AFP	α-fetoprotein
AICD	APP intracellular domain
ALB	albumin
ANOVA	analysis of variance
AP	adaptor protein
APO	apolipoprotein
APP	amyloid precursor protein
APS	ammonium persulfate
Arg	arginine
Aβ	amyloid β-peptide
B2M	β-2-microglobulin
BACE1	β-site APP cleaving enzyme-1
BCA	bicinchoninic acid
BDNF	brain-derived neurotrophic factor
BMP	bone morphogenetic protein
bp	base pairs
BSA	bovine serum albumin
bZIP	basic-region leucine zipper
cDNA	complementary DNA
CHO cells	Chinese hamster ovary cells
CNS	central nervous system
co-IP	co-immunoprecipitation
CPY	carboxypeptidase Y
Ct	cycle threshold
CTF	carboxy-terminal fragment
CTR	complement-type repeats
Cys	cysteine
d	day(s)
DAPI	4',6-diamidine-2'-phenylindole dihydrochloride
DMEM	Dulbecco's modified Eagle medium
DMSO	dimethyl sulfoxide
DNA	desoxyribonucleic acid
dNTP	deoxynucleotide
E. coli	*Eschericha coli*
EDTA	ethylenediaminetetraacetic acid

EGFP	enhanced green fluorescent protein
ELISA	enzyme-linked immunosorbent assay
EOAD	early-onset Alzheimer's disease
eQTL	expression quantitative trait locus
ER	endoplasmic reticulum
ERK	extracellular regulated kinase
EtOH	ethanol
FBS	fetal bovine serum
FLIM	fluorescence-lifetime imaging microscopy
Fn(III)	fibronectin type III repeat
FRET	fluorescence resonance energy transfer
FTLD	frontotemporal lobar degeneration
FTLD-U	FTLD with ubiquitin-positive inclusions
g	gram
GAPDH	glyceraldehyde-3-phosphate dehydrogenase
GFP	green fluorescent protein
GGA	Golgi-localizing γ-adaptin ear homology domain, ARF-interacting
GWAS	genome-wide association study
h	hour(s)
HAB	head activator binding protein
HBSS	Hank's balanced salt solution
HEK cells	human embryonic kidney cells
HNF4A	hepatocyte nuclear factor 4α
HR	homology recombination
IF	immunofluorescence
IP	immunoprecipitation
iPSCs	induced pluripotent stem cells
kb	kilo base pairs
L	liter
LAMP1	lysosomal-associated membrane protein 1
LB	lysogeny broth
LDL	low-density lipoprotein
LDLR	low-density lipoprotein receptor
LOAD	late-onset Alzheimer's disease
LRP	low-density lipoprotein receptor-related protein
M	molar
MAPT	microtubule-associated protein tau
MFG-E8	milk fat globule epidermal growth factor 8
min	minute(s)

mRNA	messenger RNA
MUT	mutant
n	number of independent experiments
NDS	normal donkey serum
NEAA	non-essential amino acids
NGN2	neurogenin-2
NHEJ	non-homologous end-joining
NP-40	Nonidet-P40
p	probability value
P/S	penicillin/streptomycin
PACS1	phosphofurin acidic cluster sorting protein 1
PAF	population-attributable fraction
PAGE	polyacrylamide gel electrophoresis
PBS	phosphate buffered saline
PBX	excision-only piggyBac™ Transposase
PCR	polymerase chain reaction
PFA	paraformaldehyde
PGRN	progranulin
PICh	proteomics of isolated chromatin segments
qRT-PCR	quantitative real-time PCR
RAB	ras-related in brain
RAP	receptor-associated protein
RFP	red fluorescent protein
RNA	ribonucleic acid
rs	reference SNP ID
RT	room temperature
sAPP	soluble APP
SD	standard deviation
SDS	sodium dodecyl sulfate
sec	second(s)
SILAC	stable isotope labeling by/with amino acids in cell culture
SNP	single nucleotide polymorphism
SORCS	sortilin-related receptor CNS expressed
SORLA	sorting-related receptor with A type repeats
SSEA4	stage-specific embryonic antigen 4
T/E	trypsin/EDTA
TAE	tris-acetate-EDTA
TALEN	transcription activator-like effector nuclease
TBS	tris-buffered saline
TDP-43	transactive response DNA-binding protein 43

TEMED	N,N,N´,N´-tetramethylendiamine
TGN	*trans*-Golgi-network
TK	thymidine kinase
Tm	melting temperature
tM1	thresholded Manders' coefficient 1
U	enzymatic unit(s)
UTR	untranslated region
v	volume
V	Voltage
VLDL	very low-density lipoproteins
VPS10P	vacuolar protein sorting 10 protein
w	weight
w/o	without
WB	Western blot
WT	wildtype

1 INTRODUCTION

1.1 Alzheimer's disease

Alzheimer's disease is a neurodegenerative disorder and the leading cause of age-related dementia, accounting for 60-70 % of all cases (World Health Organization, 2017). Today, 50 million people worldwide are affected by dementia and this number is expected to triple until 2050 (World Health Organization, 2017). This development will confront millions of patients and their families with an extreme emotional burden. Also, the dependence of late-stage patients on continuous care will create a demand for social and medical support that few public health systems will be able to manage (Huang and Mucke, 2012).

Alzheimer's disease is characterized by a progressive loss in cognitive functions, specifically a loss in short and long term memory, but symptoms also include drastic mood and personality changes (Khachaturian, 1985). Even though Alzheimer's disease is the 6th leading cause of death and decades of research have been dedicated to uncover its underlying mechanisms and potential treatment strategies, there is still no effective treatment that significantly halts or prevents the progression of Alzheimer's disease (Graham *et al.*, 2017).

The most obvious risk factor for Alzheimer's disease is aging, as documented by an almost exponential correlation of age and disease risk (Reitz and Mayeux, 2014). Additional non-genetic risk factors have been identified in various epidemiological studies, such as the association of Alzheimer's disease risk with head trauma (Jellinger, 2004) or the protective

effect of mental and physical activities (Mortimer *et al.*, 2003). Interestingly, Alzheimer's disease is also associated with a number of vascular and metabolic disorders including hypercholesterolemia, obesity, and diabetes (Mayeux, 2003). However, while environmental influences and pre-existing medical conditions seem to affect Alzheimer's disease progression, twin studies have clearly demonstrated that almost 80 % of the Alzheimer's disease risk is genetically determined (Gatz et al., 2006).

Etiologically, Alzheimer's disease can be categorized in two forms of the disease; early- versus late-onset Alzheimer's disease. While clinically indistinguishable from late-onset Alzheimer's disease (LOAD), patients with early-onset form of the disease (EOAD) develop symptoms before 65 years of age. EOAD is a rare condition, affecting less than 1% of cases (Campion *et al.*, 1999). It is typically associated with an accelerated rate of disease progression (Reitz and Mayeux, 2014). While LOAD is genetically heterogeneous, EOAD patients usually display a Mendelian autosomal-dominant inheritance of the disease, which is attributed to the higher penetrance of the underlying familial gene mutations (see Section 1.1.3).

1.1.1 Pathophysiology of Alzheimer's disease

The neuropathological hallmarks of Alzheimer's disease are so-called senile plaques, which consist mainly of aggregated amyloid-β (Aβ) peptide, and neurofibrillary tangles, which are filamentous aggregates of the hyperphosphorylated microtubule-associated protein tau. The occurrence of senile plaques and neurofibrillary tangles is accompanied by a progressive loss of neurons in the diseased brain (Selkoe, 1991). Neuronal lesions affect multiple brain regions, but pyramidal neurons of the cortical layer II and of the CA1 region of the hippocampus seem to particularly vulnerable to cell death (Gómez-Isla *et al.*, 1996). At later stages of the disease, brains of Alzheimer's disease patients display a significant decrease in overall brain volume, which is mainly caused by a wide-spread loss of synapses and dendrites (Palop *et al.*, 2006). Several pathogenic mechanisms have been implicated in this drastic loss of neuronal connections including inflammatory and neurovascular alterations, oxidative stress, neurotransmitter deficits, and hyperphosphorylation of tau (Blennow *et al.*, 2006). However, a growing body

of evidence combining genetic and functional studies from over 30 years of research lead to the wide acceptance of the fact that the Aβ peptide, the main constituent of the characteristic senile plaques, plays a central role in Alzheimer's disease pathology (Selkoe and Hardy, 2016).

1.1.2 Amyloid cascade hypothesis

The amyloid cascade hypothesis was first proposed by Hardy and Higgins in 1992 and states that the Aβ peptide is the main agent causative of Alzheimer's disease (Hardy and Higgins, 1992). This peptide is produced by proteolytic breakdown of the amyloid precursor protein (APP).

First evidence implicating the Aβ peptide in Alzheimer's disease came with the notion that the *APP* gene is located on chromosome 21 (Goldgaber *et al.*, 1987; Kang *et al.*, 1987; Tanzi *et al.*, 1987). Since it had already been established that Down's syndrome patients, that carry an extra copy of chromosome 21, invariably developed EOAD (Olson and Shaw, 1969), this finding pinpointed to APP's central role in causing Alzheimer's disease. Soon after, several mutations in the *APP* gene were found in early-onset Alzheimer's disease patients (Goate *et al.*, 1991; Hendriks *et al.*, 1992; Mullan *et al.*, 1992). Interestingly, most of the identified *APP* mutations clustered close to APP's proteolytic sites and promoted an increased production of the Aβ peptide (Citron *et al.*, 1992; Cai *et al.*, 1993; Suzuki *et al.*, 1994). Since then, many independent findings have unambiguously confirmed the central role of Aβ accumulation for Alzheimer's disease pathology (reviewed (Selkoe and Hardy, 2016)), including the observation that *PSEN1* and *PSEN2*, that encode for the catalytic enzymes producing the Aβ peptide, also harbor EOAD-causing mutations (Levy-Lahad *et al.*, 1995; Sherrington *et al.*, 1995; Scheuner *et al.*, 1996).

1.1.2.1 Amyloidogenic and non-amyloidogenic processing of APP

Since Aβ has been identified as the main causative agent in Alzheimer's disease, much has been learned about the process of Aβ production. APP is a widely expressed type-1 transmembrane protein and APP processing is a ubiquitous process occurring in many cell types. Although some physiological functions of both APP and its processing products have been described, the role of APP processing under physiological conditions is still not fully

understood (Pearson and Peers, 2006). Full length APP facilitates cell matrix adhesion and neurite outgrowth by binding several extracellular matrix proteins (Kibbey *et al.*, 1993; Small *et al.*, 1994, 1999; Beher *et al.*, 1996), while the neurotoxic Aβ peptide regulates synaptic activity under physiological conditions (Kamenetz *et al.*, 2003).

APP is mainly processed by two proteolytic pathways described as amyloidogenic or non-amyloidogenic APP processing, depending on whether the processing pathway produces the neurotoxic Aβ peptide or not (Figure 1-1). Both pathways are referred to as canonical APP processing, since alternative processing pathways, such as δ- and η-processing, have recently been identified, contributing to the increasing complexity of APP processing regulation (reviewed in Andrew *et al.*, 2016).

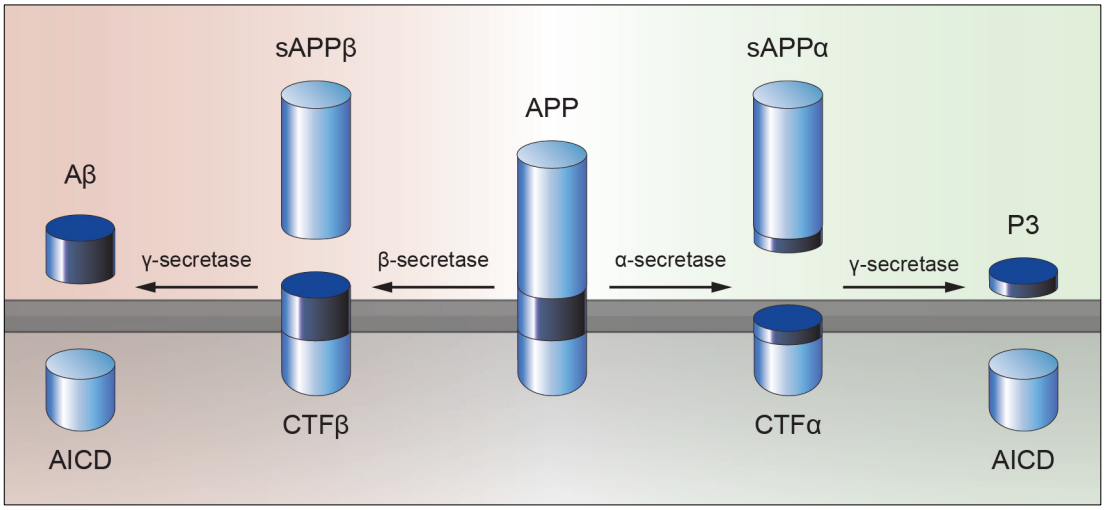

Figure 1-1: Canonical amyloidogenic and non-amyloidogenic processing of the amyloid precursor protein (APP). In the amyloidogenic pathway (left), APP is processed by β-secretase activity at the amino terminal end of Aβ, releasing soluble APPβ (sAPPβ) and the membrane-anchored carboxy-terminal fragment β (CTFβ). Further processing of CTFβ by γ-secretase activity produces the neurotoxic Aβ peptide and the APP intracellular domain (AICD). In the non-amyloidogenic pathway (right), APP is cleaved by α-secretase activity, which destroys the Aβ peptide and produces sAPPα and the membrane-anchored fragment CTFα. Subsequently, γ-secretase activity processes CTFα into the P3 peptide and the AICD. Figure adapted from Andersen *et al.*, 2016.

Canonical amyloidogenic processing is facilitated by β- and γ-secretase activities. In a first step, APP is cleaved by the β-secretase BACE1 (β-site APP cleaving enzyme-1) at the amino terminal end of the Aβ encoding

peptide sequence, releasing the soluble extracellular fragment sAPPβ (Vassar *et al.*, 1999). The remaining membrane-anchored carboxy-terminal fragment (CTFβ) is subsequently cleaved within the transmembrane domain by a multimeric γ-secretase complex, releasing the Aβ peptide and the APP intracellular domain (AICD). The γ-secretase complex consists of four subunits; PSEN1 or PSEN2, nicastrin, anterior pharynx defective 1 (APH-1), and presenilin enhancer 2 (PEN-2), with PSEN1/2 representing the catalytic domains of the protease complex (Wolfe *et al.*, 1999; Kimberly *et al.*, 2003; Steiner *et al.*, 2008). γ-secretase cleavage is imprecise, likely due to its step-wise processing of the CTFβ fragment, generating Aβ peptides with varying amino acid lengths. The predominant forms are Aβ38, Aβ40, and Aβ42 (Haass *et al.*, 2012). Interestingly, the longer Aβ42 peptide is more prone to oligomerization and aggregation than Aβ38 and Aβ40, suggesting that the imprecise γ-secretase cleavage influences neurotoxicity of the produced Aβ species (Haass and Selkoe, 2007).

In the non-amyloidogenic pathway, APP is initially processed by α-secretase activity, which cuts within the Aβ peptide sequence, producing the soluble extracellular fragment sAPPα and the membrane-anchored carboxy-terminal fragment α (CTFα) (Esch *et al.*, 1990; Sisodia *et al.*, 1990). Several members of ‘a disintegrin and metalloprotease’ (ADAM) family can process APP at the non-amyloidogenic α-site. However, α-cleavage of APP in neurons is mainly conducted by ADAM10 (Kuhn *et al.*, 2010). CTFα is also subjected to γ-secretase cleavage which releases the AICD and the p3 peptide, a benign form of the Aβ peptide that does not exhibit neurotoxicity (Dulin *et al.*, 2008).

1.1.2.2 Subcellular trafficking of APP

Whether APP is processed by amyloidogenic or non-amyloidogenic secretases depends largely on its subcellular trafficking, since α- and β-secretases are located in distinct subcellular compartments (Eggert *et al.*, 2018). While the α-secretase ADAM10 is mainly localized to the plasma membrane (Lammich *et al.*, 1999), the β-secretase BACE1 is predominantly found in endosomal compartments (Golde *et al.*, 1992; Vassar *et al.*, 1999; Sannerud *et al.*, 2011). γ-secretase complexes including the catalytic proteases PSEN1/2 locate to both cell surface and endosomal compartments

(Meckler and Checler, 2016; Sannerud *et al.*, 2016).

After biosynthesis in the endoplasmatic reticulum (ER), nascent APP enters the secretory pathway to reach the *trans*-Golgi-network (TGN), where the precursor protein is mainly localized (Palacios *et al.*, 1992; Caporaso *et al.*, 1994; Guo *et al.*, 2012). From the TGN, APP moves to the plasma membrane (Figure 1-2). There, it is subjected to non-amyloidogenic processing by α- and γ-secretases, releasing sAPPα into the extracellular space.

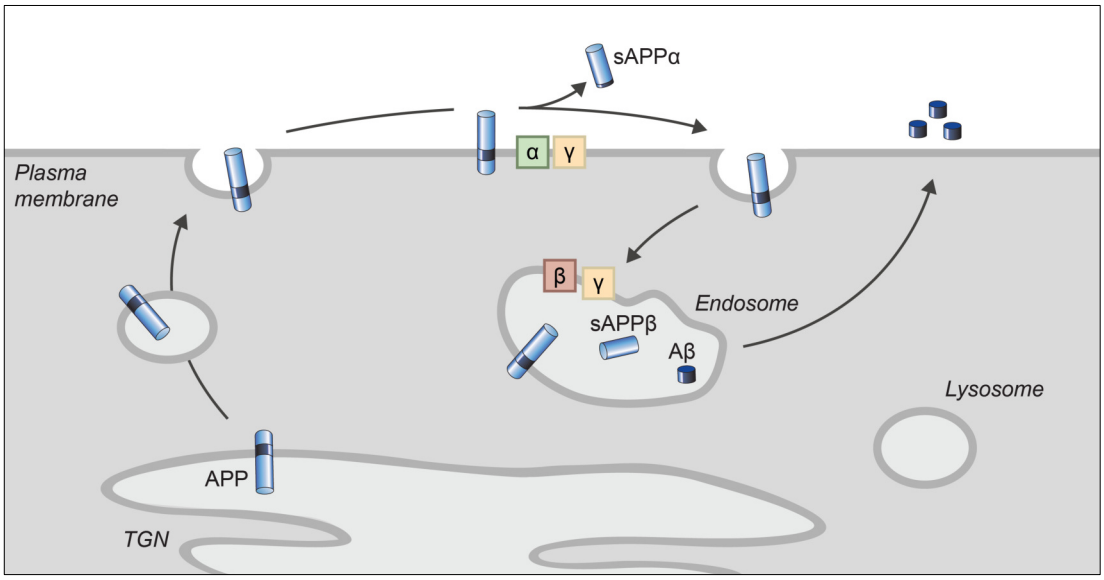

Figure 1-2: Intracellular trafficking and processing of APP. Newly synthesized APP is transported from the endoplasmatic reticulum (ER) through the Golgi apparatus to the plasma membrane. Here, APP is processed by α- and γ-secretases (non-amyloidogenic processing), releasing the soluble APPα (sAPPα). Non-processed APP molecules are internalized into endosomal compartments, where β- and γ-secretases release sAPPβ and the neurotoxic Aβ from APP (amyloidogenic processing). Aβ peptides are secreted from the cell through different exocytic pathways, including exosomes (Rajendran *et al.*, 2006).

Non-processed APP molecules are rapidly internalized from the cell surface. Endocytosis of APP is facilitated by several adaptor proteins that bind to a carboxy-terminal YENPTY motif in the cytosolic domain of APP (Lai *et al.*, 1995; Haass *et al.*, 2012). In endosomal compartments, APP is processed by β- and γ-secretases, producing sAPPβ and the neurotoxic Aβ peptide. A small fraction of internalized APP is recycled back to the cell surface (Das *et al.*, 2013) or sorted to lysosomes for degradation (Cole *et al.*, 1992; Haass *et al.*, 1992).

Apart from cytosolic adaptor proteins (reviewed in King and Scott Turner, 2004), APP's intracellular trafficking route is also influenced by the sorting of several type-I transmembrane receptors interacting with APP (Eggert et al., 2018).

1.1.3 Genetic risk factors for Alzheimer's disease

As mentioned above, approximately 80 % of the Alzheimer's disease risk is genetically determined (Gatz et al., 2006). EOAD is caused by rare gene mutations exhibiting more than 85 % penetrance (Reitz and Mayeux, 2014). These gene mutations are inherited in an autosomal-dominant pattern and invariably lead to Alzheimer's disease pathology. In contrast, LOAD is genetically heterogeneous and its risk is likely determined by a combination of common genetic variants with lower individual risk sizes (Bertram *et al.*, 2010).

1.1.3.1 Gene mutations causing EOAD

After the initial finding that *APP* duplications and mutations invariably cause EOAD (Olson and Shaw, 1969; Goldgaber *et al.*, 1987; Goate *et al.*, 1991), many more pathogenic *APP* mutations have been identified. At present, over fifty mutations in the *APP* gene are known to cause EOAD (AD mutation database, http://www.molgen.ua.ac.be/). Interestingly, most pathogenic *APP* mutations cluster close to the target sites for α-, β-, and γ-secretases and aberrantly promote amyloidogenic processing by β- and γ-secretases (Citron *et al.*, 1992; Cai *et al.*, 1993; Suzuki *et al.*, 1994; Hardy and Selkoe, 2002).

While the discovery of pathogenic *APP* mutations was central for the formulation of the amyloid cascade hypothesis, 82% of currently identified EOAD-causing mutations locate to *PSEN 1* and *PSEN2* (Zou *et al.*, 2014). Most of the over 200 identified mutations in *PSEN1* and *PSEN2* favor production of the aggregation-prone Aβ42 peptide over that of Aβ40 (Selkoe and Hardy, 2016). Collectively, the identified mutations in *APP*, *PSEN1,* and *PSEN2* are estimated to account for 30–50 % of EOAD cases (Zou *et al.*, 2014), indicating the existence of further EOAD-causing gene mutations with high penetrance yet to be identified.

1.1.3.2 LOAD risk genes

The most significant determinants of LOAD risk are genetic variants of the *APOE* gene, encoding for the predominant apolipoprotein in the brain, apolipoprotein E (APOE) (Corder *et al.*, 1993; Lambert *et al.*, 2013). Two coding single nucleotide polymorphisms (SNPs) in the *APOE* gene determine the amino acid residues at position 112 and 158 of APOE, being either cysteine (Cys) or arginine (Arg). Accordingly, APOE exists in three different isoforms in the human genome called ε2 (Cys112, Cys158), ε3 (Cys112, Arg158), and ε4 (Arg112, Arg158). Their global frequencies are 8 %, 78 %, and 14 %, respectively (Farrer *et al.*, 1997). Individuals carrying at least one ε4 risk allele face a significantly higher risk of developing LOAD, as well as a lower age of clinical onset compared to carriers of the common ε3 allele. By contrast, the rare ε2 allele seems to have a protective effect over ε3 (Corder *et al.*, 1993; Farrer *et al.*, 1997). In the brain, APOE is mainly expressed and secreted by astrocytes to facilitate lipid transport into neurons. Various mechanisms have been proposed to explain the LOAD risk conferred by the APOE ε4 allele. Conceptually, these mechanisms entail either gain of neurotoxic functions for APOE ε4, such as increased Aβ aggregation and aberrant brain activity, or loss of neuroprotective activities of APOE ε3, such as mitochondrial function and lipid metabolism (Liu *et al.*, 2013). Interestingly, APOE binds soluble Aβ and mediates Aβ clearance through receptor-mediated uptake by neurons and glia (Kim *et al.*, 2009; Kanekiyo *et al.*, 2011). Compared to APOE ε2 and ε3, APOE ε4 is less efficient in mediating Aβ clearance, likely due to a reduced isoform-specific Aβ binding affinity (LaDu *et al.*, 1994; Castellano *et al.*, 2011).

Besides *APOE*, 19 other genetic loci reached significant genome-wide association with Alzheimer's disease risk in a recent large meta-analysis of genome-wide association studies (GWAS) (Lambert *et al.*, 2013). Of note, many of the associated gene loci are implicated in Alzheimer's disease relevant processes such as APP trafficking or lipid transport. Compared to the APOE ε4 allele, other risk genes displayed significantly smaller risk sizes (population-attributable fractions (PAF) of 1-8 % compared to 27 % PAF of APOE ε4 (Lambert *et al.*, 2013)). This observation highlights the complexity of LOAD risk, being conferred by a combination of multiple genetic risk loci and environmental stressors (Bertram *et al.*, 2010).

1.2 VPS10P domain receptors in human health and disease

One group of intracellular sorting receptors has gained increasing attention for the genetic and function implication of their family members in neurodegenerative diseases. This VPS10P domain receptor family comprises a group of seven type-1 transmembrane proteins that share an extracellular protein domain, called vacuolar protein sorting 10 protein (VPS10P) domain (Figure 1-3).

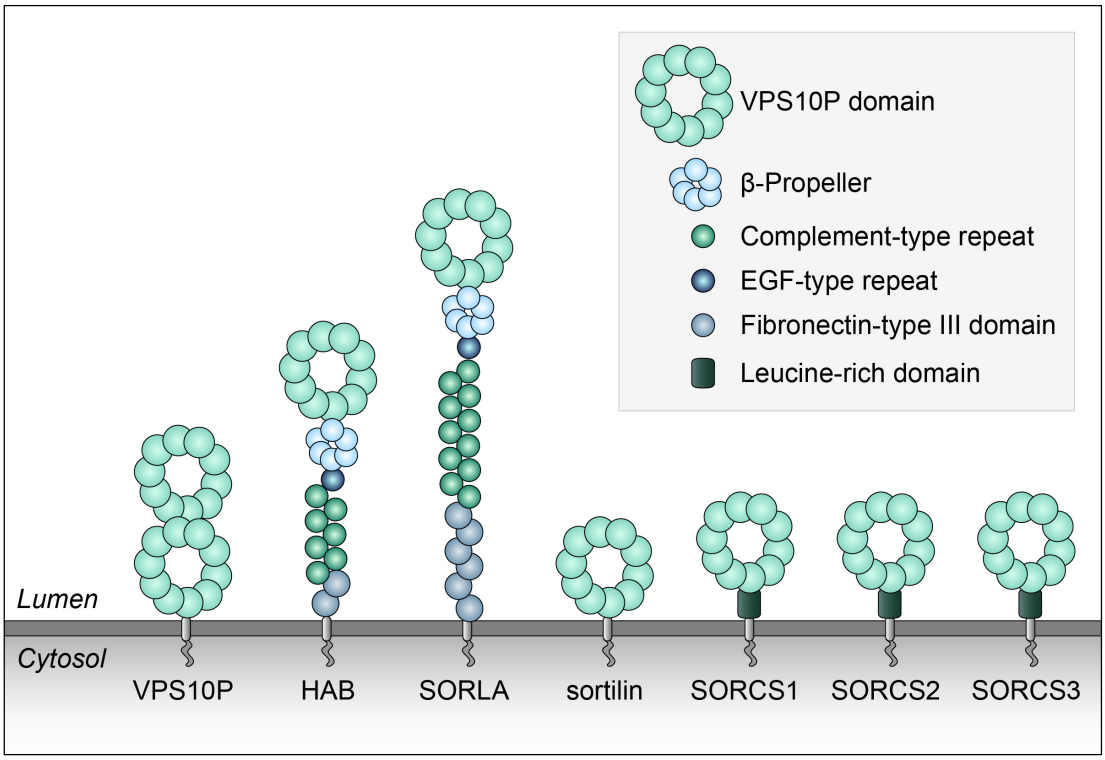

Figure 1-3: Structural organization of the vacuolar protein sorting 10 protein (VPS10P) domain receptor family. VPS10P (*Saccharomyces cerevisiae*), head activator binding protein (HAB) (*Chlorohydra viridissima*), sorting protein-related receptor with A-type repeats (SORLA), sortilin, sortilin-related receptors CNS expressed (SORCS) 1, 2, and 3 are type-1 transmembrane receptors that share a common extracellular domain (the VPS10P domain). Some receptors of the family carry additional functional domains required for ligand binding such as the complement-type repeats in SORLA and HAB. The intracellular tail of the receptors mediates subcellular trafficking through binding of cytosolic adaptor proteins. Figure adapted from Andersen *et al.*, 2016.

This domain has first been described in a protein in *Saccharomyces cerevisiae* called VPS10P, which acts as an intracellular trafficking receptor for transport of carboxypeptidase Y (CPY) to the vacuole (Marcusson et al.,

1994; Cooper and Stevens, 1996). The VPS10P domain was also found in the head activator binding protein (HAB), a transmembrane receptor for the head activator neuropeptide that regulates stem cell proliferation and differentiation in *Chlorohydra viridissima* (Hampe *et al.*, 1999).

The first two mammalian members of the VPS10P domain receptor family, the sorting protein-related receptor with A-type repeats (SORLA) and sortilin, were identified in a screen for novel lipoprotein receptors, which bind the receptor-associated protein (RAP) (Jacobsen *et al.*, 1996; Petersen *et al.*, 1997). RAP is a molecular chaperone that delivers newly synthesized low-density lipoprotein receptors (LDLR) from the ER to the Golgi (Lee *et al.*, 2007). The 250 kDa protein SORLA is the largest member of the VPS10P domain receptor family and the only one sharing structural ligand-binding domains with the LDLR family (Willnow and Andersen, 2013). SORLA is widely expressed in neurons of the central nervous system, including cortex, hippocampus and cerebellum, but also in adipocytes (Motoi *et al.*, 1999; Schmidt *et al.*, 2016). The 95 kDa VPS10P domain receptor family member sortilin is also highly expressed in neurons of the central and peripheral nervous systems, including cerebral cortex and hippocampus, as well as in hepatocytes and white blood cells (Petersen *et al.*, 1997; Sarret *et al.*, 2003; Jansen *et al.*, 2007). Subsequently, three structurally related receptors were identified, namely the 130 kDa sortilin-related receptors CNS expressed (SORCS) 1, 2, and 3 (Hermey *et al.*, 1999; Hampe *et al.*, 2001; Rezgaoui *et al.*, 2001), which are also highly expressed in neurons.

The structural similarities to the extracellular domain and the cytosolic tail of VPS10P in yeast, that mediate ligand binding and subcellular trafficking, respectively, suggested that the five mammalian VPS10P domain receptors might also play a role in intracellular protein sorting. Meanwhile, the receptor family attracted increasing attention as genetic association studies implicated VPS10P domain receptors in a wide range of neurological disorders. Most established is the association of *SORL1*, the gene encoding for SORLA, with Alzheimer's' disease (see Section 1.2.2), but the other mammalian VPS10P domain receptors have also been association with this disease (Grupe *et al.*, 2006; Reitz *et al.*, 2011b, 2013; Andersson *et al.*, 2016). *SORT1*, the gene encoding sortilin, is associated with frontotemporal

lobar degeneration (FTLD), the second most common form of early-onset dementia (Carrasquillo *et al.*, 2010), and with senescence of the brain (Lu *et al.*, 2004). *SORCS2* is associated with bipolar disorder and schizophrenia (Baum *et al.*, 2008; Christoforou *et al.*, 2011), whereas *SORCS1, 2,* and *3* are associated with attention deficit hyperactivity disorders (Lionel *et al.*, 2011; Alemany *et al.*, 2015).

Considering the well-known link between neurodegenerative and metabolic disorders (Frisardi *et al.*, 2010), it is interesting to note that VPS10P domain receptors were also genetically implicated in metabolic and cardiovascular diseases. *SORL1* is associated with obesity (Smith *et al.*, 2010; Parks *et al.*, 2013), *SORT1* with hypercholesterolemia and risk of myocardial infarction (Samani *et al.*, 2007; Kathiresan *et al.*, 2008, 2009; Teslovich *et al.*, 2010), whereas *SORCS1* and *3* are associated with type-2 diabetes (Clee *et al.*, 2006; Granhall *et al.*, 2006).

1.2.1 Subcellular trafficking of SORLA and sortilin

Conceptually, members of the VPS10P domain receptors rely on two functional modules for subcellular sorting of ligands. As best described for SORLA and sortilin, the luminal receptor domains contain ligand-specific binding sites, including interaction motifs in the VPS10P domain (Quistgaard *et al.*, 2009; Kitago *et al.*, 2015) and in SORLA's complement type repeats (Mehmedbasic *et al.*, 2015). The cytosolic receptor tails harbor recognition sites for adaptor proteins that mediate subcellular trafficking of the receptors (Willnow *et al.*, 2008).

Both SORLA and sortilin contain a propeptide in their unprocessed precursor form that is cleaved off by furin or furin-like proprotein convertases in the TGN before they enter the constitutive secretory pathway (Petersen *et al.*, 1999; Jacobsen *et al.*, 2001). The propeptide prevents ligand binding to the VPS10P domain of the receptors during biosynthesis and, at least for sortilin, also acts as an endogenous chaperone to facilitate transport to the Golgi compartment (Petersen *et al.*, 1999; Jacobsen *et al.*, 2001; Westergaard *et al.*, 2004). At the cell surface, SORLA and sortilin can shed their extracellular domains which is mediated by ADAM17 cleavage (Hampe *et al.*, 2000; Navarro *et al.*, 2002; Hermey *et al.*, 2006). While extracellular

shedding disrupts the sorting function of the receptors, the soluble form of SORLA can act as a signaling molecule binding to bone morphogenetic protein (BMP) receptors and the head activator peptide (Hampe *et al.*, 2000; Whittle *et al.*, 2015). Still, only a small fraction of SORLA and sortilin resides at the cell surface at any given time. Rather, most receptor molecules relocate from the cell surface back to endosomes and the TGN (Petersen *et al.*, 1997; Jacobsen *et al.*, 2001; Nielsen, 2001). To achieve this, receptor molecules at the cell surface are rapidly internalized by binding of the adaptor protein 2 (AP2) to acidic cluster dileucine-like and YXXΦ motifs in their cytosolic tails (Jacobsen *et al.*, 2001; Nielsen, 2001). Subsequently, SORLA and sortilin sort retrogradely from early endosomes to the TGN (Seaman, 2004, 2007; Nielsen *et al.*, 2007; Mari *et al.*, 2008). The retrograde transport of SORLA and sortilin to the TGN depends on several adaptor proteins binding to specific motifs in their cytosolic domains, including the retromer complex (Seaman, 2004, 2007; Canuel *et al.*, 2008; Fjorback *et al.*, 2012) and the phosphofurin acidic cluster sorting protein 1 (PACS1) (Schmidt *et al.*, 2007; Burgert *et al.*, 2013). Both receptors can also traffic anterogradely from the TGN to endosomal compartments, from where ligands are delivered to the lysosomes for degradation. Anterograde sorting of SORLA and sortilin is dependent on binding of the Golgi-localizing γ-adaptin ear homology domain, ARF-interacting (GGA) proteins 1 and 2 (Nielsen, 2001; Jacobsen *et al.*, 2002; Schmidt *et al.*, 2007; Herskowitz *et al.*, 2012).

1.2.2 SORLA is a risk factor for Alzheimer's disease

1.2.2.1 *SORL1* is genetically associated with Alzheimer's disease

SORLA was initially implicated in LOAD by the observation that SORLA protein levels are decreased in brains of patients compared to healthy controls (Scherzer *et al.*, 2004). This finding was substantiated by the genetic association of several single nucleotide polymorphisms (SNPs) in the *SORL1* gene with occurrence of LOAD. In the initial association study, a candidate gene approach revealed association of two haplotypes with highly linked SNPs at the 3' and at the 5' end of *SORL1* with LOAD in Caucasians (Rogaeva *et al.*, 2007). Subsequent association studies gave conflicting results as some reproduced the association of certain *SORL1* SNPs with

LOAD, while others did not. This controversy was likely caused by small cohort sizes of some of the studies and the allelic heterogeneity in different ethnicities (reviewed in Reitz *et al.*, 2011a). However, recent meta-analyses combining several studies (Reitz *et al.*, 2011a; Jin *et al.*, 2013; Wang *et al.*, 2016) and large genome-wide association studies (GWAS) (Lambert *et al.*, 2013; Miyashita *et al.*, 2013) finally confirmed the association of *SORL1* with LOAD.

Since the validation of *SORL1* as an LOAD risk gene, several studies have focused on analyzing the functional relevance of the identified genetic risk variants. Some LOAD-associated risk SNPs in the 3' and 5' haplotypes of the *SORL1* gene are associated with reduced *SORL1* mRNA levels (Rogaeva *et al.*, 2007; Grear *et al.*, 2009; McCarthy *et al.*, 2012), suggesting that some non-coding risk variants act through decreasing *SORL1* transcription efficiency. Indeed, recent analysis of iPSC-derived neurons carrying either minor or major variants of the 5' haplotype block revealed a loss of brain-derived neurotrophic factor (BDNF)-stimulated *SORL1* expression in the risk variant carriers (Young *et al.*, 2015). BDNF induces *SORL1* gene expression through activation of the extracellular regulated kinase (ERK) pathway (Rohe *et al.*, 2009). Another non-coding risk variant (rs73595277) was suggested to regulate alternative splicing of *SORL1* by *in silico* prediction (Kölsch *et al.*, 2009). In addition to the impact on transcriptional regulation of *SORL1* by the associated risk variants, some SNPs also affect *SORL1* translation efficiency. The minor variant of rs2070045 causes an exchange of a frequently used codon in the major variant to a rare codon, thereby lowering SORLA translation efficiency (Caglayan *et al.*, 2012).

Overall, LOAD-associated risk variants in the *SORL1* gene affect *SORL1* transcription, splicing or translation efficiency and therefore likely confer LOAD risk by reducing SORLA levels in the brain.

1.2.2.2 SORLA is a trafficking receptor for both APP and Aβ

Numerous studies in cultured cells and transgenic mouse models have revealed two distinct molecular mechanisms by which SORLA reduces Aβ burden in the brain (Andersen *et al.*, 2016). In one mechanism, SORLA protects APP from proteolytic processing by sorting APP retrogradely from

endosomal compartments back to the TGN (Andersen et al., 2005; Schmidt et al., 2007) (see Figure 1-4). While loss of SORLA increases Aβ levels and senile plaque burden in Alzheimer's disease mouse models (Andersen *et al.*, 2005; Dodson *et al.*, 2008; Rohe *et al.*, 2008), SORLA overexpression reduces the amount of all APP processing products, including Aβ, in various cell lines (Andersen *et al.*, 2005; Offe *et al.*, 2006; Rogaeva *et al.*, 2007).

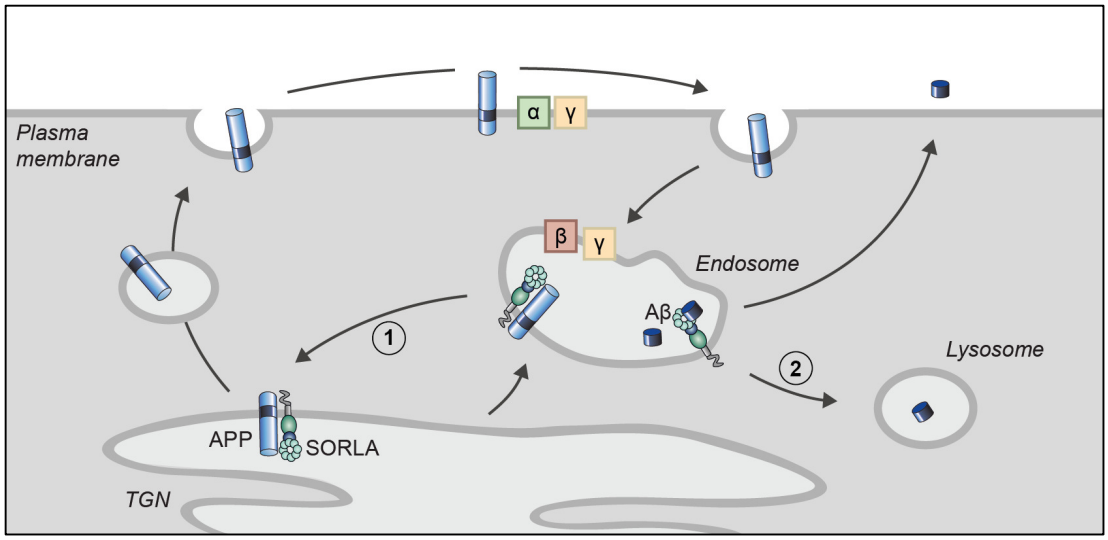

Figure 1-4: SORLA reduces Aβ peptide accumulation by two distinct mechanisms. (1) SORLA binds to full length APP and sorts it retrogradely from endosomes to the *trans*-Golgi-network (TGN). As secretases are localized mainly to the plasma membrane and to endosomal compartments, APP in the TGN is protected from being processed by amyloidogenic and non-amyloidogenic secretases. (2) SORLA also acts as a sorting receptor for newly produced Aβ molecules in endosomal compartments by anterograde trafficking from endosomes to lysosomes where both SORLA and Aβ are degraded.

The APP binding site in SORLA locates to the cluster of complement-type repeats in SORLA's extracellular domain, which is essential for shuttling APP to the TGN and thereby protecting it from processing (Andersen *et al.*, 2005, 2006; Mehmedbasic *et al.*, 2015). Even small reductions in SORLA levels significantly alter APP processing rates, as SORLA's interaction with APP prevents the formation of APP oligomers, which are the preferred form of substrate for α- and β-secretases (Schmidt *et al.*, 2011). The retrograde transport from endosomes to TGN of SORLA, and thus APP, depends on binding of PACS1 (Schmidt *et al.*, 2007; Burgert *et al.*, 2013) and the VPS26 subunit of the retromer complex to SORLA's cytosolic tail (Seaman, 2004,

2007; Fjorback *et al.*, 2012; Dumanis *et al.*, 2015). Anterograde transport of SORLA from the TGN to endosomes, that serves to restore receptor levels in endosomal compartments for retrieval of APP, is mediated by the adaptor proteins GGA1 and 2 (Jacobsen *et al.*, 2002; Schmidt *et al.*, 2007; Herskowitz *et al.*, 2012; Dumanis *et al.*, 2015).

The second mechanism whereby SORLA lowers Aβ levels in the brain relies on anterograde sorting of the receptor. Specifically, SORLA directly interacts with newly generated Aβ peptides in endosomal compartments and sorts Aβ to the lysosomes for degradation (Caglayan *et al.*, 2014) (Figure 1-4). Interestingly, Aβ binds to the VPS10P domain of SORLA, but not of sortilin, even though both VPS10P domains form structurally similar ten-bladed β-propeller folds with ligand binding domains at the center (Quistgaard *et al.*, 2009; Kitago *et al.*, 2015).

1.2.2.3 *SORL1* is implicated in early-onset Alzheimer's disease

As discussed above, EOAD is caused by rare gene mutations with high penetrance and an autosomal-dominant pattern of inheritance (Reitz and Mayeux, 2014). Intriguingly, known mutations in *APP* or *PSEN1/2* only account for 30–50 % of EOAD cases (Zou *et al.*, 2014), indicating that further EOAD-causing mutations still remain to be uncovered.

Recently, potentially pathogenic sequence variations in *SORL1* were found in EOAD patients (Pottier *et al.*, 2012; Nicolas *et al.*, 2016; Verheijen *et al.*, 2016). In a first report, whole exome sequencing of EOAD patients carrying neither *APP* nor *PSEN1/2* mutations revealed seven novel potentially pathogenic mutations in *SORL1* that were not found in healthy individuals (Pottier *et al.*, 2012). Subsequent studies uncovered further rare mutations in *SORL1* in EOAD patients that potentially damage SORLA function, including nonsense, frame shift, and missense variants (Nicolas *et al.*, 2016; Verheijen *et al.*, 2016). While these observations suggest *SORL1* as a novel EOAD gene, many questions still remain open. The proposed pathogenicity of most of the EOAD-associated *SORL1* mutations so far relies on *in silico* predictions. Functional characterization of these mutations will have to prove whether they in fact impair SORLA function. Also, limited availability of genomic DNA from other affected relatives so far precluded pedigree analysis for most discovered EOAD-associated mutations

(Pottier *et al.*, 2012).

Still, *SORL1* was substantiated as a potential novel EOAD gene by recent work studying the functional relevance of the G511R mutation (Pottier *et al.*, 2012). This mutation was also found in the affected mother of the EOAD patient. G511R locates to the VPS10P domain of SORLA and disrupts SORLA's Aβ binding site, resulting in impaired lysosomal targeting of Aβ by the mutant receptor (Caglayan *et al.*, 2014). This observation suggests that not only increased APP processing, as observed for *APP* and *PSEN1/2* mutations, but also impaired SORLA-mediated lysosomal degradation of Aβ may cause EOAD.

Most of the potentially pathogenic *SORL1* variants found in EOAD patients still lack functional validation. Analyzing especially the protein coding EOAD-associated mutations in cell and mouse models will improve our understanding of SORLA's structural domains fulfilling different functions in the context of Alzheimer's disease. It may also elucidate how some genetic variants in the *SORL1* gene confer relatively small Alzheimer's disease risk sizes for LOAD, while others exhibit high penetrance and cause the aggressive early-onset form of the disease.

1.2.3 Sortilin is implicated in neurodegenerative and cardiovascular diseases

Similar to SORLA, sortilin is a sorting receptor for proteins along the endocytic and secretory pathways. Sortilin was initially recognized for its central role in regulating neurotrophic and apoptotic processes in the brain by both controlling the release of pro-neurotrophins (Chen *et al.*, 2005), and by sorting neurotrophin receptors (Nykjaer *et al.*, 2004; Vaegter *et al.*, 2011). Interestingly, neurotrophic signaling is altered both in Alzheimer's disease patients and in the aging brain, implicating sortilin-mediated neurotrophin regulation in age-related neurodegeneration (Fahnestock *et al.*, 2001; Al-Shawi *et al.*, 2008; Terry *et al.*, 2011). Besides its role in global neurotrophic signaling, sortilin is specifically implicated in both Alzheimer's disease and frontotemporal lobar degeneration (FTLD) (Ratnavalli *et al.*, 2002; Kumar-Singh, 2011).

1.2.3.1 Role of sortilin in Alzheimer's disease

Aβ accumulation and senile plaque formation in the brain is thought to result from an imbalance of Aβ production and clearance (Blennow *et al.*, 2006). Aβ clearance from the interstitial fluid is facilitated by different mechanisms, including receptor-mediated clearance of the peptide by neurons, astrocytes, or microglia. Transport across the blood brain barrier as well as proteolytic degradation in the brain interstitial fluids by Aβ-degrading proteases (Saido and Leissring, 2012; Liu *et al.*, 2013) also contribute to removal of the peptide from the brain parenchyma. APOE plays an important role in mediating Aβ clearance by binding soluble Aβ and facilitating cellular uptake of APOE-Aβ complexes by APOE receptors (Kim *et al.*, 2009; Kanekiyo *et al.*, 2011). Several members of the LDL receptor family have been described to act as APOE receptors and to contribute to the cellular uptake and catabolism of Aβ, including LDLR and the LDLR-related protein 1 (LRP1) (Holtzman *et al.*, 2012).

Recent work now also suggests a role for sortilin as a major clearance receptor for APOE-Aβ complexes in neurons (Carlo et al., 2013). First evidence for sortilin facilitating APOE clearance in the brain originated from the observation that APOE accumulates in the brain of *Sort1* deficient mice (Carlo et al., 2013). Also, Alzheimer's disease mouse models deficient

for *Sort1* display increased Aβ levels and senile plaque burden compared to wildtype controls (Carlo et al., 2013). Finally, APOE/Aβ uptake experiments revealed a 70 - 80 % reduction in uptake of APOE/Aβ complexes in *Sort1* deficient compared to wildtype primary neurons, confirming that APOE/Aβ uptake in neurons largely depends on sortilin (Carlo et al., 2013).

Besides facilitating Aβ clearance in the brain, sortilin has also been proposed to increase Aβ production by trafficking both APP (Gustafsen *et al.*, 2013) and the β-secretase BACE1 (Finan *et al.*, 2011).

1.2.3.2 Role of sortilin in frontotemporal lobar degeneration

Frontotemporal lobar degeneration (FTLD) is the second leading cause of early-onset dementia (Ratnavalli *et al.*, 2002; Kumar-Singh, 2011). FTLD is a clinically heterogeneous disease characterized by symptoms like behavioral changes and gradual language dysfunction that are caused by progressive atrophy of the frontal and temporal lobes of the brain (Neary et al., 1998). Histologically, the disease is characterized by protein inclusions in the brain that stain positive for the microtubule-associated protein tau (MAPT), for ubiquitin or for transactive response DNA-binding protein 43 (TDP-43) (Sampathu *et al.*, 2006). Based on these neurobiological targets, FTLD is classified into three major subtypes (Kumar-Singh and Van Broeckhoven, 2007). A major cause of FTLD with ubiquitin-positive inclusions (FTLD-U) are heterozygous mutations in the *GRN* gene (Baker *et al.*, 2006; Cruts *et al.*, 2006; Gass *et al.*, 2006; Mackenzie *et al.*, 2006; Mukherjee *et al.*, 2006; Snowden *et al.*, 2006). Most of these mutations are nonsense or frame shift mutations resulting in haploinsufficiency of the protein progranulin (PGRN), suggesting PGRN as a protective factor against FTLD (Gass *et al.*, 2012). The mechanism by which PGRN protects from FTLD is not fully understood, although mechanisms in neurotrophin signaling and inflammation regulation have been proposed (He *et al.*, 2003; Van Damme *et al.*, 2008). However, since PGRN deficiency clearly causes FTLD-U, a major potential therapeutic strategy for FTLD is to restore PGRN levels in FTLD patients. One promising approach is to target the PGRN sorting receptor sortilin. Sortilin determines PGRN levels by mediating PGRN endocytosis and rapidly delivering it to the lysosomes for degradation (Hu *et al.*, 2010). PGRN levels are increased 2.5- to 5-fold in mice lacking sortilin and disrupting *Sort1* expression in

haploinsufficient *GRN*+/− mice completely restores PGRN levels (Hu *et al.*, 2010). Targeting the sortilin-PGRN interaction using small molecules in human FTLD patient iPSC-derived neurons also restored PGRN levels, confirming the potential of targeting sortilin as a therapeutic strategy for FTLD (Lee *et al.*, 2014). In line with the central role of sortilin for regulation PGRN levels, a SNP near the *SORT1* gene locus is associated with PGRN plasma levels (Carrasquillo *et al.*, 2010).

1.2.3.3 Role of sortilin in hypercholesterolemia and myocardial infarction

Besides sortilin's causal role in neurodegenerative diseases, recent work uncovered that sortilin also controls the release of lipoproteins in the liver (Kjolby *et al.*, 2010; Musunuru *et al.*, 2010).

Levels of LDL-associated cholesterol in the circulation are 50 % genetically determined and represent a major risk factor for myocardial infarction (Heller *et al.*, 1993; Rader *et al.*, 2003). Both hypercholesterolemia and myocardial infarction have been associated with rs646776, a non-coding SNP close to the *SORT1* gene locus, by numerous GWAS (Samani *et al.*, 2007; Kathiresan *et al.*, 2008, 2009; Teslovich *et al.*, 2010). *SORT1* expression in the liver is increased 4-fold in carriers of the protective minor variant compared to major risk variant carrying controls. This observation suggests that sortilin acts as a protective factor for hypercholesterolemia (Musunuru *et al.*, 2010). Molecular dissection of this cardiovascular risk locus indicated that indeed rs12740374, a SNP closely linked to rs646776, regulates *SORT1* expression levels in the liver by generating a C/EBP enhancer site in the minor variant (Musunuru *et al.*, 2010). Mechanistically, sortilin regulates the hepatic release and clearance of both LDLs and of very low-density lipoproteins (VLDL), that are converted to LDLs in the bloodstream (Kjolby *et al.*, 2010; Linsel-Nitschke *et al.*, 2010; Musunuru *et al.*, 2010; Strong *et al.*, 2012). Increased *SORT1* expression in the liver correlates with decreased LDL-C plasma levels in humans and thus lower risk of myocardial infarction in humans.

The genetic and functional evidence that proposes sortilin as an important protective factor against myocardial infarction also provides an intriguing link between lipoprotein regulation in the liver and neurodegenerative processes in the brain. The association of *SORT1*

expression levels in hepatocytes with rs646776 was established by analyzing human liver samples, however, whether this SNP, or other genetically linked SNPs, also predict *SORT1* expression in the brain remains to be elucidated. Interestingly, the same genetic variant that confers risk of hypercholesteloremia and myocardial infarction (rs646776) is also associated with PGRN levels in human plasma (Carrasquillo *et al.*, 2010).

2 AIMS OF THIS STUDY

The VPS10P domain receptors SORLA and sortilin have been genetically associated with neurodegenerative diseases. Studies in cultured cells and transgenic mouse models substantiated their functional role for Alzheimer's disease and FTLD. Still, the molecular mechanisms whereby certain genetic variants predispose carriers to Alzheimer's disease and FTLD are unclear. In my PhD thesis I aimed at functionally characterizing disease-associated genetic variants in *SORL1* and *SORT1* and assess their relevance for neurodegenerative diseases.

2.1 Human iPSC-derived neurons as a model system to study the functional relevance of the *SORT1* risk locus in neurons

The myocardial infarction risk SNP rs646776 was demonstrated to predict *SORT1* expression in the liver. However, analysis of the genomic region revealed rs12740374 as a more likely candidate to affect SORT1 expression as it created a C/EBP recognition site in the minor variant. Whether this SNP also predicts *SORT1* expression in the brain remained to be elucidated. To assess whether rs12740374 regulates *SORT1* expression in hepatocytes and in neurons, I differentiated human iPSCs carrying minor or major variants into hepatocytes and cortical neurons. I used donor and genome-edited iPSC lines to assess both whether the risk locus predicts *SORT1* expression levels in neurons in general and whether rs12740374 is indeed the causal variant (Figure 2-1).

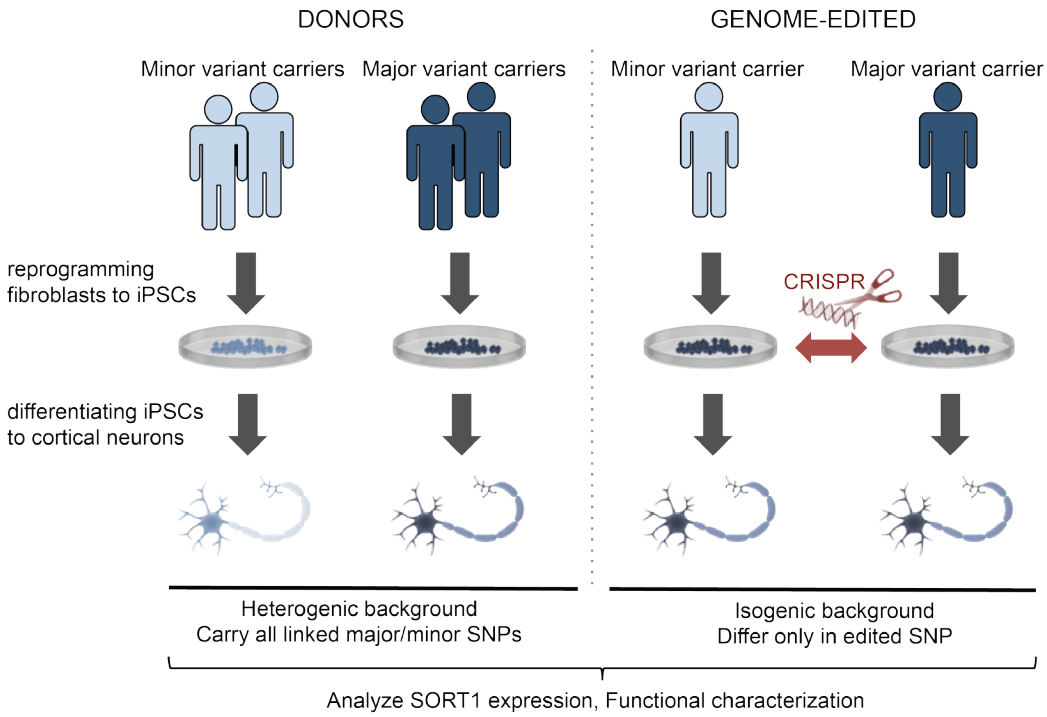

Figure 2-1: Schematic depiction of the two approaches used to analyze functional relevance of *SORT1* minor/major variants. *SORT1* expression and its functional relevance in human neurons can be modelled by reprogramming primary fibroblasts from donors to iPSCs and to further differentiate them into cortical neurons. In a first approach (left), iPSC-derived neurons from donors carrying either the minor or major variant of the SNP of interest were analyzed for their difference in *SORT1* expression. Of note, these cells do not only differ in the SNP of interest but also in minor/major variants of all genetically linked SNPs as well as in their entire genetic background. To conclusively attribute potential effects on *SORT1* expression to a distinct SNP, iPSCs can be genome-edited using CRISPR/Cas9 to carry minor or major SNP variants (right). The seamless exchange of the SNP of interest (see Figure 4-8) allows testing of its direct effect on *SORT1* expression and its functional relevance.

2.2 Functional validation of coding *SORL1* mutations associated with early-onset Alzheimer's disease

Most of the recently identifed *SORL1* mutations in EOAD patients have not been functionally characterized yet. Studying these mutations in cellular models and determing their relevance for EOAD-relevant processes would not only validate *SORL1* as a novel EOAD-causative gene but also deepens our knowledge of SORLA's role in neurodegeneration. The coding missense *SORL1* mutations identified in EOAD patients are thought to have a strong effect on SORLA function to cause the aggressive early-onset form of Alzheimer's disease, presumably by affecting SORLA's functional domains and therefore binding of interaction partners. To test this hypothesis, I overexpressed the mutant receptor variants in an established neuronal cell line (SH-SY5Y) and analyzed their effect on amyloidogenic processes.

3 MATERIALS AND METHODS

3.1 Materials

3.1.1 General reagents and chemicals

Reagent/Chemical	**Provider (Cat. No.)**
Agar	BD Biosciences (214010)
Agarose	VWR Peqlab (35-1020)
Ammonium persulfate (APS)	Sigma-Aldrich (A3678)
Ampicillin	Biomol (01503)
AmpliTaq Gold™ DNA-Polymerase	Thermo Fisher (N8080241)
Ara-C (Cytosine β-D-arabinofuranoside)	Sigma-Aldrich (C1768)
Arg0 (L-arginine-HCl)	Sigma-Aldrich (A6969)
Arg10 (L-arginine-HCl, $^{13}C_6$, $^{15}N_4$)	Sigma-Aldrich (608033)
B-27 supplement (50x)	Thermo Fisher (17504044)
Bacto Tryptone	BD Biosciences (211699)
Bacto Yeast Extract	BD Biosciences (212720)
Bambanker™ freezing medium	Lymphotec Inc. (302-14681)
BDNF (brain-derived neurotrophic factor)	R&D systems (248-BD-025)
Bromophenol blue	Sigma-Aldrich (B8026)
BSA (Bovine serum albumin)	Thermo Fisher (23209)
Chloroquine	Sigma-Aldrich (C6628-25g)
DMEM (Dulbecco´s Modified Eagle Medium)	Thermo Fisher (41966029)
DMEM for SILAC	Thermo Fisher (88364)
DMEM/ F12 (Dulbecco's Modified Eagle Medium/Nutrient Mixture F-12)	Thermo Fisher (11330-032)
DMSO (dimethylsulfoxide)	Sigma-Aldrich (D2650)
DNase I Set (RNase-free)	Qiagen (79254)
dNTP (deoxynucleotide) set	Sigma-Aldrich (DNTP100-1KT)
Doxycycline	Clontech (631311)
EDTA (Ethylene diamine tetraacetic acid)	Roth (80432)
Ethanol	Merck Millipore (1009862500)
Ethidium bromide	Sigma-Aldrich (E1510)

Reagent/Chemical	**Provider (Cat. No.)**
ExoSAP-IT™ PCR Product Cleanup reagent	Thermo Fisher (78201.1.ML)
FBS (Fetal bovine serum)	Thermo Fisher (10270-106)
FGF-2 (fibroblast growth factor 2)	Peprotech (100-18B)
Fluorescence mounting medium	Dako (S3023)
Glacial acetic acid	Sigma-Aldrich (537020)
GlutaMax™ (100x)	Thermo Fisher (350-038)
Glycerol	Serva (23176)
HBSS (Hanks' balanced salt solution)	Lonza (BE10-547F)
Hygromycin B	Thermo Fisher (10687010)
Insulin	CS Bio (C9212-1G)
Isopropanol	Roth (9866.5)
L-ascorbic acid 2-phosphate	Sigma-Aldrich (A8960)
Laminin mouse protein	Thermo Fisher (23017-015)
Lenti-X Concentrator	Clontech (631231)
Lipofectamine™ 2000 Transfection Reagent	Thermo Fisher (11668027)
Lipofectamine™ 3000 Transfection Reagent	Thermo Fisher (L3000008)
Lys0 (L-lysine-HCl)	Sigma-Aldrich (L8662)
Lys8 (L-lysine-HCl, $^{13}C_6$,$^{15}N_2$)	Silantes (211604102)
Matrigel™ Basement Membrane Matrix	BD Biosciences (354277)
Methanol	Roth (KK44.1)
N-2 supplement (100x)	Thermo Fisher (17502048)
NEAA (non-essential amino acids, 100x)	Thermo Fisher (11140-035)
Neurobasal medium	Thermo Fisher (21103-049)
Nitrocellulose membrane	GE Healthcare (10600016)
NP-40 (Nonidet-P40)	US Biological (N3500)
NT-3 (neurotrophin 3)	R&D systems (267-N3-025)
Opti-MEM	Thermo Fisher (51985034)
P/S (penicilin/streptomycin, 100x)	Thermo Fisher (15140-122)
Papain	Sigma-Aldrich (P4762)
PBS (phosphate-buffered saline, 10x)	Thermo Fisher (14200-067)
PFA (paraformaldehyde)	Sigma-Aldrich (16005)
Pierce™ NHS-Activated Magnetic Beads	Thermo Fisher (88826)
Poly-L-lysine solution (0.01 %)	Sigma-Aldrich (P4832-50ml)
Polybrene	Merck Millipore (TR-1003-G)
PowerUp™ SYBR™ Green Master Mix	Thermo Fisher (A25742)
Precision Plus Protein™ Dual Color standard	Bio-Rad (161-0374)
Protease Inhibitor cOmplete cocktail	Roche (04693116001)
Puromycin	Thermo Fisher (A1113803)
Rotiphorese gel 30 % (37.5:1)	Roth (30291)
SDS (sodium dodcyl sulfate, pellets)	Serva (2076503)
Skim milk powder	Sigma-Aldrich (70166)
Sodium chloride (NaCl)	Roth (9265.3)

Reagent/Chemical	**Provider (Cat. No.)**
Sodium hydroxide (NaOH)	Roth (P031.2)
Sodium Pyruvate (100 mM)	Thermo Fisher (11360039)
Sodium selenite	Sigma Aldrich (S5261-10G)
StemPro™ Accutase™	Thermo Fisher (A11105-01)
SuperSignal West Femto Maximum Sensitivity Substrate	Thermo Fisher (34095)
SYBR™ green PCR Master Mix	Thermo Fisher (4344463)
TaqMan™ Gene Expression Master Mix	Thermo Fisher (4369016)
TaqMan™ Gene Expression Master Mix	Thermo Fisher (4369016)
TaqMan™ Genotyping Master Mix	Thermo Fisher (4371355)
TEMED (N,N,N′,N′-Tetramethylethylenediamine)	Sigma-Aldrich (T9281)
TGF-β1 (transforming growth factor β1)	Peprotech (100-21C)
Transferrin	Sigma Aldrich (T3705-1G)
Tris PUFFERAN® ($C_4H_{11}NO_3$)	Roth (AE15.4)
Triton X-100	Roth (3051.2)
Trypan Blue Stain (0.4 %)	Thermo Fisher (T10282)
Trypsin/EDTA, 0.05 %	Thermo Fisher (25300-054)
Tween-20	Sigma-Aldrich (P1379)
XL1-Blue Supercompetent Cells	Stratagene (200236)
Y27632 (ROCK inhibitor)	Selleck Chemicals (S1049)
Zeocin™ Selection Reagent	Thermo Fisher (R25001)
β-Mercaptoethanol	Roth (42273)

3.1.2 Kits

Kit	**Provider (Cat. No.)**
Aβ V-PLEX Kit (human, 6E10)	Mesoscale (K15200E)
Cellartis iPS Cell to Hepatocyte Differentiation Kit	Clontech (Y30055)
CytoTune™-iPS 2.0 Sendai Reprogramming Kit	Thermo Fisher (A16517)
DNeasy Blood and Tissue Kit	Qiagen (69504)
High-Capacity RNA-to-cDNA™ Kit	Thermo Fisher (4387406)
MFG-E8 ELISA (human)	R&D Systems (DGFE80)
MFG-E8 ELISA (mouse)	R&D Systems (MFGE80)
Nucleobond Xtra Plasmid Midiprep Kit	Macherey Nagel (740410.100)
Pierce™ BCA Protein Assay Kit	Thermo Fisher (23225)
Progranulin ELISA (human)	Adipogen (AG-45A-0018YEK-K101)
QIAquick Gel Extraction Kit	Qiagen (28704)
RNeasy Mini Kit	Qiagen (74106)
sAPPα/sAPPβ Duplex Kit (human)	Mesoscale (K15120E)
TALEN Musunuru/Cowan Lab TALEN Kit	Addgene (Kit #1000000034)

3.1.3 DNA primers

DNA oligonucleotides were purchased from Eurofins Genomics.

Table 3-1: DNA primers for TALENs targeting of *SORT1* ATG.

Application	Sequence (5'-3')	Annealing temperature
Sequencing cloned TALENs constructs	GGCCAGTTGCTGAAGATCG (TALseq+)	-
	CGCTACAAGATGATCATTAGTG (TALseq-)	
Amplifying *SORT1* ATG region (528 bp)	forward: CGTTCCAGCCAATCAGTCCC	63 °C
	reverse: AGCTTGGCGACGAAGTCC	

Table 3-2: DNA primers for CRISPR-HR targeting of the *SORT1* SNP.

Application	Sequence (5'-3')	Annealing temperature
Sequence sgRNA in Cas9 vector	GAGGGCCTATTTCCCATGATT (hU6-forward)	-
Check for genomic integration of HR vector (left)	forward_gen_left: ATCTCCACTCTTCATGACTTCAGG	60 °C
	reverse_gen_right: CTCCAGAAGGAAAGTCAGTGACA	
	reverse_vector: AGACCGATAAAACACATGCGTCAA	
Check for genomic integration of HR vector (right)	forward_gen_left: ATCTCCACTCTTCATGACTTCAGG	60 °C
	reverse_gen_right: CTCCAGAAGGAAAGTCAGTGACA	
	forward_vector: GTCCTAAATGCACAGCGACG	

Table 3-3: DNA primers for site-directed introduction of *SORL1* mutations (red).

Primer ID	Sequence (5'-3')	Annealing temperature
N924S_A	GCGGCCGCATGGCGACACGGAGCAGCAGGAGG	72 °C
N924S_B	CAGAGATGCCACTGGGCCACTTCACATCC	72 °C
N924S_C	GGATGTGAAGTGGCCCAGTGGCATCTCTG	72 °C
N924S_D	CATCCTGGCAATCTTGGTGG	72 °C
N1358S_A	AAGAGAATGTCCACAGCTGG	72 °C
N1358S_B	GTTTTCGCAGCTGGCTTCATCAGAATAATC	72 °C
N1358S_C	ATTATTCTGATGAAGCCAGCTGCGAAAACC	72 °C
N1358S_D	CATCCTGGCAATCTTGGTGG	72 °C
G1681D_A	CTTGCAAACGTCACTGCTGCCTCC	72 °C
G1681D_B	ACTCACGGATGAGGTCATGGGTGTGGATGG	72 °C
G1681D_C	CCATCCACACCCATGACCTCATCCGTGAG	72 °C
G1681D_D	TCAGGCTATCACCATGGGGACGTCATCTGAAAATC	72 °C

3.1.4 Quantitative real-time PCR primers

Quantitative real-time PCR was performed using either TaqMan™ probes ordered from Thermo Fisher (Cat. No.: 4331182) or SYBR™ green dye (Thermo Fisher) and DNA oligonucleotides purchased from Eurofins Genomics.

Table 3-4: TaqMan™ probes used for qRT-PCR.

Gene name	Assay ID
OCT4	Hs0999632_s1
NANOG	Hs02387400_g1
TUJ1	Hs00964963_g1
MAP2	Hs00258900_m1
SYN1	Hs00199577_m1
SORT1	Hs00361760_m1
GAPDH	Hs02758991_g1
B2M	Hs00984230_m1
C/EBPα	Hs00269972_s1

Table 3-5: DNA oligonucleotides used with SYBR™ green dye for qRT-PCR.

Gene name	Sequence (5'-3')
ALB	forward: CCTGTTGCCAAAGCTCGATG
	reverse: GAAATCTCTGGCTCAGGCGA
HNF4α	forward: ACATGGACATGGCCGACTAC
	reverse: CGTTGAGGTTGGTGCCTTCT
CYP3A4	forward: GTCTTTGGGGCCTACAGCAT
	reverse: TTGAGAGAAAGAATGGATCCAAAAA
GAPDH	forward: AGCTCACTGGCATGGCCTTC
	reverse: CGCCTGCTTCACCACCTTCT
APOA2	forward: GTCAAGAGCCCAGAGCTTCA
	reverse: GCTGTGTTCCAAGTTCCACG
AFP	forward: ACTGAATCCAGAACACTGCATAG
	reverse: GCTTCTTGAACAAACTGGGCA
OCT4	forward: CCGAAAGAGAAAGCGAACCAG
	reverse: ATGTGGCTGATCTGCTGCAGT
NANOG	forward: TCCAACATCCTGAACCTCAGC
	reverse: CAGGCATCCCTGCGTCAC

3.1.5 SNP genotyping primers

TaqMan™-based SNP genotyping assays were ordered from Thermo Fisher (Cat. No.: 4351379).

Table 3-6: TaqMan™ probes used for SNP genotyping.

Target SNP (minor/major variant)	Assay ID
rs646776 (C/T)	C_31432916_10
rs12740374 (G/T)	C_3160062_10

3.1.6 Plasmids

Plasmid	Antibiotic resistance	Provider (Cat. No.)
TALENs targeting plasmid	Ampicillin	Addgene (Kit #1000000034)
CRISPR Cas9 sgRNA vector	Ampicillin	Addgene (48138)
Homologous recombination vector	Ampicillin	Sanger Institute (pENTR-PGKpuroΔtk)
piggyBac™ Transposase (PBX)	Ampicillin	Transposagen (SPB-002)
GFP (neuronal differentiation)	Ampicillin	T. Südhof (Stanford University)
NGN2 (neuronal differentiation)	Ampicillin	T. Südhof (Stanford University)
NGN2-GFP (neuronal differentiation)	Ampicillin	T. Südhof (Stanford University)
rtTA (neuronal differentiation)	Ampicillin	T. Südhof (Stanford University)
pRSV-Rev (lentivirus packaging)	Ampicillin	Addgene (12253)
pRRE (lentivirus packaging)	Ampicillin	Addgene (12251)
VSV-G (lentivirus packaging)	Ampicillin	Addgene (8454)

3.1.7 Antibodies

Table 3-7: Primary antibodies used for Western Blot and co-IP analyses.

Target protein	Host species	Provider (Cat. No.)	Dilution
SORTILIN	mouse	BD Biosciences (612101)	1:1000
α-TUBULIN	mouse	Merck Millipore (CP06)	1:1000
SORLA	goat	Thomas E. Willnow (homemade)	1:1000
APP	rabbit	Thomas E. Willnow (homemade)	1:1000

Horseradish-peroxidase (HRP) labeled secondary antibodies for Western blot were purchased from Sigma-Aldrich and used at a dilution of 1:5000.

Table 3-8: Primary antibodies used for immunofluorescence stainings.

Target protein	Host species	Provider (Cat. No.)	Dilution
ALBUMIN	rabbit	DakoCytomation (A0001)	1:200
HNF4A	goat	Santa Cruz (sc-6556)	1:200
MAP2	guinea pig	Synaptic Sytems (188004)	1:200
NANOG	rabbit	Thermo Fisher (PA1-097)	1:200
OCT4	mouse	Abcam (ab59545)	1:200
SOX2	rabbit	Abcam (ab97959)	1:200
SSEA4	mouse	Abcam (ab16287)	1:200
TUJ1	mouse	Sigma (T8578	1:1000

Fluorophore-conjugated secondary antibodies for immunocytochemistry were purchased from Thermo Fisher (Alexa Fluor™ 488/555/647 Dyes) and used at a dilution of 1:2000.

3.1.8 Buffers, solutions and cell culture media

3.1.8.1 Buffers and solutions for microbiology methods

LB (Lysogeny broth) medium, pH: 7.2
BactoYeast Extract (5 g/L)
Bacto Tryptone (10 g/L)
Sodium chloride (NaCl) (10 g/L)

LB agar
LB medium
Agar (15 g/L)

SOC (Super Optimal broth with Catabolite repression) medium, pH: 7.0
Bacto yeast extract (5 g/L)
Bacto tryptone (20 g/L)
NaCl (0.6 g/L)
KCl (0.2 g/L)
MgCl2 (10 mM)
Glucose (20 mM)

3.1.8.2 Buffers and solutions for molecular biology methods

Protein lysis buffer
Tris-HCl, pH: 8.0 (20 mM)
NaCl (20 mM)
Sodium deoxycholate (0.6 %, w/v)
Nonidet P-40 (NP-40) (0.6 %, v/v)
cOmplete protease Inhibitor cocktail (1x)

TBS (Tris-buffered saline, 10x)
Tris-HCl (250mM), pH 7.4
NaCl (1.37M)
KCl (27mM)

TBS-T
1x TBS
Tween-20 (0.1 % v/v)

Blocking solution for Western Blot	TBS-T Skim milk powder (5 %, w/v)
Transfer buffer for Western Blot (10x)	Tris-HCl, pH: 7.5 (181.6 mM) Glycine (1.49 M)
TAE (Tris-acetate-EDTA) buffer	Tris-HCl, pH: 8.0 (40 mM) EDTA (1 mM) Glacial acetic acid (20 mM)
Laemmli buffer (4x)	Tris-HCl, pH: 6.8 (250mM) Glycerin (40 %, v/v) SDS (8 %, w/v)
SDS PAGE Running buffer (5x)	Glycine (1.25 M) Tris-HCl, pH 8.3 (125 mM) SDS (0.5 %, w/v)

3.1.8.3 Buffers, solutions and media for cell culture methods

E8 (iPSC medium)	DMEM/F12 L-ascorbic acid 2-phosphate (64 µg/ml) Insulin (20 µg/ml) Transferrin (5 µg/mL) Sodium selenite (14 ng/ml) human FGF-2 (100 ng/ml) TGF-β1 (2 ng/ml)
E7 medium (for reprogramming)	DMEM/F12 L-ascorbic acid 2-phosphate (64 µg/ml) Insulin (20 µg/ml) Transferrin (5 µg/mL) Sodium selenite (14 ng/ml) human FGF-2 (100 ng/ml)
Dissociation solution	PBS EDTA (0.5M)
DMEM growth medium (for HEK cells, CHO cells, human fibroblasts and mouse primary glia)	DMEM FBS (10 %) P/S (1x)
SY5Y growth medium	DMEM/F12 FBS (10 %) NEAA (1x) P/S (1x)

F12-N2 medium (for neuronal differentiation)	DMEM/F12 N-2 supplement (1x) NEAA (1x) BDNF (10 ng/ml) NT-3 (10 ng/ml) Laminin (0.2 µg/ml) Doxycycline (2 µg/ml)
NB-B27 medium (for neuronal differentiation)	Neurobasal medium B-27 supplement (1x) GlutaMax™ (1x) BDNF (10 ng/ml) NT-3 (10 ng/ml) Ara-C (2 µM) Doxycycline (2 µg/ml)
Digestion solution (for preparation of mouse primary glia)	HBSS Papain (850 U/ml) EDTA (0.5 mM)
Freezing medium (2x, for HEK cells, human fibroblasts mouse primary glia and SY5Y cells)	Respective growth medium (40% v/v) FBS (40 %, v/v) DMSO (20 %, v/v)
SILAC labeling base medium	DMEM for SILAC FBS (10 %) GlutaMax™ (1x) NEAA (1x) Sodium Pyruvate (1 mM)

3.1.8.4 Buffers and solutions for immunocytochemistry methods

Fixative solution	PBS Paraformaldehyde (4 % w/v)
Blocking/Permeabilization solution	PBS Normal goat serum (5 %) Triton X-100 (0.1 %)

3.2 Microbiology methods

3.2.1 Transformation of bacteria with plasmid DNA

For propagation of plasmid DNA, plasmids were transformed into the chemocompetent *Escherichia (E.) coli* strain XL1 Blue (Stratagene) according to manufacturer's instructions. In short, 100 µl of the bacteria

suspension were mixed with 1.7 µl β-mercaptoethanol and incubated for 10 min at 4 °C. Plasmid DNA (10 ng) was added to the mix and incubated for 30 min at 4 °C, then 45 seconds at 42 °C, and again 2 min at 4 °C. Pre-warmed SOC medium (1 ml) was added and cells were incubated 1 h at 37 °C while shaking at 300 rpm. After incubation, 150 µl of the cell suspension were plated on a LB-Agar plate containing 100 µg/ml ampicillin.

3.2.2 Cryopreservation of bacteria

Transformed *E. coli* were incubated over night in LB medium, containing 100 µg/ml ampicillin. For cryopreservation, cultured bacteria were mixed by 1:1 with glycerol, mixed by pipetting and frozen at -80 °C.

3.2.3 Plasmid DNA isolation from bacteria

Plasmid DNA from *E. coli* was isolated using the Nucleobond Xtra Plasmid Midiprep Kit (Macherey Nagel) according to manufacturer's instructions.

3.3 Molecular biology methods

3.3.1 Isolation of genomic DNA from cells

Genomic DNA was extracted from cell pellets using the DNeasy Blood and Tissue Kit (Qiagen) according to manufacturer's instructions. DNA concentrations were determined using the NanoDrop™ ND-1000 spectrophotometer.

3.3.2 PCR amplification of DNA fragments

AmpliTaq Gold™ DNA polymerase (Thermo Fisher) was used to amplify DNA fragments from genomic regions by polymerase chain reaction (PCR).
For reasons of lower error rate, Phusion High-Fidelity DNA Polymerase (Thermo Fisher) was used for PCR amplification for cloning of constructs. Primer sequences and melting temperatures are specified in Section 3.1.3.

Table 3-9: AmpliTaq Gold™ PCR 10 µl reaction mix.

AmpliTaq Gold™ DNA polymerase	5 µl
GC enhancer	1.2 µl
H_2O	2.7 µl
Forward primer (10 µM)	0.3 µl
Reverse primer (10 µM)	0.3 µl
Genomic DNA (2 ng/µl)	0.5 µl

Table 3-10: AmpliTaq Gold™ PCR program.

Step	Temperature	Time	Repeat cycle
Initial denaturation	95 °C	10 min	-
Denaturation	95 °C	30 sec	35x
Primer annealing	50 - 72 °C	30 sec	
Extension	72 °C	30 sec/kb	
Final extension	72 °C	7 min	-
Hold	4 °C	∞	-

Table 3-11: Phusion High-Fidelity PCR 25 µl reaction mix.

Phusion High-Fidelity Polymerase	0.25 µl
Phusion High-Fidelity Buffer (5x)	5 µl
forward primer (10 µM)	1.25 µl
reverse primer (10 µM)	1.25 µl
dNTPs (10mM)	0.5 µl
DMSO	1 µl
template DNA	250 ng
H_2O	ad 25 µl

Table 3-12: Phusion High-Fidelity PCR program.

Step	Temperature	Time	Repeat cycle
Initial denaturation	98 °C	3 min	-
Denaturation	98 °C	10 sec	35x
Primer annealing	50 - 72 °C	10 sec	
Extension	72 °C	30 sec/kb	
Final extension	72 °C	10 min	-
Hold	4 °C	∞	-

3.3.3 Agarose gel electrophoresis of DNA fragments

Digested plasmids and PCR products were separated on 0.8 - 2 % agarose gels containing 0.5 µg/ml ethidium bromide in TAE buffer for 30-60 min at 80 V. UV light was used to visualize the DNA. To isolate DNA fragments from agarose gels, bands where cut under UV light and the DNA purified using the QIAquick Gel Extraction Kit (Qiagen) according to manufacturer's instructions.

3.3.4 DNA sequencing

PCR products were purified using the ExoSAP-IT™ PCR Product Cleanup reagent (Thermo Fisher) which enzymatically digests primers and dNTPs. Ten µl of PCR product were mixed with 4 µl ExoSAP-IT™ PCR Product Cleanup reagent and incubated for 15 min at 37 °C for digestion followed by 15 min at 80 °C for enzyme deactivation. Sanger sequencing was performed by LGC Genomics GmbH. Sequences were analysed using the DNAStar SeqMan Software Version 13.0.0.

3.3.5 SNP genotyping

SNP genotyping was performed using pre-designed TaqMan™-based SNP genotyping assays (Thermo Fisher). These assays contain two allele-specific probes labeled either with FAM™ or VIC™ dye that specifically recognize the minor or the major allele, respectively. Genomic DNA was diluted to a concentration of 1 ng/µl and 5 µl of the diluted DNA solution were pipetted into a 384-well-plate. A water sample was included as negative control. Covered with a dry paper tissue, wells were dried over night before adding the SNP genotyping probe-mastermix. PCR amplification and fluorescent measurement of the wells was performed using the QuantStudio 6 Flex Real-Time PCR-System (Thermo Fisher). SNP genotypes of all samples were assigned by the software based on FAM™/VIC™ fluorescence ratios.

Table 3-13: SNP genotyping reaction mix per well.

TaqMan™ SNP Genotyping Assay	0.0625 µl
TaqMan™ Genotyping Master Mix	2.5 µl
H_2O	2.44 µl

Table 3-14: SNP genotyping PCR program.

Step	Temperature	Time	Repeat cycle
Initial denaturation	95 °C	10 min	-
Denaturation	92 °C	15 sec	40x
Annealing/Extension	60 °C	1 min	
Hold	16 °C	∞	-

3.3.6 Transcription activator-like effector nuclease (TALEN) cloning

Transcription activator-like effector nucleases (TALENs) are engineered endo-nucleases designed to target a genomic locus based on their modular DNA-binding domain structure. Here, TALEN constructs were designed to target the *SORT1* start codon using the TALEN Targeter (Cornell University, https://tale-nt.cac.cornell.edu/node/add/talen) (see Table 3-15).

Table 3-15: TALEN sequences to target the *SORT1* start codon.

Vector ID	TALEN sequence (LEFT TALEN - spacer - RIGHT TALEN)	Segment I	Segment II	Segment III	Segment IV
SORT1 ATG left -GFP	TCGGCGGCATTCGGCG - gcgatggagcggc - CCTGGGGAGCTGCGGA	CGGC	GGCA	TTCG	GCG
SORT1 ATG right -RFP		CCGC	AGCT	CCCC	AGG

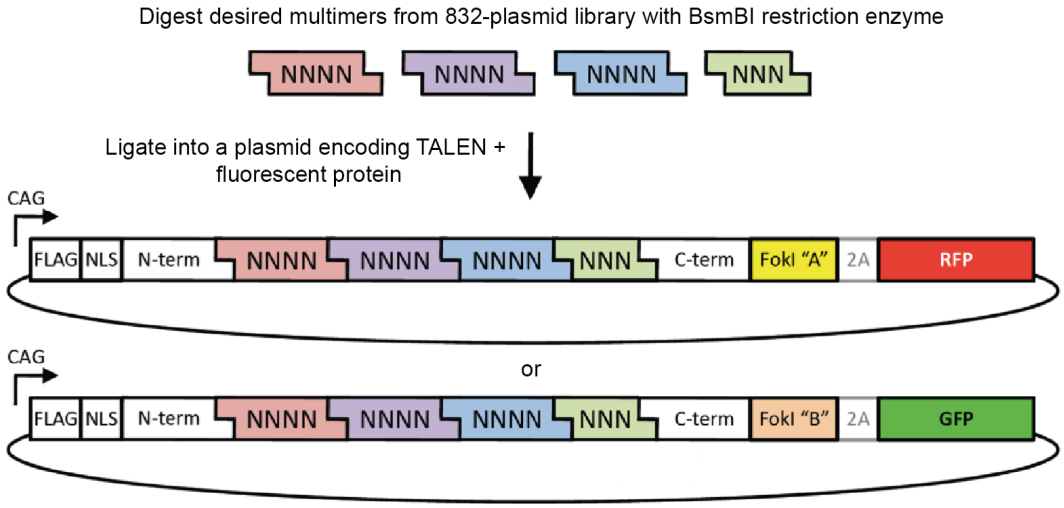

Figure 3-1: Schematic representation of the modular cloning strategy for TALENs constructs using a plasmid library. Designed multimers encoding the DNA-binding domain were digested from a plasmid library representing all variations of mulitmers (NNN/NNNN). Cloning into the TALEN target vector was performed in a single ligation step. The TALEN targeting vector contains the BsmBI restriction site, the FokI endonuclease domain, and either green or red fluorescent protein (GFP/RFP) under the control of a CAG promoter. Scheme adapted from Ding *et al.*, 2013.

The DNA binding encoding segments were cloned into one vector as described in Ding *et al.*, 2013). In short, the four desired segments were digested from an 832-plasmid library (Addgene; provided by the MDC stem cell core facility) using the BsmBI restriction enzyme and ligated into the TALENs vector carrying a FokI endonuclease domain, and either GFP or RFP (see Figure 3-1).

3.3.7 CRISPR and Homology Recombination (HR) vector cloning

SgRNAs were designed to target close to the *SORT1* SNP using the Optimized CRISPR design tool (Massachusetts Institute of Technology, http://crispr.mit.edu/). SgRNA target sequence and antisense strands were purchased as single-stranded (ss) DNA oligonucleotides from Eurofins Genomics with sticky ends complementary to the BbsI-digested CRISPR Cas9 sgRNA vector (Addgene) (see Table 3-16). After ligation of the two ssDNA oligonucleotides by incubation for 5 min at 95 °C followed by gradual annealing at -0.1 C/s, the DNA fragment was ligated into the CRISPR Cas9 sgRNA vector. Correct insertion was verified by sequencing with the hU6-forward primer (see Table 3-2).

Table 3-16: Single-stranded oligonucleotides encoding for *SORT1* SNP sgRNA.

DNA oligonucleotide	Sequence (5'-3')
Sense Oligo	CACC-G-AGCGCAACTTAACACATGAC
Antisense Oligo	AAAC-GTCATGTGTTAAGTTGCGCT-C

For cloning of the *SORT1* SNP homology vector, a TTAA sequence was identified close to the SNP of interest that served as a recognition site for excision of the selection cassette by the piggybag™ transposase (see Section 3.4.3). Left and right homology arms (500 bp upstream and downstream of the TTAA with attached restriction sites) were ordered as Strings™ DNA Fragments (Thermo Fisher) (see Table 3-17). The fragments were digested and subsequently ligated into the pENTR-PGKpuroΔtk homology recombination vector (Sanger Institute).

Table 3-17: Homology arms for introducing the *SORT1* SNP. Restriction sites for cloning homology arms into the Homology Recombination (HR vector) are underlined (NotI and BsiWI for *SORT1* left and NsiI and AscI for *SORT1* right, respectively). The TTAA recognition site for piggybag™ transposase excision is highlighted in green. The introduced mutation (minor variant) is highlighted in red.

Homology arm	Sequence (5'-3')
SORT1 left	TGGGTC**GCGGCCGC**CCTTTCCCTTCCCAAAGAGGATAG GACCTCCCAGGATGCTTCCCAGCCTCTCCTCAGTTTCC CATCTGCTGTGCCTCTGGGAGGAGAGGGACTCCTGGG GGGCCTGCCCCTCATACGCCATCACCAAAAGGAAAGGA CAAAGCCACACGCAGCCAGGGCTTCACACCCTTCAGGC TGCACCCGGGCAGGCCTCAGAACGGTGAGGGGCCAGG GCAAAGGGTGTGCCTCGTCCTGCCCGCACTGCCTCTCC CAGGAACTGGAAAAGCCCTGTCCGGTGAGGGGGCAGA AGGACTCAGCGCCCCTGGACCCCCAAATGCTGCATGAA CACATTTTCAGGGGAGCCTGTGCCCCCAGGCGGGGGT CGGGCAGCCCCAGCCCCTCTCCTTTTCCTGGACTCTGG CCGTGCGCGGCAGCCCAGGTGTTTGCTCAGTTGCTGA CCCAAAAGTGCTTCATTTTTCCTGCCCGCCCCGCGCCC CGGGCAGGCCAGTCATGTG**TTAA**CCCTAGAAAGATAAT CATATTGTGA**CGTACG**TT
SORT1 right	TCAAGA**ATGCAT**GCGTCAATTTTACGCAGACTATCTTTC TAGGG**TTAA**GTTGCGCTTCTTTGCTGTGATGTGGGTGG GGGAGGAAGAGTAAACACAGTGCTGGCTCGGCTGCCC TGAGGTTGCTCAATCAAGCACAGGTTTCAAGTCTGGGTT CTGGTGTCCACTCACCCACCCCACCCCCCAAAATCAGA CAAATGCTACTTTGTCTAACCTGCTGTGGCCTCTGAGAC ATGTTCTATTTTTAACCCCTTCTTGGAATTGGCTCTCTTC TTCAAAGGACCAGGTCCTGTTCCTCTTTCTCCCCGACTC CACCCCAGCTCCCTGTGAAGAGAGAGTTAATATATTTGT TTTATTTATTTGCTTTTTGCGTTGGGATGGGTTCGTGTC CAGTCCCGGGGGTCTGATATGGCCATCACAGGCTGGG TGTTCCCAGCAGCCCTGGCTTGGGGGCTTGACGCCCTT CCCCTTGCCCCAGGCCATCATCTCCCCACCTCTCCTCC CCTCTCCTCAGTTTTGCCGACTGCTTTTCATCTGAGTCA CCATTTACTCC**GGCGCGCC**TGCAT

3.3.8 Site-directed mutagenesis for introduction of *SORL1* mutations

SORL1 mutations were introduced into a *SORL1* expression vector (pcDNA3.1zeo+) using site-directed mutagenesis (see Figure 3-2). Primers A-D for PCR amplification are specified in Section 3.1.3. The N1358S mutation was also introduced into *SORL1* expression vectors encoding for SORLA fused to GFP (for FLIM/FRET experiment, see Section 3.5.4) or for the His-tagged SORLA ectodomain (for purification of SORLA from conditioned medium, see Section 3.3.16) using the same cloning strategy. All *SORL1* expression vectors were kindly provided by Dr. Vanessa Schmidt (Lab Willnow, MDC Berlin).

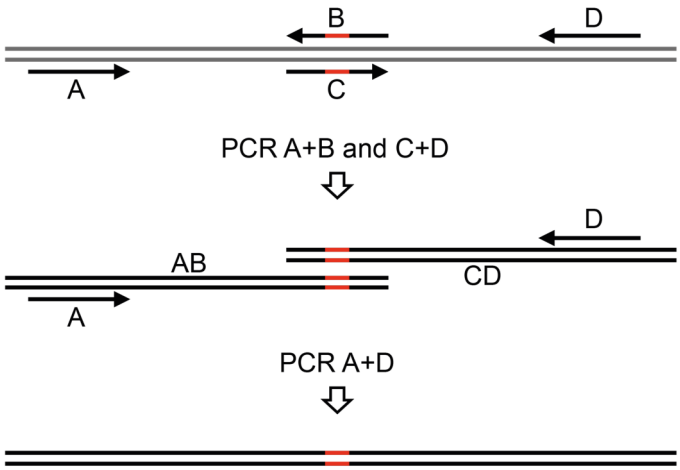

Figure 3-2: Site-directed mutagenesis for introduction of *SORL1* mutations. The *SORL1* expression vector was amplified using primers A and B and primers C and D, with primers B and C carrying the mutation to be introduced (red). The two PCR products AB and CD where then amplified in one reaction using primers A and D and the mutated PCR product was introduced into the vector by restriction enzyme digestion and ligation.

3.3.9 RNA isolation from cells

Total RNA was extracted from cells using the RNeasy Mini Kit (Qiagen) according to manufacturer's instructions. DNase treatment of the sample was performed directly on the purification column by addition of 80 µl RNase-free DNase I (Qiagen) prepared according to manufacturer's instructions and incubated for 15 min at room temperature after the first washing step. RNA concentrations were determined using the NanoDrop™ ND-1000 spectrophotometer.

3.3.10 Reverse transcription of RNA

Reverse transcription of the isolated RNA into complementary DNA (cDNA) was performed using the High Capacity RNA to cDNA™ Kit (Thermo Fisher) according to manufacturer's instructions. A total RNA amount of 50 ng to 1 µg was used for cDNA synthesis.

3.3.11 RNA quantification using quantitative real-time PCR

Quantitative real-time PCR (qRT-PCR) was performed using either predesigned TaqMan™ probes (Thermo Fisher) or DNA oligonucleotides flanking the target region and SYBR™ green dye (Thermo Fisher). TaqMan™ probes and DNA oligonucleotides are specified in Section 3.1.3.

qRT-PCR using SYBR™ green dye was performed by Silvia Ruzittu (Lab Spagnoli, MDC Berlin).

Table 3-18: TaqMan™ reaction mix per well.

TaqMan™ Gene Expression Assay	0.5 µl
TaqMan™ Gene Expression Master Mix	5 µl
cDNA (1:10 diluted)	4 µl
H_2O	0.5 µl

Table 3-19: TaqMan™ qRT-PCR program.

Step	Temperature	Time	Repeat cycle
Digestion of dUTP-containing DNA	50 °C	2 min	-
Denaturation, polymerase activation	95 °C	10 min	-
Denaturation	95 °C	15 sec	40
Primer annealing, extension	60 °C	1 min	

Table 3-20: SYBR™ green reaction mix per well.

SYBR™ green PCR Master Mix	5 µl
Forward primer (10 µM)	0.2 µl
Reverse primer (10 µM)	0.2 µl
cDNA (1:10 diluted)	3 µl
H_2O	1.6 µl

Table 3-21: SYBR™ green qRT-PCR program.

Step	Temperature	Time	Repeat cycle
Denaturation, polymerase activation	95 °C	10 min	-
Denaturation	95 °C	15 sec	40
Primer annealing, extension	60 °C	1 min	

Samples were measured in triplicates using the 7900 HT Fast Real time PCR System (Thermo Fisher). The data were analyzed using the comparative cycle threshold (Ct) method, also known as 2^{-ddCt} method (Schmittgen and Livak, 2008). The Ct value of each sample represents the number of cycles needed for the emitted fluorescence signal to cross a defined threshold. The abundance of the target mRNA is therefore inversely correlated to the Ct value. The Ct value for a house keeping mRNA was substracted from the Ct value for the mRNA of interest to ensure equal amount of cDNA in each well (dCt). For comparison of multiple samples, the dCt value of the internal control was substracted from the dCt values of the other samples (ddCt) and data were presented as $\log_2$ change in expression. Relative fold change between the samples was calculated as 2^{-ddCt}.

3.3.12 Protein preparation from cells

Confluent 6-wells were scraped in 1 ml ice-cold 1x PBS and cells were pelleted by centrifugation at 300 x g for 5 min at 4 °C. Cell pellets were lysed in 80 µl protein lysis buffer containing proteinase inhibitors for 1 h at 4 °C. Cell debris was removed by centrifugation for 10 min at 20,000 x g at 4 °C and the supernatant was transferred to a new tube. Protein lysates were either analyzed by Western Blot immediately or stored at -80 °C until further use.

3.3.13 Determining protein concentration in cell lysates

Protein concentrations in cell lysates were determined using the Pierce™ BCA Protein Assay Kit (Thermo Fisher) according to manufacturer's instructions. In short, 2 µl of the cell lysate were mixed with 23 µl H_2O and 200 µl of the kit's mixed reagents (reagent A : reagent B, 50:1) in a 96-well-plate. BSA solutions with a total protein content ranging from 0.78 µg to 50 µg were used as a standard curve and also mixed with reagent A and B. A blank sample (protein lysis buffer) was included to subtract the background absorbance. After incubation at 37 °C for 30 min, absorbance was measured in a plate reader set to 562 nm.

3.3.14 SDS polyacrylamide gel electrophoresis and Western Blot

Separation of proteins was performed by SDS polyacrylamide gel electrophoresis (PAGE) on 8 % SDS polyacrylamide gels prepared in a multiple gel caster (SE215, Hoefer Inc.). Ammonium persulfate (APS) and N,N,N´,N´-tetramethylendiamine (TEMED) were added shortly before usage as these components start polymerization of the gel matrix. Isopropanol was added on top of the separation gel layer to ensure a smooth interface between the gels, and removed before adding the stacking gel. SDS polyacrylamide gels were stored wrapped in wet tissues for up to 2 weeks at 4 °C. Cell lysates (50-100 µg of total protein) were mixed with 1x Laemmli buffer containing 10 % β-Mercaptoethanol and boiled for 5 min at 95 °C. Precision Plus Protein™ Dual Color Standard (Bio-Rad) and denatured samples were loaded on the SDS polyacrylamide gel and proteins were separated by electrophoresis for 1.5-2 h at 80 V in SDS-PAGE Running

buffer. Proteins were transferred from the SDS polyacrylamide gels onto 0.2 µm nitrocellulose membranes in Transfer Buffer for 2 h at 350 mA using the Mini Protean 3 Western transblot cell setup (BioRad). The membrane was then blocked by shaking for 1 h at room temperature in blocking solution to prevent non-specific antibody binding. The primary antibody was diluted in blocking solution, added to the membrane, and incubated while shaking o/n at 4 °C. After washing the membrane three times for 10 min with TBS-T, it was incubated with the secondary antibody, also diluted in blocking solution, for 1 h at RT. The membrane was washed again three times for 10 min with TBS-T and then incubated with protein detection reagent (SuperSignal West Femto Maximum Sensitivity Substrate, Thermo Scientific). Protein bands were imaged using the Raytest 3200 Stella system.

Table 3-22: Separation gel (8 %) for SDS-PAGE.

Reagent	Volume
Rotiphorese gel 30 % (37.5:1)	26,67 ml
Tris-HCl, pH: 8.8 (1.5 M)	25 ml
SDS (20 %)	500 µl
Ammonium persulfate (APS, 10%)	1 ml
N,N,N´,N´-tetramethylendiamine (TEMED)	100 µl
H_2O	46,33 ml

Table 3-23: Stacking gel for SDS-PAGE.

Reagent	Volume
Rotiphorese gel 30 % (37.5:1)	8.38 ml
Tris-HCl, pH: 6.8 (1 M)	6.25 ml
SDS (20 %)	250 µl
Ammonium persulfate (APS, 10%)	500 µl
N,N,N´,N´-tetramethylendiamine (TEMED)	50 µl
H_2O	33.75 ml

3.3.15 SORLA and APP co-immunoprecipitation

CHO cells stably overexpressing APP were transiently transfected with constructs encoding wildtype or mutant SORLA as described in Section 3.4.8. Two days after transfection, cells were lysed in 100 µl protein lysis buffer, incubated for 1 h at 4 °C and cleared from cell debris by centrifugation for 10 min at 20,000 x g at 4 °C. Two µl of SORLA antibody (goat, homemade) was added to 600 µg protein lysate and incubated for 30 min at

4°C under continuous rotation. To purify the antibody/protein complexes from the lysates, 50 µl immobilized protein G agarose beads (Roche) were added and incubated o/n at 4 °C under continuous rotation. Then, beads were washed three times with cold PBS. Finally, proteins were eluted by adding 30 µl 4x Laemmli buffer to the washed beads and boiling them for 5 min at 95 °C. The presence of SORLA and APP in the elute was analyzed by Western Blot (see Section 3.3.14).

3.3.16 Surface Plasmon Resonance

Surface Plasmon Resonance (SPR) analysis was carried out by Dr. Olav Michael Andersen (Aarhus University, Denmark) using a BIAcore2000 system as described in Andersen *et al.*, 2005. In short, the ectodomains of $SORLA^{WT}$ and $SORLA^{N1358S}$ (hexa-His-tagged fragments of SORLA including residues 728-1526) were transfected into HEK293-EBNA cells and purified from the conditioned medium purified using Ni^{2+} affinity chromatography. Purified ectodomains of SORLA were immobilized on a CM5 Biacore chip at a density of 56 fmol/mm^2. The sensor chip was incubated with a concentration series (10, 20, 50, 100 and 200 nM) of the ectodomain of APP (APP_{695}) in running buffer (10 mM Hepes, pH: 7.4, 150 mM NaCl, 5 mM $CaCl_2$, 0.005% Tween 20). The difference in Biacore response signals between SORLA-coated and non-coated control was recorded as relative response units (RU).

3.4 Cell culture methods

3.4.1 Human induced pluripotent stem cell (iPSC) culture

iPSC lines and human primary fibroblasts were tested for the absence of human pathogenic viruses (HIV, HBV, HCV) by the Leibniz-Institute DSMZ, German Collection of Microorganisms and Cell Cultures, Braunschweig, Germany.

Table 3-24: Human iPSC line information. Cell line ID (as used in this study), provider of iPSC (i) or fibroblast (f) cell line and provider ID as well as entry at the Human Pluripotent Stem Cell Registry (hPSC^{reg}, https://hpscreg.eu/) for all iPSC lines used in this study.

Cell line ID	Provider (iPSC(i)/fibroblast(f), Provider ID)	hPSC^{reg} ID
parental line for *SORT1* KO	MDC stem cell core facility (i: LMNA Pt5 mRNA Clone 1, SCVI 111)	BIHi005-A
donor_minor_1	MDC stem cell core facility (f: MDCH0003)	BIHi013-A
donor_minor_2	Wellcome Trust Sanger Institute (i: HPSI1113i-qorq_2)	WTSIi081-A
donor_major_1	Wellcome Trust Sanger Institute (i: HPSI1113i-podx_1)	WTSIi005-A
donor_major_2	Wellcome Trust Sanger Institute (i: HPSI1113i-wetu_2)	WTSIi227-A
isogenic_parental_major	MDC stem cell core facility (i: LMNA Pt6 Sendai Clone 1)	BIHi049-A

Human iPSC cultures were maintained on plates coated with Matrigel™ (BD Biosciences) in E8 medium at 37 °C in humidified atmosphere containing 5% CO_2. The medium was changed every day. For regular passaging (twice a week), cells at 80 % confluency were incubated with 1 ml dissociation solution (0.5 M EDTA in PBS) per 6-well for 5-7 min at room temperature. Afterwards, the dissociation solution was removed, and cell clumps carefully resuspended in E8 medium and transferred onto Matrigel^{TM}-coated plates at a ratio of 1:4-1:8. For single cell seeding and counting, cells were dissociated by incubation in 1 ml StemPro^{TM} Accutase^{TM} (Thermo Fisher) for 5 min at 37 °C. The single cell suspension was diluted with 5 ml E8 medium and centrifuged at 300 x g for 3 min. The cell pellet was resuspended in E8 supplemented with 10 µM ROCK-1 inhibitor Y-27632 (LC Laboratories) to reduce apoptosis of single iPSCs after dissociation. Cells were counted using the Countess II Automated Cell Counter (Thermo Fisher) and seeded on Matrigel^{TM}-coated plates. iPSCs were cryopreserved by dissociating 80 %

confluent cell wells using StemPro™ Accutase™ as described above. Cell pellets were resuspended in 1 ml Bambanker™ freezing medium (Lymphotec Inc.), transferred to cryovials, and frozen at -80°C in Nalgene™ cryo freezing containers. Cells were thawed at 37 °C, diluted with 10 ml E8 medium and centrifuged at 300 x g for 3 min. The cell pellets were resuspended in E8 supplemented with 10 µM ROCK-1 inhibitor and cells plated on Matrigel™-coated plates. Plasmid DNA transfections were performed using Lipofectamine™ 3000 (Thermo Fisher) according to manufacturer's instructions.

3.4.2 Reprogramming of human fibroblasts to human iPSCs

Human primary fibroblasts were reprogrammed into iPSCs using the CytoTune™-iPS 2.0 Sendai Reprogramming Kit (Thermo Fisher) according to manufacturer's instructions. The non-transmissible Sendai virus vector encoded for the four pluripotency factors (*SOX2*, *KLF-4*, *OCT4*, *c-MYC*), known to efficiently reprogram somatic cells into iPSCs (Takahashi and Yamanaka, 2006). The reprogrammed iPSCs were characterized by immunofluorescence stainings for the pluripotency markers OCT4, SOX2, NANOG and SSEA4. Genomic DNA was submitted to the MDC stem cell core facility (in cooperation with the Hübner Lab) for SNP karyotyping using the Infinium OmniExpressExome-8 Kit and the iScan system from Illumina. CNV and SNP visualization were performed using KaryoStudio v1.4 (Illumina).

3.4.3 Generation of a *SORT1* knock-out iPSC line using TALENs

Ablation of *SORT1* expression in iPSCs by deleting the *SORT1* start codon ATG was performed as described in (Ding *et al.*, 2013). In short, TALEN pairs, designed and cloned as described in Section 0, were transfected into iPSCs using Lipofectamine™ 3000 (Thermo Fisher) according to manufacturer's instructions. Cells were subjected to fluorescence activated cell sorting (FACS) 48 h post-transfection based on GFP and RFP expression. The double-positive sorted cells were replated at low density and left to recover and expand until forming distinct single cell colonies. Colonies were expanded and genomic DNA was isolated to amplify the ATG region of

SORT1 (see Section 3.1.3 for PCR primers). PCR products were analyzed on 2 % agarose gels to identify insertions or deletions at the ATG region. PCR products were sequenced to verify homozygous deletion of the ATG and the ATG knock-out clone was expanded. Ablation of *SORT1* expression was confirmed by Western Blot analysis.

3.4.4 Generating genome-edited isogenic iPSC lines using CRISPR

The seamless exchange of a SNP in iPSCs using CRISPR and the piggybac™ transposon system was performed as described in (Yusa, 2013) (see also Figure 4-8). In short, sgRNA-Cas9 construct and homology recombination (HR) vector, designed and cloned as described in Section 3.3.7, were transfected into iPSCs using Lipofectamine™ 3000 (Thermo Fisher) according to manufacturer's instructions. Cells were selected for integration of the HR vector's selection cassette at the target site by puromycin treatment (1 µg/ml) for approximately two weeks, until distinct puromycin-resistant cell colonies had formed. Colonies were expanded and genomic DNA was isolated. To test for integration of the HR cassette, the genomic DNA was amplified using a set of three primers (specified in Table 3-2), two of them binding in the genomic region, not included in the homology arms of the vector, and one of them binding in the vector's selection cassette (see scheme in

). PCR products were analyzed on 1 % agarose gels to identify wildtype (WT, 0.6 kb) and homology cassette integrated (HR, 1.1 kb) alleles. Cell clones with integration of the homology cassette in both alleles (absence of WT band) were sequenced to ensure integrity of left and right homology arms and correct introduction of the desired mutation. Correct cell clones were expanded under continuous puromycin selection and transfected with excision-only piggybac™ (PBX) transposase using Lipofectamine™ 3000 (Thermo Fisher) according to manufacturer's instructions. PBX transposase recognizes transposon-specific inverted terminal repeat sequences (ITRs) located on both sites of the selection cassettes and excises the complete selection cassettes by fusing the TTAA sequences on both homology arms. Negative selection for thymidine kinase (TK) by ganciclocir (GCV) treatment allows for enrichment of cells that have excised the selection cassette from

both alleles. Ganciclovir is a guanosine analogue that, upon phosphorylation by TK, causes premature DNA chain termination and therefore apoptosis in TK expressing cells (Fillat *et al.*, 2003). Cells were treated with 0.3 µM GCV for three days and single cell colonies were expanded. Genomic DNA was isolated and amplified with the same set of three primers for WT/HR allele amplification. Cell clones that had excised the homology cassette in both alleles (only the WT band present) were sequenced to verify the exchange of the SNP and the integrity of the target site.

3.4.5 Differentiation of human iPSCs into cortical neurons

Human iPSCs were differentiated into cortical neurons using the rapid neuronal differentiation protocol described in (Zhang *et al.*, 2013) (see also Figure 4-1). In brief, 0.6-1 x 10^5 iPSCs were plated on Matrigel™-coated 24-wells cells (day -2). The next day (day -1), cells were transduced with lentiviruses encoding for the transcription factor neurogenin-2 (NGN2) and for the enhanced green fluorescent protein (EGFP), either as fused (NGN2-EGFP) or as separate (NGN2 and EGFP) constructs, as well for the reverse tetracycline-controlled transactivator (rtTA) that activates transcription of NGN2 and EGFP upon additon of doxycycline. One µl of each virus preparation per well (see Section 3.4.7 for lentivirus production) and 7 µg/ml polybrene were diluted in E8 medium and added to the cells. One day after transduction, medium was changed to F12-N2 medium which contained doxycycline to induce NGN2 expression (day 0). On the next day (day 1), the medium was changed to F12-N2 medium supplemented with 1 µg/ml puromycin to enrich for transduced cells. On day 2, glia cell cultures prepared from P1 mouse cortices (see Section 3.4.8) were added in NB-B27 medium to the differentiating iPSCs to support neuronal growth. Half of the medium was replaced with fresh NB-B27 medium every 2-3 days. Mature neurons were usually harvested at day 14 or day 21.

3.4.6 Differentiation of human iPSCs into hepatocytes

Human iPSCs were differentiated into hepatocytes using the Cellartis Hepatocyte Differentiation Kit (Clontech) according to manufacturer's instructions. All media and coating solutions were included in the kit. In short,

0.6-1 x 10^6 iPSCs were seeded in definitive endoderm differentiation day 0 medium in 6-wells coated with definitive endoderm coating. Medium was changed at day 1, 2, 3, 4, and 6 with the respective medium. On day 7, definitive endoderm cells were either seeded for further hepatocyte differentiation or cryopreserved in Bambanker™ freezing medium for later use (see Section 3.4.1). Hepatocyte differentiation was performed in 24-wells coated with hepatocyte coating using 2-6 x 10^5 definitve endoderm cells per well seeded in hepatocyte seeding medium. Manufacturer's instructions were followed until day 30 when differentiated hepatocytes were harvested for analysis.

3.4.7 Lentiviral production in HEK-293TN cells

HEK-293TN cells used herein expressed the mutated SV40 large T antigen. Transfected plasmids carrying the SV40 origin of replication can therefore replicate in HEK-293TN cells and reach a high copy number, which greatly increases the amount of lentivirus produced by these cells. HEK-293TN cells were grown in DMEM growth medium at 37 °C, 5 % CO_2 and 95 % humidity. At 90 % confluency, cells were split at a 1:6 - 1:12 ratio using 0.05 % trypsin/EDTA. Plasmid DNA transfections were performed using Lipofectamine™ 2000 (Thermo Fisher) according to manufacturer's instructions. For production of lentiviruses, 1 x 10^7 HEK-293TN cells were seeded in OptiMEM with 5 % FBS in T75 flasks coated with 0.01 % poly-L-lysine for 1 h. The next day, the medium was changed to OptiMEM w/o FBS containing 25 µM chloroquine (to reduce plasmid degradation), before co-transfection of the three packaging plasmids and the viral construct of interest (see Table 3-25) was performed. Six hours after transfection or the next morning, the medium was replaced by 10 ml OptiMEM w/o FBS and cells incubated for an additional 24 h. After incubation, the medium was collected and stored at 4 °C, while the incubation of the transfected cells with 10 ml OptiMEM was repeated for the following two days. Once 30 ml of lentivirus-containing medium were collected, dead cells were removed from the medium by centrifugation at 500 x g for 15 min at 4 °C. The cleared medium was transferred to a new 50 ml tube and mixed with 10 ml of cold Lenti-X Concentrator (Clontech) by gentle inversion. The Lenti-X

Concentrator contained polyethylene glycol to precipitate the produced lentivirus and to enable virus purification without ultracentrifugation. Lentivirus-containing supernatants mixed with Lenti-X Concentrator were incubated o/n at 4 °C and then centrifuged at 1500 x g for 45 min at 4 ºC. The supernatant was removed carefully removed and the white pellet was resuspended in 300 µl cold PBS, aliquoted and snap frozen in liquid nitrogen. Aliquoted virus preparations were stored at -80 °C.

Table 3-25: Lipofectamine™ 2000 transfection for lentivirus production.

DNA mix		**Lipofectamine™ 2000 mix**	
OptiMEM	1000 µl	OptiMEM	1000 µl
VSV-G	6 µg	Lipofectamine™ 2000	50 µl
pRRE	8 µg		
pRSV-REV	4 µg		
Construct of interest	12 µg		

3.4.8 Preparation and culture of primary mouse glia

Primary mouse glial cells were prepared from the forebrain of newborn wildtype mice as described in (Franke *et al.*, 1998). In short, two P1 mouse forebrains were dissected in HBSS and digested by incubation in 5 ml digestion solution containing papain for 30 min at 37 °C. Cells were dissociated by harsh pipetting to avoid survival of neurons, diluted with 5 ml DMEM growth medium, and centrifuged at 300 x g for 10 min. The cell pellet was resuspended in 15 ml DMEM growth medium and plated into a T75 flask. Primary mouse glia reached confluency one week after plating and were passaged using 0.05 % trypsin/EDTA. To support neuronal growth during neuronal differentiation of iPSCs, mouse glia were used from passage 1-3. One T75 flask of primary mouse glia sufficed for three 24-well-plates of differentiating iPSCs. Mouse glia were dissociated using 0.05 trypsin/EDTA, washed with DMEM growth medium, and centrifuged at 300 x g for 5 min. The cell pellet was resuspended in NB-B27 medium (for neuronal differentiation) and directly seeded on top of the differentiating iPSCs.

3.4.9 SH-SY5Y cell culture

SH-SY5Y cells were maintained in SY5Y growth medium at 37 °C, 5 % CO_2 and 95 % humidity. At 90 % confluency, cells were split at a 1:2 - 1:6 ratio using 0.05 % trypsin/EDTA. Plasmid DNA transfections were performed using Lipofectamine™ 2000 (Thermo Fisher) according to manufacturer's instructions. Stable cell lines were generated by transfecting either APP or SORLA encoding expression plasmids and by selecting transfected cells with Hygromycin B (150 µg/ml) or Zeocin™ (50 µg/ml), respectively, for at least two weeks until all non-transfected cells had died. Single cell colonies were picked, expanded, and tested for APP/SORLA expression by immunofluorescence staining and Western Blot. Stable cell lines were cultured in the presence of the respective antibiotic.

3.4.10 CHO cell culture

CHO cells were grown in DMEM growth medium at 37 °C, 5 % CO_2 and 95 % humidity. At 90 % confluency, cells were split at a 1:6 - 1:12 ratio using 0.05 % trypsin/EDTA. Plasmid DNA transfections were performed using Lipofectamine™ 2000 (Thermo Fisher) according to manufacturer's instructions.

3.4.11 Preparation of exosomes

Exosomal preparation was perfomed as described in (Théry *et al.*, 2006). In detail, stable SH-SY5Y cells were grown in two T175 cell culture flasks per exosome preparation and conditioning was started at 80 % confluency. Normal SY5Y growth medium was used for conditioning (35 ml per flask). Prior to use, the FBS solution was ultracentrifuged at 100,000 x g for 90 min to clear it from FBS-specific exosomes. After 5 days of conditioning, the medium was collected and the cells scraped in cold PBS for protein purification (see Section 0). All centrifugation steps were performed at 4 °C and samples were kept on ice throughout the procedure. First, medium was cleared from dead cells and cell debris by a series of centrifugation steps at 300 x g for 10 min, at 2000 x g for 20 min, and at 10,000 x g for 30 min. A non-conditioned medium sample was included as a negative control. The cleared supernatant was subjected to ultracentrifugation at 100,000 x g for 60

min. Ultracentrifugation was performed using the SW40 Ti Swinging-Bucket Rotor (Beckman) with 14 ml tubes. In each step, 13 ml of conditioned medium was ultracentrifuged, the supernatant carefully removed from the exosome pellet, and the tube refilled with 13 ml of conditioned medium until exosomes of the complete 70 ml medium were pelleted. The exosome pellet was resuspended in 13 ml cold PBS, incubated on ice for 1 h, and centrifuged at 100,000 x g for 60 min. Exosomes were lysed either in 4x Laemmli buffer for Western Blot or in protein lysis buffer for MFG-E8 ELISA.

3.4.12 DAPT experiment

DAPT is a γ-secretase inhibitor that stops cellular production of Aβ. SY5Y cells were seeded in triplicates and the experiment was started at 80 % confluency. Cells were washed once with SY5Y growth medium w/o FBS. DAPT was diluted in FBS-free SY5Y growth medium to a final concentration of 5 µM and added to the cells. After incubating at 37 °C for 0, 0.5, 1, 2, and 3 h, cells were washed once with PBS and scraped in cold PBS. Cells were lysed in protein lysis buffer containing protease inhibitors according to Section 0 and analyzed for Aβ levels using the Aβ V-PLEX Kit (Mesoscale) according to manufacturer's instructions.

3.4.13 SILAC-based interactome study

SH-SY5Y stable cell lines were labeled with either heavy or light isotope aminoacids for three weeks before performing the interactome experiment. For this purpose, cells were cultured in SILAC labeling base medium supplemented with normal L-arginine (Arg0) and L-lysine (Lys0) ("light"), or with the heavy isotope variants Arg10 and Lys8 ("heavy"). Heavy and light isotope aminoacids were purchased from Silantes or Sigma-Aldrich (see Section 3.1.1). Cell pellets were lysed as described in Section 0. SORLA antibody (goat, homemade) was coupled to Pierce™ NHS-Activated Magnetic Beads according to manufacturer's instructions and used for immunoprecipitation. After elution with 6 M guanidium-HCl for 10 min at 70 °C, the eluted proteins were precipitated using ethanol and digested with trypsin. Peptides were ionized using an electrospray ionization (ESI) source (Thermo Fisher) and analyzed on a Q-exactive plus Orbitrap instrument

(Thermo Fisher). Protein precipitation, trypsin digest and peptide quantification by mass spectrometry were performed by Katrina Meyer (Lab Selbach, MDC Berlin).

3.5 Immunocytochemistry, microscopy and image analysis

3.5.1 Immunocytochemistry

Cells were grown on coated glass coverslips (Matrigel™ for iPSCs, 0.1 % gelatine in PBS for SH-SY5Y cells) in 24-wells and fixed with fixative solution containing 4 % PFA for 10 min at room temperature. Cells were then washed three times for 5 min each with PBS and either stored submerged in PBS at 4 °C, or used immediately for immunofluorescence staining. Blocking of non-specific antibody binding and membrane permeabilization was performed by 10 min incubation at room temperature with Blocking/Permeabilization solution. Primary antibodies were diluted in PBS as specified in Table 3-8 and incubated at 4 °C o/n. The next day, the cells were washed three times for 5 min with PBS before incubation with secondary antibody solution. Fluorophore-conjugated secondary antibodies were diluted 1:2000 in PBS together with DAPI, which was diluted 1:10,000, and incubated for 1 h at room temperature. After washing three times for 5 min with PBS, cells were rinsed with H_2O before mounting cover slips on microscope slides using Fluorescence mounting medium (Dako).

3.5.2 Microscopy

Immunofluorescently stained cells were imaged using the Leica TCS SPE (true point-scanning, spectral system) confocal microscope at the MDC imaging core facility or the DeltaVision Elite Imaging system (GE Healthcare) for high magnification and high resolution images. Lower magnification overview images were acquired using the EVOS FL Cell Imaging System (Thermo Fisher). Image processing was performed using ImageJ software (National Institutes of Health).

3.5.3 Colocalization quantification

Immunofluorescence staining and confocal microscopy of SORLA, APP, and cell compartment markers were performed as described in Sections 3.5.1 and 3.5.2. Colocalization of pixels was analyzed using ImageJ software (National Institutes of Health). In detail, three confocal planes of 0.2 µm each were projected to a single plane and regions of interest were defined by marking single cell perimeters. The colocalization analysis function calculated the Manders' coefficient (tM) that is proportional to the fluorescence intensity of the colocalizing pixels in each channel with tM=0 representing no colocalization and tM=1 representing perfect colocalization (Manders *et al.*, 1993).

3.5.4 Fluorescence-lifetime imaging microscopy

Fluorescence-lifetime imaging microscopy (FLIM) of fluorescence resonance energy transfer (FRET) between two fluorophore-coupled proteins can be used to study protein-protein interaction in living cells (Chen *et al.*, 2003). FRET occurs when an excited donor fluorophore (here green fluorescent protein, GFP) is in close proximity (<10 nm) to an acceptor fluorophore (here red fluorescent protein, RFP) with an excitation spectrum similar to the donor's emission spectrum. The transfer of resonance energy leads to a shorting of the donor's fluorescence lifetime and can be used as measure as to how many donor fluorophores are in close proximity to the acceptor fluorophores. To analyze the SORLA-APP interaction in living cells, SORLA-GFP was used as the donor fluorophore, while APP-RFP served as the acceptor fluorophore. COS-7 cells were seeded on glass cover slips coated with 0.1 % gelatine. Upon 70 % confluency, cells were transfected with GFP, $SORLA^{WT}$, or $SORLA^{N1358S}$ either alone or in combination with APP-RFP. 2 days after transfection, the GFP lifetime was measured. A ps diode laser (473 nm) with 40 MHz repetition rate (pulses repeating every 25 ns) was used to excite the donor fluorophore (GFP). Images were acquired using a DCS-120 Confocal FLIM Scanning System (given as a loan to the MDC), using a hybrid detector and TCSPC (time correlated single photon counting) electronics (Becker & Hickl GmbH, Berlin). The fluorescence lifetime of GFP was measured on a pixel-by-pixel basis. Detection of GFP fluorescence was

performed using a 525/50 nm band pass filter to separate it from the acceptor (RFP) emission. Analysis was carried out using the SPCImage software (Becker & Hickl GmbH, Berlin). Donor fluorescence lifetimes were fitted to a monoexponential decay function, equivalent to the average GFP lifetime. The reduced GFP lifetimes in the presence of the acceptor indicated FRET, i.e., the interaction that occured between the corresponding proteins.

3.5.5 Statistics

Statistical analysis was performed using the GraphPad Prism 7.0 software. Two experimental groups were compared using an unpaired Student's t-test. Three or more experimental groups were compared using a one-way analysis of variance (ANOVA) with Dunnett's multiple comparison post-test. When testing for the influence of two independent variables on one dependent variable (e.g., the influence of genotype and time on Aβ levels), two-way ANOVA with Sidak's multiple comparison post-test was used. P-values of less than 0.05 were considered statistically significant with * representing $p<0.05$, ** representing $p<0.01$, *** representing $p<0.001$, and **** representing $p<0.0001$. All quantitative data are shown as mean ± standard deviation (SD).

4 RESULTS

4.1 Human iPSC-derived neurons as a model system to study the functional relevance of the *SORT1* risk locus in neurons

Genome-wide association studies have uncovered a SNP upstream of the *SORT1* gene (rs646776) to be associated with hypercholesterolemia and risk of myocardial infarction (Samani *et al.*, 2007; Kathiresan *et al.*, 2008, 2009; Teslovich *et al.*, 2010). Individuals carrying the minor variant of this SNP display a 4-fold increased expression of *SORT1* in liver samples as compared to major variant carrying controls (Musunuru *et al.*, 2010). Molecular dissection of the SNP locus revealed that rs646776 is closely linked with rs12740374 and that the minor variant of rs12740374 generates a C/EBP enhancer site that is disrupted in the major variant, suggesting that rather rs12740374 (but not rs646776) determines *SORT1* expression levels in hepatocytes (Musunuru *et al.*, 2010). To determine whether rs12740374 also predicts *SORT1* expression in the brain, and thereby affects the risk of neurodegenerative diseases, such as frontotemporal lobar degeneration and Alzheimer's disease (Hu *et al.*, 2010; Carlo *et al.*, 2013), I assessed the functional relevance of this SNP in human iPSC-derived neurons.

4.1.1 Human iPSC-derived cortical neurons express mature neuronal markers and induce *SORT1* expression

As a model system for *SORT1* expression in the brain, I established a previously described one-step differentiation protocol to generate cortical neurons from human iPSCs (Zhang *et al.*, 2013). iPSCs were transduced

with a lentiviral construct encoding for the neuronal transcription factor neurogenin-2 (NGN2), which induces neuronal differentiation upon forced expression in human iPSCs (Figure 4-1A).

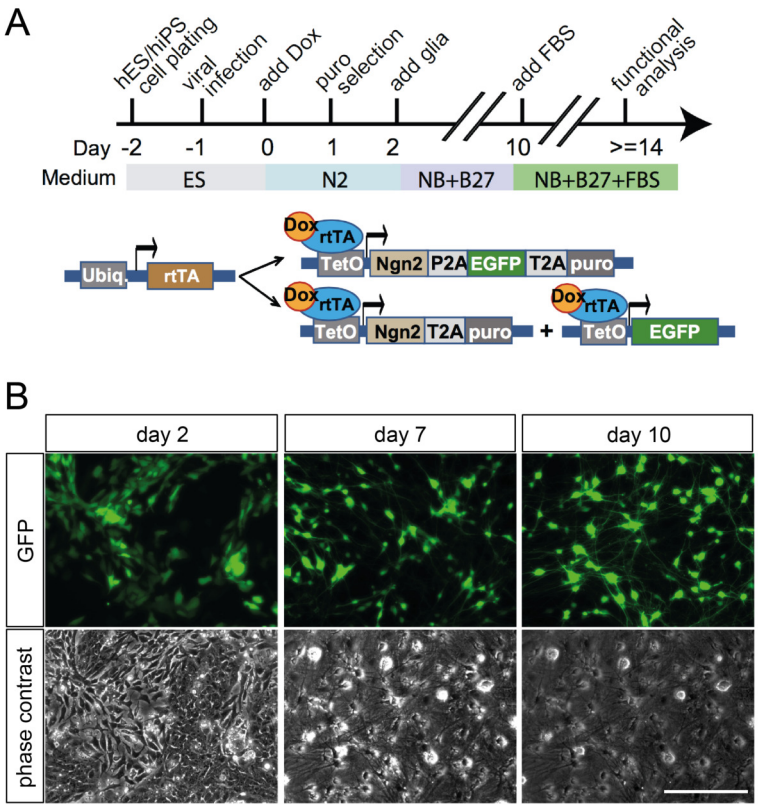

Figure 4-1: Rapid one-step differentiation protocol for generation of cortical neurons from human iPSCs. (A) Timeline and expression constructs required for neuronal differentiation (adapted from Zhang *et al.*, 2013). On day -1, iPSCs are transduced with a lentiviral construct encoding for the transcription factor neurogenin-2 (NGN2) and for the enhanced green fluorescent protein (EGFP), either as fused (above) or as separate (below) constructs, as well as for a puromycin resistance cassette (puro), with coding sequences separated by the cleavage sequences P2A/T2A. A second transduced construct encodes for the reverse tetracycline-controlled transactivator (rtTA) driven by the human constitutive ubiquitin C promoter (Ubiq.). One day after transduction, gene expression is activated by doxycycline (Dox) that binds to rtTA and enables gene transcription from the tetracycline response element (TetO). On day 1, transduced cells show EGFP expression and can be enriched by selection with puromycin. Glia cell cultures are prepared from P1 mouse cortices and added to the differentiating iPSCs to support neuronal growth and survival. After 10 days, cells show neuronal morphology indicated by small cell bodies and neuronal processes. Mature neurons are usually harvested at day 14 or 21. (B) Appearance of human iPSCs at day 2, 7, and 10 of neuronal differentiation. Scale bar, 200 µm.

Lentiviral constructs also encoded for the enhanced green fluorescent protein (EGFP) to mark transfected cells, as well as a puromycin resistance cassette to allow for their selection. Puromycin selection was performed one day after induction of NGN2 expression using doxycycline. The next day, primary mouse glia were added to the differentiating iPSCs to support neuronal cell growth. At day 10 of neuronal differentiation, cells displayed smaller cell bodies compared to iPSCs and had formed neuronal processes, indicating their neuronal fate (Figure 4-1B). Neurons were harvested at day 21 of differentiation to analyze neuronal marker expression by quantitative real-time (qRT) PCR and immunocytochemistry. Transduced cells, as marked by GFP expression, stained positive for the neuronal markers TUJ1 and MAP2 (Figure 4-2A).

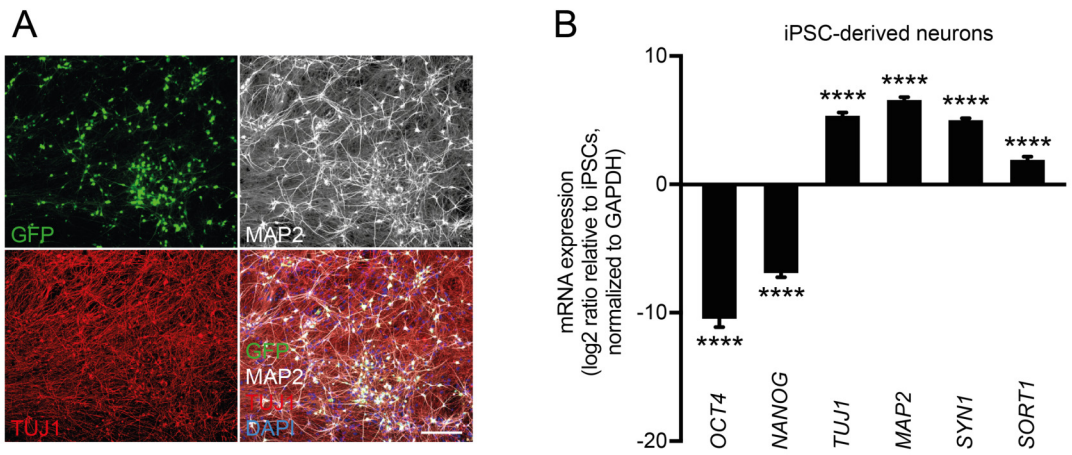

Figure 4-2: Human iPSC-derived neurons express neuronal markers and induce *SORT1* expression. Human iPSC-derived cortical neurons were analyzed 21 days after lentiviral transduction for expression of neuronal markers. (A) Expression of the neuronal markers TUJ1 and MAP2 was analyzed using immunofluorescence microscopy. Cell nuclei were counterstained with DAPI. Scale bar, 200 µm. (B) Also, mRNA levels of pluripotency markers *OCT4* and *NANOG*, of neuronal markers *TUJ1*, *MAP2*, and *SYN1* as well as of *SORT1* were tested using quantitative real-time (qRT) PCR, normalized to *GAPDH* and compared to iPSC levels. Data are shown as mean ± SD (n=1 experiment with 3 biological replicates; 2way ANOVA multiple comparison to iPSCs; ****, p<0.0001).

Compared to iPSCs, mRNA expression levels of the pluripotency markers *OCT4* and *NANOG* were significantly decreased in the differentiated neurons, while expression of the neuronal markers *TUJ1*, *MAP2* and *synapsin I* (*SYN1*) was significantly increased after three weeks of

differentiation. *SORT1* expression levels were increased 3.8-fold in iPSC-derived neurons as compared to iPSC levels (Figure 4-2B).

4.1.2 A genetically engineered *SORT1*$^{-/-}$ iPSC line demonstrates altered PGRN metabolism in *SORT1* deficient iPSC-derived neurons

Having successfully established a protocol to differentiate human iPSCs into mature cortical neurons, I next generated an iPSC line with a targeted deletion of *SORT1*. This cell line was intended as a negative control of receptor function for analysis of iPSC lines with the *SORT1* risk locus variants. For targeted disruption of *SORT1*, I used transcription activator-like effector nuclease (TALEN) constructs flanking the *SORT1* start codon (Figure 4-3A). TALENs are engineered endonucleases designed to target a genomic locus based on their modular DNA-binding domain structure. Targeting TALENs to induce a double-strand break at a gene's start codon provokes non-homologous end-joining (NHEJ), which often results in small insertions or deletions at the target site and consequently disruption of gene expression (Gaj *et al.*, 2013). The TALEN constructs targeting the *SORT1* start codon were kindly generated by Dr. Sebastian Diecke (MDC stem cell core facility) and transfected into human iPSCs as described before (Ding *et al.*, 2013).Transfected cells were identified by expression of markers GFP and RFP encoded by the TALEN constructs, FACS sorted, and expanded into single cell derived clones (Figure 4-3B). 36 clones were screened by PCR amplification and sequencing of the ATG region. Clone 11 displayed a 23 bp homozygous deletion that included the ATG start codon and caused a frame shift in the coding sequence (Figure 4-3C). Western Blot analysis of the parental iPSC line, the ATG knock-out clone (clone 11) and a non-targeted clone (clone 13) confirmed the successful disruption of *SORT1* expression in clone 11 (Figure 4-3D).

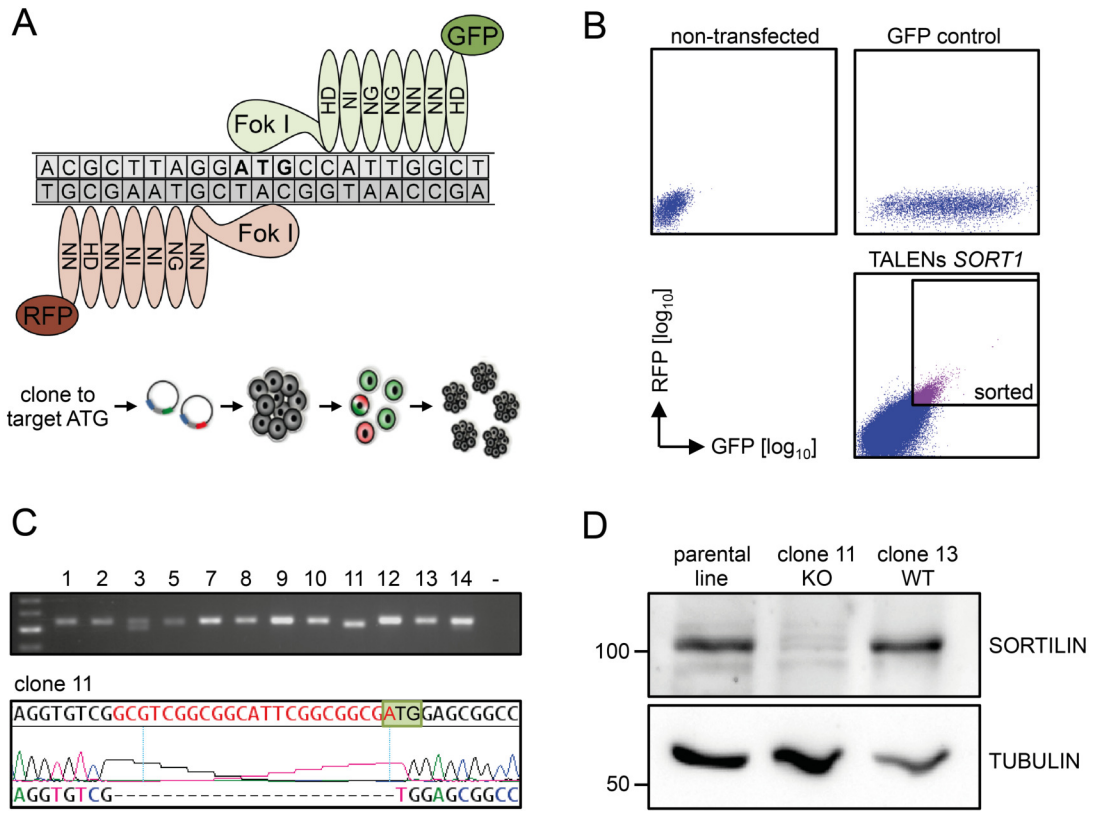

Figure 4-3: Generating a *SORT1* knock-out iPSC line by deleting the *SORT1* start codon (ATG) using transcription activator-like effector nucleases (TALENs). (A) Scheme (above) and workflow (below) of the TALENs targeting. Scheme: Each TALEN consists of a modular DNA binding domain and a FokI endonuclease that, as a homodimer, causes DNA double-strand breaks. TALENs used here are also fused to either green or red fluorescent protein (GFP/RFP) that allow for sorting of transfected cells. DNA binding of each nucleotide at the target site is mediated by a set of two amino acids in the DNA binding domain (NN for G; HD for C; NI for A; NG for T). By designing two TALENs binding shortly upstream and downstream of the *SORT1* start codon, the two Fok1 domains cause a double-strand break close to the ATG. The DNA break is repaired by non-homologous end joining (NHEJ) which often causes insertions or deletions at the target site, which in turn disrupt gene expression. Workflow: The two TALENs constructs are designed and cloned to target the start codon of *SORT1* and transfected into human iPSCs. GFP^+/RFP^+ double positive cells are sorted using fluorescence-activated cell sorting (FACS) and seeded for picking clonal colonies. After expansion, individual clones are analyzed for insertions/deletions at the *SORT1* ATG and for loss of *SORT1* expression. Workflow adapted from Peters, 2014). (B) Human iPSCs were transfected with two *SORT1* TALENs constructs or with a GFP control, and analyzed 48 h after transfection for expression of GFP and RFP using FACS. A non-transfected pool of iPSCs was analyzed in parallel to identify non-specific autofluorescence. Double positive cells (pink) were sorted and replated for picking individual colonies.

Figure legend continues on next page.

Continued figure legend:

(C) Genomic DNA was isolated from expanded clones and the *SORT1* ATG region was amplified by PCR and sequenced. Clone 11 shows a 23 base pair deletion including the ATG (ATG KO). (D) Comparative Western Blot analysis of the parental cell line, the ATG KO clone (clone 11) as well as a non-targeted clone (clone 13) confirmed the ablation of *SORT1* expression in clone 11. Detection of tubulin served as loading control. Molecular weights are given on the left in kilodaltons (kDa).

Clones 11 (*SORT1* KO) and 13 (*SORT1* WT) were expanded and the expression of pluripotent stem cell markers analyzed by immunocytochemistry. Like the parental iPSC line used for targeting, the generated *SORT1* WT and KO clones uniformly expressed the pluripotency markers OCT4, NANOG, SSEA4 and SOX2, verifying their pluripotent stem cell identity (Figure 4-4). Karyotype analysis was performed by the MDC stem cell core facility using the Infinium OmniExpressExome-8 Kit and the iScan system from Illumina. The *SORT1* WT and KO cell lines displayed normal karyotypes without larger areas of insertions or deletions (Supplementary Figure 7-2).

To determine the functional relevance of *SORT1* deficiency in human iPSC-derived neurons, I next differentiated the *SORT1* WT and KO iPSC lines into cortical neurons. Immunocytochemical analysis of TUJ1 and MAP2 revealed no obvious defects in neuronal differentiation capacity when differentiating the *SORT1* KO clone, suggesting that loss of *SORT1* expression does not impair neuronal differentiation (Figure 4-5A).

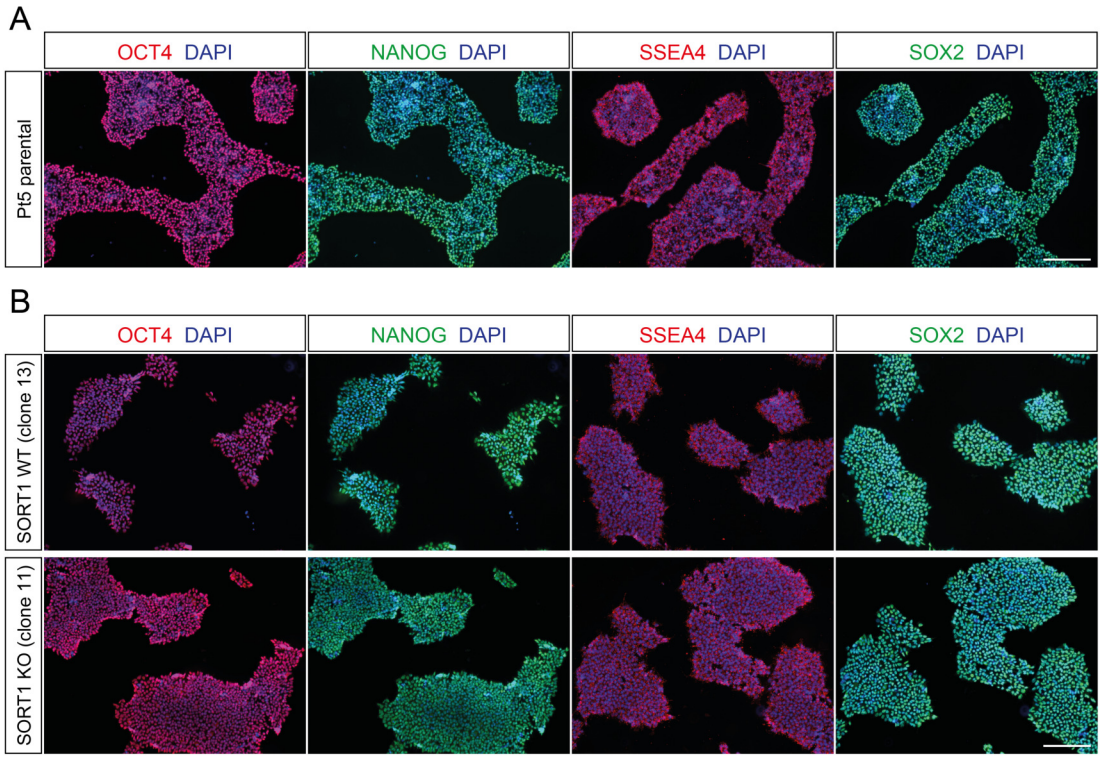

Figure 4-4: Immunocytochemical characterization of the *SORT1* knock-out iPSC line. (A, B) Representative immunofluorescence microscopy images of pluripotency marker expression in the parental iPSC line (A) and the generated *SORT1* wildtype (WT) and knock-out (KO) cell lines (B). All cell lines express the pluripotency markers OCT4, NANOG, SSEA4, and SOX2. Cell nuclei were counterstained with DAPI. Scale bar, 200 µm.

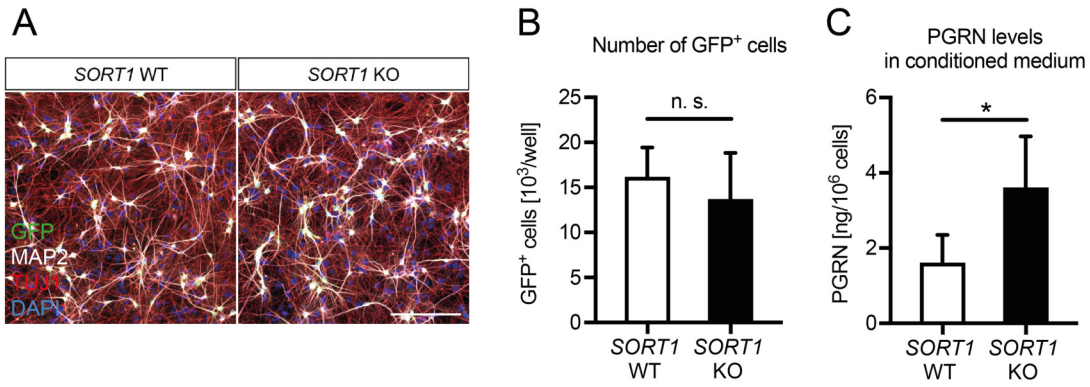

Figure 4-5: Disruption of *SORT1* in iPSC-derived cortical neurons impacts PGRN metabolism. (A) *SORT1* wildtype (WT) and knock-out (KO) iPSC lines were differentiated for 3 weeks into cortical neurons and analyzed for expression of the neuronal markers TUJ1 and MAP2 using immunofluorescence microscopy. Cell nuclei were counterstained with DAPI. Scale bar, 200 µm. (B) Number of NGN2-transduced cells (GFP^+) were counted to ensure comparable numbers of iPSC-derived neurons. (C) PGRN levels in conditioned media of the indicated neuronal cultures were measured using ELISA, and normalized to the number of GFP^+ cells. Data are shown as mean ± SD (n=1 experiment with 3 biological replicates shown; representative for 3 independent experiments performed; t test; *, $p<0.05$).

Next, I assessed the impact of *SORT1* deficiency on PGRN metabolism. PGRN is secreted by mature neurons (Van Damme *et al.*, 2008; Petkau *et al.*, 2010) and re-endocytosed and sorted for lysosomal degradation by sortilin (Hu *et al.*, 2010). As haploinsufficieny of PGRN causes FTLD (Baker *et al.*, 2006; Cruts *et al.*, 2006), restoring PGRN levels by targeting sortilin-mediated endocytosis is a potential therapeutic strategy for FTLD treatment (Lee *et al.*, 2014).

To ensure comparable numbers of differentiated neurons, which both secrete PGRN and clear it from the medium, I first counted the number of *SORT1* WT and KO GFP^+ neurons per well (Figure 4-5B). I then measured PGRN levels in the conditioned medium of the iPSC-derived neurons using ELISA and normalized them to the number of GFP^+ neurons. PGRN levels were significantly increased in the medium of *SORT1* KO iPSC-derived neurons compared the WT control, validating iPSC-derived neurons as a model for the functional relevance of *SORT1* (Figure 4-5C).

4.1.3 Generation of iPSC lines from minor and major *SORT1* SNP variant carriers

Having established iPSC-derived neurons as a model for *SORT1* expression and function in the brain, I next generated iPSC lines carrying either the minor or major variant of the *SORT1* risk locus. I obtained one minor variant carrying iPSC line from the Wellcome Trust Sanger Institute and one fibroblast sample from the Hamburg City Health Study. Control major variant donor cell lines were also obtained from the Wellcome Trust Sanger Institute (see Table 3-24). Verification of the rs12740374 and rs646776 SNP genotypes was performed using allele-specific TaqMan™-based SNP genotyping assays (Figure 4-6). The carriers of the minor variant of rs12074374 also carried the minor variant of rs646776, confirming their linkage.

I reprogrammed primary fibroblasts carrying the minor SNP variants into iPSCs using a non-transmissible Sendai virus encoding for the four pluripotency factors (*SOX2*, *KLF-4*, *OCT4*, *c-MYC*), known to efficiently reprogram somatic cells into iPSCs (Takahashi and Yamanaka, 2006). The reprogrammed iPSCs were characterized by immunofluorescence stainings for the pluripotency markers OCT4, NANOG, SSEA4, and SOX2 (Figure

4-7). All cell lines uniformly expressed these four pluripotency markers, verifying their pluripotent stem cell identity. Karyotype analysis of the reprogrammed cell line MDCH0003/BIH013-A was performed by the MDC stem cell core facility using the Infinium OmniExpressExome-8 Kit and the iScan system from Illumina. The iPSC line displayed a normal karyotype without larger areas of insertions or deletions (Supplementary Figure 7-2). Karyotype integrity and exosome sequencing data on the iPSC lines obtained from the Wellcome Trust Sanger Institute is available online (http://www.hipsci.org).

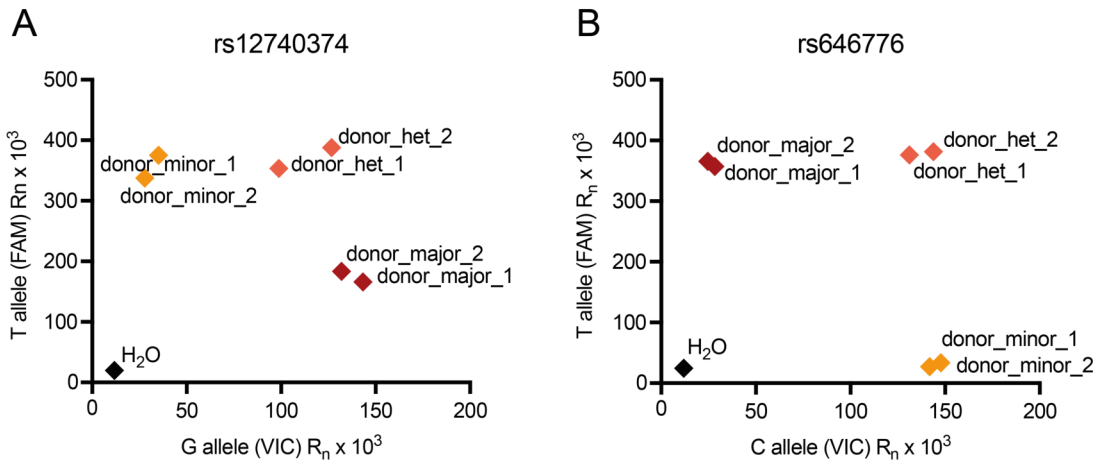

Figure 4-6: Donor iPSC lines carrying major or minor variants of SNP rs12740374. (A, B) SNP genotypes of rs12740374 (A) and rs646776 (B) were analyzed by allele-specific quantitative real-time (qRT) PCR in 6 donor cell lines. Due to linkage, minor variant carriers of SNP rs12740374 (homozygous T/T) also carry the minor variant of the diagnostic SNP rs646776 (homozygous C/C).

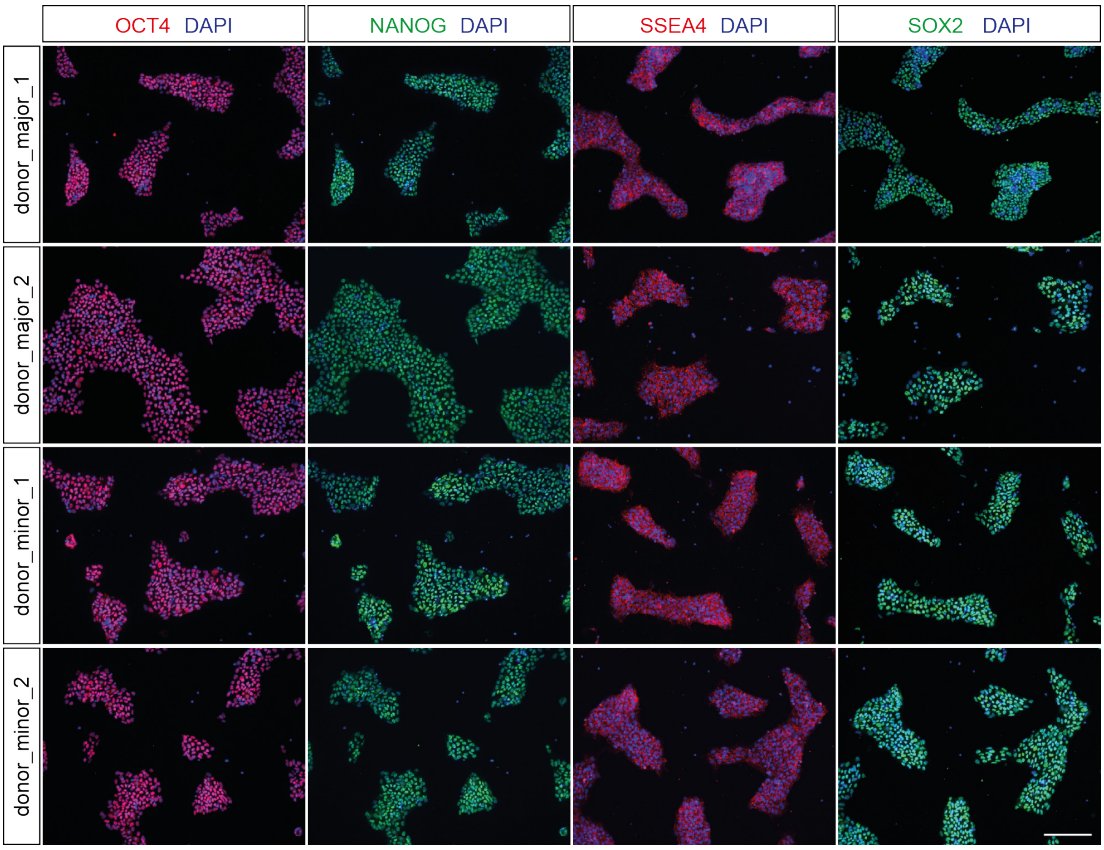

Figure 4-7: Immunocytochemical characterization of major and minor variant donor iPSC lines. Representative immunofluorescence microscopy images of the indicated pluripotency marker expression in two major and two minor variant carrying iPSC lines. All cell lines uniformly express the pluripotency markers OCT4, NANOG, SSEA4, and SOX2. Cell nuclei were counterstained with DAPI. Scale bar, 200 µm.

4.1.4 Seamless introduction of the minor *SORT1* SNP variant into a major variant iPSC line using CRISPR/Cas9 and the piggybac™ transposon system

Importantly, donor iPSC lines carrying either the minor or major variant of the *SORT1* risk locus do not only differ in the SNP of interest (rs12740374), but also in the minor/major variants of all genetically linked SNPs, in particular rs646776, as well as in their general genetic background. To conclusively attribute potential effects on *SORT1* expression to rs12740374, I also generated isogenic iPSC lines that carry either the minor or major variant of the proposed functional *SORT1* SNP. For this purpose, I utilized a combination of CRISPR/Cas9 and the piggybac™ transposon system that enables the seamless exchange of single nucleotides (Yusa, 2013).

As a first step, a single guide (sg) RNA-Cas9 fusion construct targeting close to the rs12740374 locus was co-transfected with a homologous recombination (HR) vector containing a selection cassette for puromycin and thymidine kinase (TK), as well as two 500 bp long homology arms harboring the minor SNP variant (Figure 4-8). The Cas9-induced double-strand break is repaired by the HR vector, integrating both the selection cassette as well as the minor variant at the genomic locus. HR-integrated clones were selected by puromycin treatment. Subsequently, the selection cassette was excised by transfecting the excision-only piggybac™ transposase (PBX). HR-excised cells were purified by negative selection for TK using ganciclovir treatment. Upon phosphorylation, the guanosine analogue Ganciclovir causes premature DNA chain termination and therefore apoptosis in TK expressing cells (Fillat *et al.*, 2003).

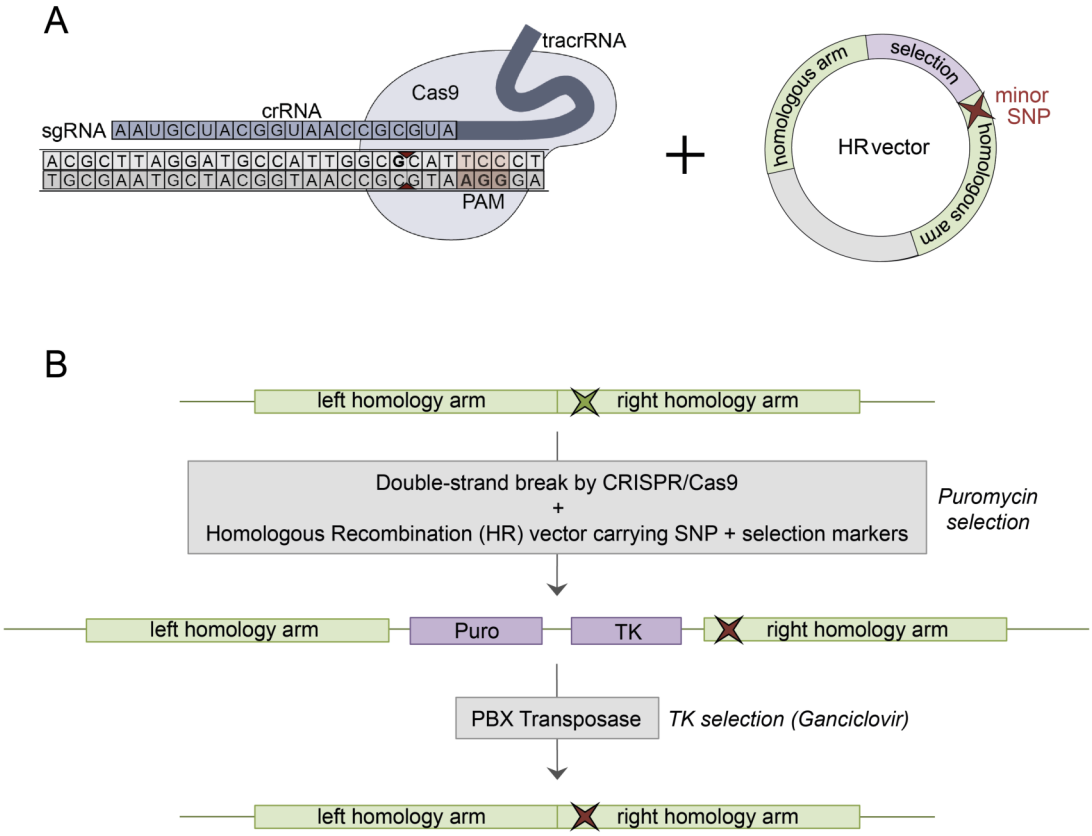

Figure 4-8: Seamless introduction of a single nucleotide polymorphism (SNP) into the genome of an iPSC line using CRISPR/Cas9 and the piggybac™ transposon system. (A) Schematic depiction of the CRISPR/Cas9 system with the 20 bp long single guide (sg) RNA consisting of the crispr (cr) RNA, that binds to the target region in the iPSC genome, and of the transactivating crispr (tracr) RNA that recruits Cas9. Cas9 is an endonuclease that causes a double-strand DNA break upstream of the protospacer adjacent motif (PAM) 5'-NGG-3'. The homology recombination (HR) vector contains selection cassettes for puromycin resistance (Puro; positive selection) and thymidine kinase (TK; negative selection), as well as homology arms of the target gene region encoding the SNP to be introduced into the genome. (B) Workflow of introducing a minor SNP variant into the parental iPSC line carrying the major SNP allele. The sgRNA is designed to target close to the endogenous SNP of interest (green star) and encoded on the same plasmid as Cas9. The transfection reaction also includes the HR vector that carries the homology arms of the target gene region and encodes the desired minor SNP variant (red star). Cell clones having integrated the HR vector into their genome are selected by puromycin. Successful insertion of the minor SNP allele is confirmed by PCR-based sequencing. Thereafter, transfection with a construct encoding excision-only piggybac™ transposase (PBX) is performed to excise the selection cassettes (negative selection for TK) from positively targeted iPSC clones. Using this seamless approach, parental and genome-edited cell line only differ in the exchanged SNP of choice.

To monitor the integration and excision of the HR vector, I amplified genomic DNA of the targeted clones using a set of three primers, two of them binding in the genomic region, not included in the homology arms of the vector, and one of them binding in the vector's selection cassette (Figure 4-9). PCR products were analyzed using agarose gel electrophoresis to identify wildtype (WT, 0.6 kb) and homology cassette integrated (HR, 1.1 kb) alleles. After transfection of the sgRNA-Cas9 construct and the HR vector, I screened for homozygously targeted clones that had integrated the HR vector into both alleles and therefore lacked the WT band (Figure 4-9A). Excision of the selection cassette by the PBX transposase was verified using the same set of primers, only now screening for clones that had excised the HR vector from both alleles and therefore showed reappearance the WT band (Figure 4-9B). Sequencing confirmed that the genome-edited iPSC clone ('isogenic_edited_minor') carried the homozygous minor variant of the rs12740374 SNP (T/T), while the parental iPSC line carried the homozygous major variant (G/G, 'isogenic_parental_major') (Figure 4-9C).

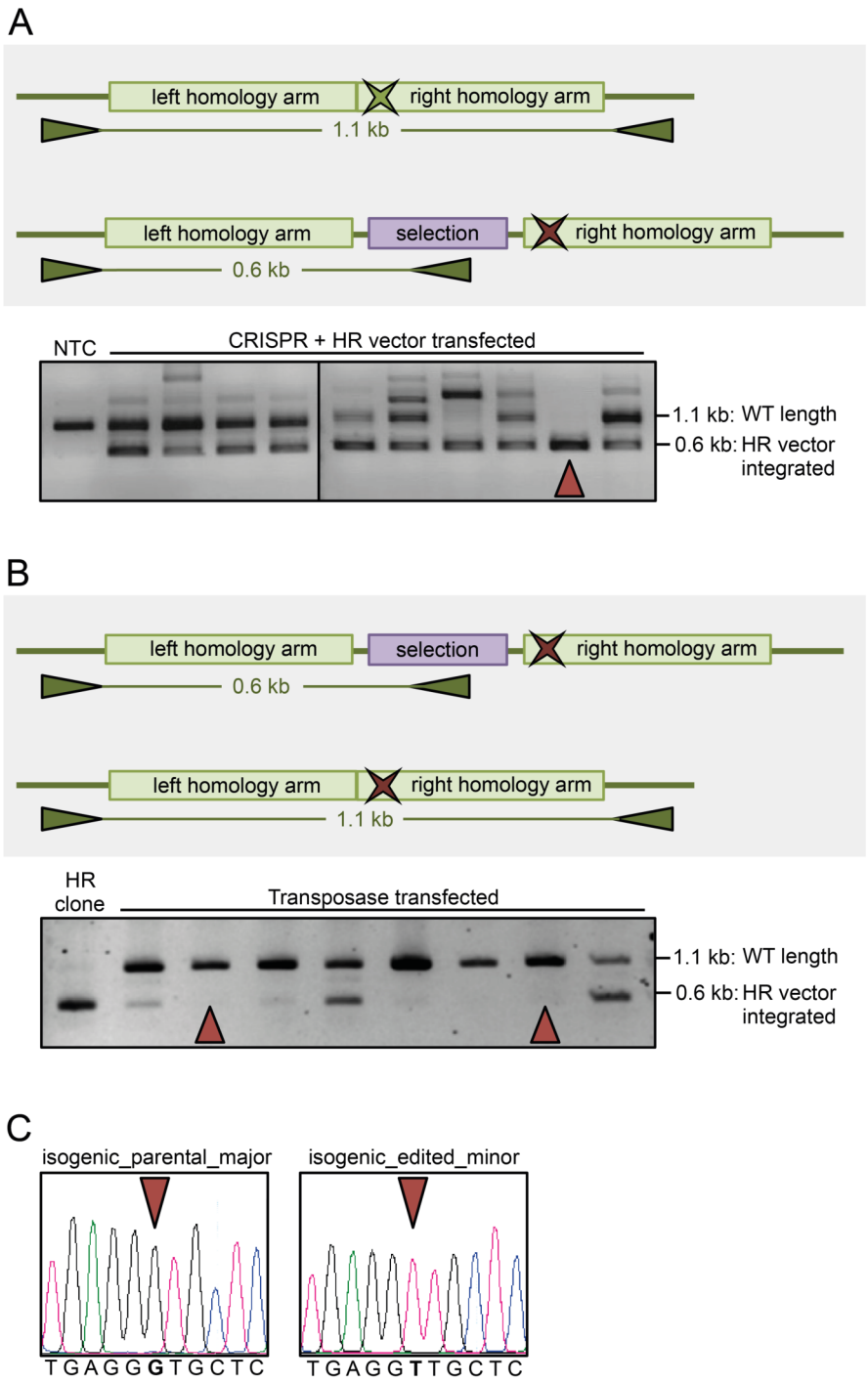

Figure 4-9: Introducing the homozygous minor variant of rs12740374 into a major variant carrying human iPSC line. (A) Human iPSCs were transfected with the sgRNA-Cas9-CRISPR construct and the HR vector, selected with Puromycin, and seeded for picking clonal colonies. After expanding individual clones, genomic DNA was isolated and the wildtype (WT) allele (1.1 kb, primers outside of homologous arms) and the targeted alleles, having integrated the homology recombination (HR) vector (0.6 kb, left primer outside of homologous arm, right primer inside selection cassette), were amplified. NTC: non-transfected control. The red arrow highlights the homozygously targeted clone that has integrated the HR vector into both alleles and lacks the WT band.

Figure legend continues on next page.

Continued figure legend:

(B) The targeted clone was expanded and transfected with piggybac™ transposase (PBX) to excise the selection cassette. After Ganciclovir selection for loss of TK (thymidine kinase), purified DNA from the picked clones was amplified for WT and HR integrated alleles. Red arrows highlight clones that had excised the selection cassettes from both alleles and only showed WT bands. (C) Sequencing confirmed that the parental iPSC line and genome-edited clone differ only in the SNP of interest. After genome-editing, the cell line carried the homozygous minor variant T/T.

The genome-edited, as well as the parental iPSC line were characterized by immunofluorescence stainings for the pluripotency markers OCT4, NANOG, SSEA4 and SOX2 (Figure 4-10). All cell lines uniformly expressed these four pluripotency markers, verifying their pluripotent stem cell identity. Karyotype analysis was performed by the MDC stem cell core facility using the Infinium OmniExpressExome-8 Kit and the iScan system from Illumina. Both cell lines displayed normal karyotypes without larger areas of insertions or deletions (see Supplementary Figure 7-3).

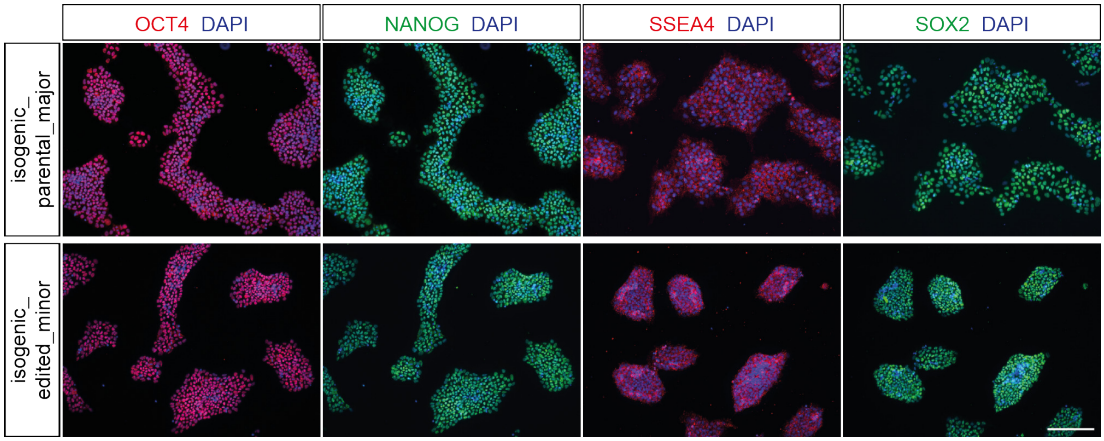

Figure 4-10: Immunocytochemical characterization of the genome-edited isogenic minor variant iPSC line. Representative immunofluorescence microscopy images of pluripotency marker expression in iPSC lines carrying the parental major and the genome-edited minor variant of rs12740374. Both cell lines uniformly express the pluripotency markers OCT4, NANOG, SSEA4 and SOX2. Cell nuclei were counterstained with DAPI. Scale bar, 200 µm.

In conclusion, I have generated a *SORT1* deficient iPSC line as a negative control, two homozygous minor and two homozygous major *SORT1* risk variant carrying iPSC lines from donors, as well as a pair of isogenic iPSC

lines that differ only in rs12740374, the proposed functional SNP for regulating *SORT1* gene expression.

4.1.5 *SORT1* expression in iPSC-derived cortical neurons is not affected by the *SORT1* risk locus

To determine the functional relevance of the *SORT1* risk locus in human iPSC-derived neurons, I next differentiated the two homozygous minor and two homozygous major *SORT1* risk variant carrying iPSC lines from donors into cortical neurons. All four lines generated mature neurons as demonstrated by immunocytochemical staining of TUJ1 and MAP2, suggesting that the *SORT1* risk locus does not affect neuronal differentiation (Figure 4-11A).

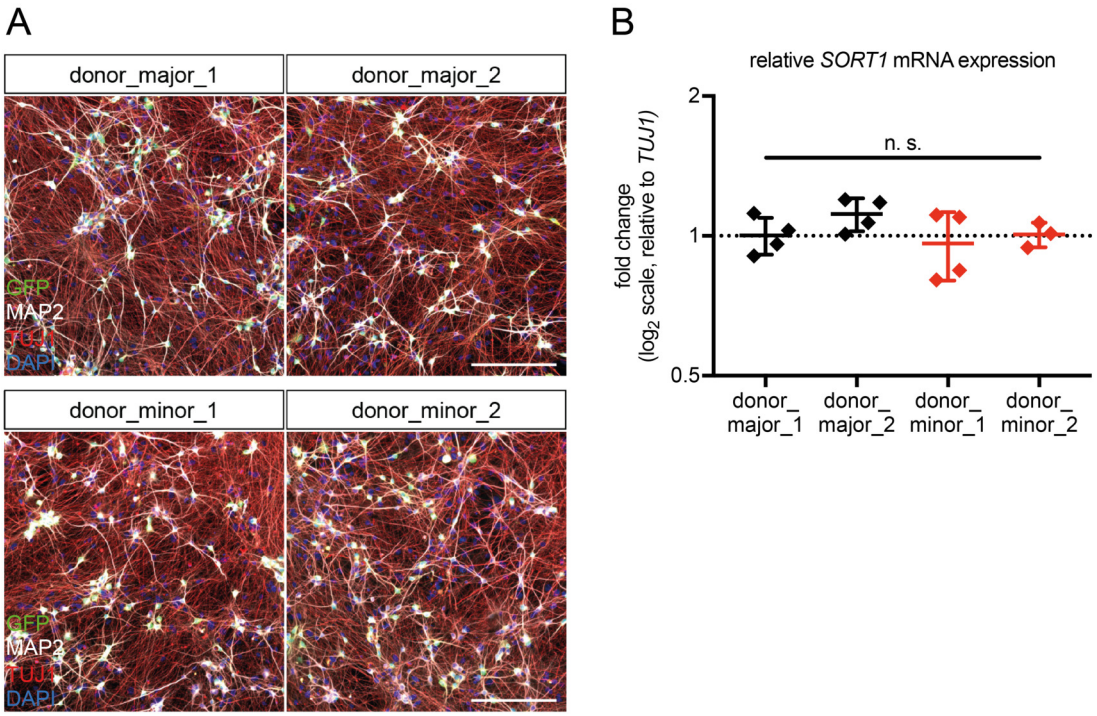

Figure 4-11: No difference in SORT1 expression comparing cortical neurons from iPSCs carrying the major or minor variant of rs12740374. (A) Donor iPSC lines were differentiated for 3 weeks into cortical neurons and analyzed for expression of neuronal markers TUJ1 and MAP2 using immunofluorescence microscopy. Cell nuclei were counterstained with DAPI. Scale bar, 200 µm. (B) *SORT1* mRNA levels were determined by quantitative real-time (qRT) PCR, normalized to *TUJ1* and depicted as relative fold change. Data are shown as mean ± SD (n=1 experiment with 3 biological replicates shown; representative for a total of 3 independent experiments performed; one-way ANOVA; n. s., p>0.05).

I analyzed *SORT1* expression in the iPSC-derived neurons using qRT-PCR and normalized *SORT1* mRNA levels to *TUJ1* mRNA levels to control for variabilites in neuronal differentiation efficiency. *SORT1* mRNA expression levels were not significantly different between homozygous minor and homozygous major *SORT1* risk variant carrying iPSC-derived neurons (Figure 4-11B).

Evaluation of iPSC-derived neurons generated from the genome-edited isogenic iPSC lines, which differ only in rs12740374, did also not reveal any defects in neuronal differentiation as both lines gave rise to mature neurons as demonstrated by immunocytochemical staining of TUJ1 and MAP2 (Figure 4-12A). As observed for the donor iPSC lines, *SORT1* mRNA expression levels, as measured by qRT-PCR and normalized to *TUJ1* mRNA levels, did not differ between the minor and major variant carrying iPSC-derived isogenic neurons (Figure 4-12B).

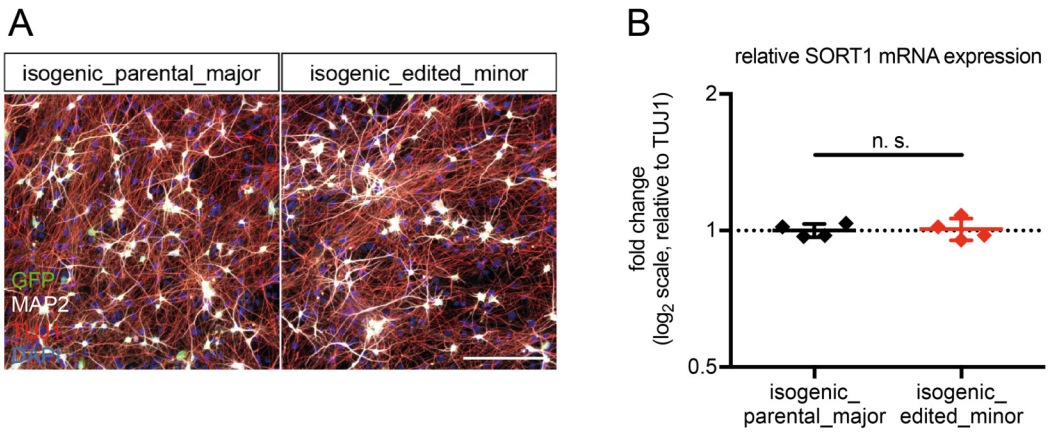

Figure 4-12: No difference in *SORT1* expression comparing isogenic iPSC-derived cortical neurons carrying the major or minor variant of rs12740374. (A) Isogenic iPSC lines were differentiated for 3 weeks into cortical neurons and analyzed for expression of neuronal markers TUJ1 and MAP2 using immunofluorescence microscopy. Cell nuclei were counterstained with DAPI. Scale bar, 200 µm. (B) *SORT1* mRNA levels were determined by quantitative real-time (qRT) PCR, normalized to *TUJ1* and depicted as relative fold change. Data are shown as mean ± SD (n=1 experiment with 3 biological replicates shown; representative for a total of 3 independent experiments performed; t test; n. s., p>0.05).

In conclusion, the *SORT1* risk locus did not predict *SORT1* expression levels in this model of human iPSC-derived cortical neurons.

4.1.6 Hepatic differentiation of minor/major variant iPSC lines suggests that rs12740374 predicts *SORT1* expression in hepatocytes

As mentioned above, *SORT1* expression in human liver samples was found to be affected by the *SORT1* risk locus (Musunuru *et al.*, 2010). To determine whether the *SORT1* risk locus affects *SORT1* expression levels only in hepatocytes, but not in neurons, I also assessed *SORT1* expression in minor/major *SORT1* risk variant carrying iPSC-derived hepatocytes.

For this purpose, I established a hepatic differentiation protocol using the Cellartis Hepatocyte Differentiation Kit from Clontech. iPSCs were first differentiated into definitive endoderm cells for 7 days and, after replating, further differentiated into hepatocytes (Asplund *et al.*, 2016). All media und and coating reagents were provided with the kit and and the formulation is proprietary to Clontech. Hepatocytes were harvested at day 30 of differentiation to analyze hepatocyte marker expression by immunocyto-chemistry and qRT-PCR in collaboration with Silvia Ruzittu (Lab Spagnoli, MDC Berlin).

iPSC-derived hepatocytes stained positive for the mature hepatocyte markers HNF4α (hepatocyte nuclear factor 4 α) and albumin (Figure 4-13A). Compared to iPSCs, mRNA expression levels of the pluripotency markers *OCT4* and *NANOG* were significantly decreased in the differentiated hepatocytes, while mRNA expression of the hepatocyte markers *albumin* and *HNF4α*, the hepatic enzyme *CYP3A4 (cytochrom P450 3A4)*, and the apolipoprotein *APOA2* were increased after 30 days of differentiation (Figure 4-13B). *CYP3A4*, *HNF4α*, and *APOA2* were expressed at similar levels in iPSC-derived hepatocytes as in primary human hepatocytes. However, *albumin* mRNA expression was decreased compared to primary human hepatocytes and the immature hepatocyte marker *AFP* (*α-fetoprotein*) was strongly expressed after 30 days of hepatic differentiation, suggesting that the culture still contained some immature hepatocytes.

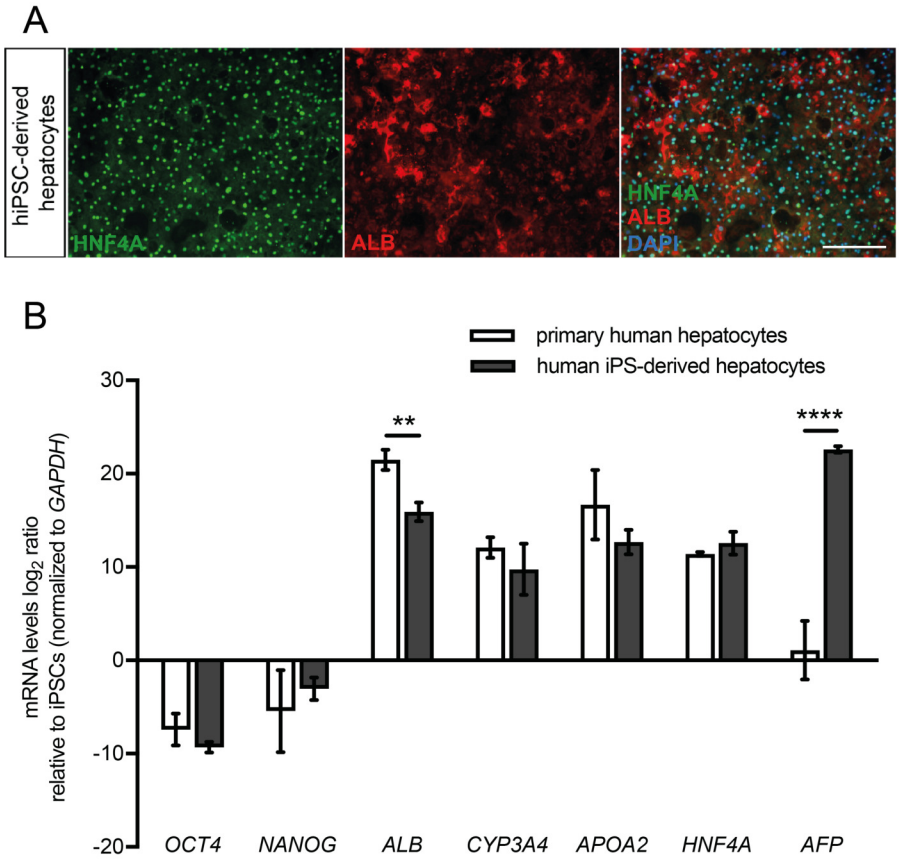

Figure 4-13: Human iPSC-derived hepatocytes express hepatocyte markers profiles comparable to that of primary human hepatocytes. (A) iPSC-derived hepatocytes were analyzed after 30 days of differentiation for expression of mature hepatocyte markers HNF4A and albumin (ALB) using immunofluorescence microscopy. Cell nuclei were counterstained with DAPI. Scale bar, 200 µm. (B) Also, mRNA levels of pluripotency markers *OCT4* and *NANOG*, of mature hepatocyte markers *ALB*, *CYP3A4*, *APOA2*, and *HNF4A,* and of immature hepatocyte marker *AFP* were tested using quantitative real-time (qRT) PCR. Levels were normalized to *GAPDH* and compared to iPSC levels. Data are shown as mean ± SD (n=1 experiment with 2-3 biological replicates shown; 2way ANOVA multiple comparison to iPSCs; **, p<0.01; ****, p<0.0001).

However, as the majority of cells expressed mature hepatocyte markers, I went on to determine *SORT1* mRNA expression levels in hepatocytes generated from one homozygous minor and one homozygous major *SORT1* risk variant carrying donor iPSC line. Both cell lines gave rise to mature hepatocytes with uniform expression of HNF4α and albumin as demonstrated by immunofluorescence staining (Figure 4-14A). *SORT1* mRNA expression was measured by qRT-PCR and normalized to either *B2M* (β-2-microglobulin) or *HNF4α* mRNA levels. While *B2M* is a common housekeeping gene for qRT-PCR normalization, as it is expressed by all cell

types, *HNF4α* is only expressed in mature hepatocytes and therefore controls for differences in differentiation efficiency. The minor variant carrying hepatocytes displayed significantly increased *SORT1* mRNA expression compared to the major variant carrying control when normalized to *B2M* (Figure 4-14B) and a tendency for increased *SORT1* mRNA expression when normalized to *HNF4α* (Figure 4-14C).

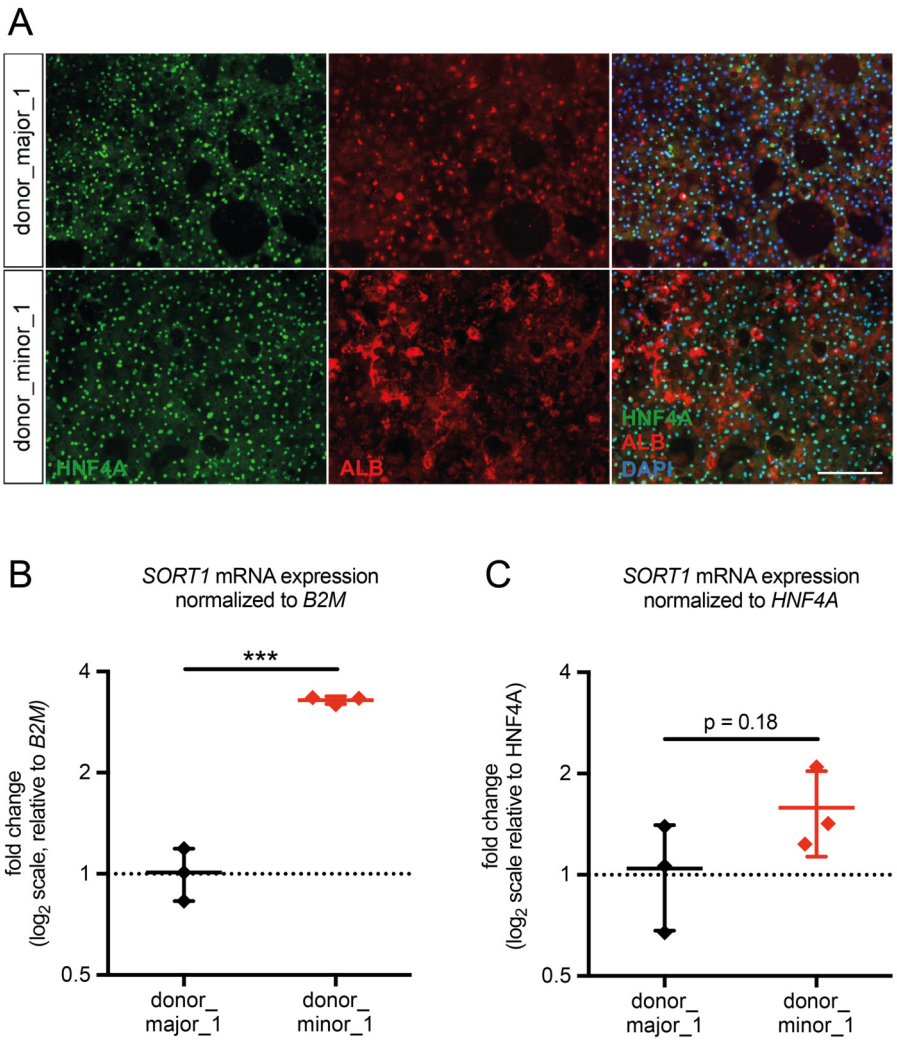

Figure 4-14: Increased *SORT1* expression in hepatocytes carrying the minor as compared to the major variant of *SORT1* SNP rs12740374. (A) Donor iPSC lines were differentiated for 30 days into hepatocytes and analyzed for expression of mature hepatocyte markers HNF4A and albumin (ALB) using immunofluorescence microscopy. Cell nuclei were counterstained with DAPI. Scale bar, 200 µm. (B, C) *SORT1* mRNA levels were determined using quantitative real-time (qRT) PCR, normalized to *B2M* (B) or *HNF4A* (C), and depicted as relative fold change. Data are shown as mean ± SD (n=1 experiment with 3 biological replicates; t test; ***, p<0.001).

To determine whether the increase in *SORT1* expression in the minor variant carrying donor hepatocytes is indeed caused by the minor variant of rs12740374, I also analyzed *SORT1* expression in hepatocytes generated from the isogenic iPSC lines.

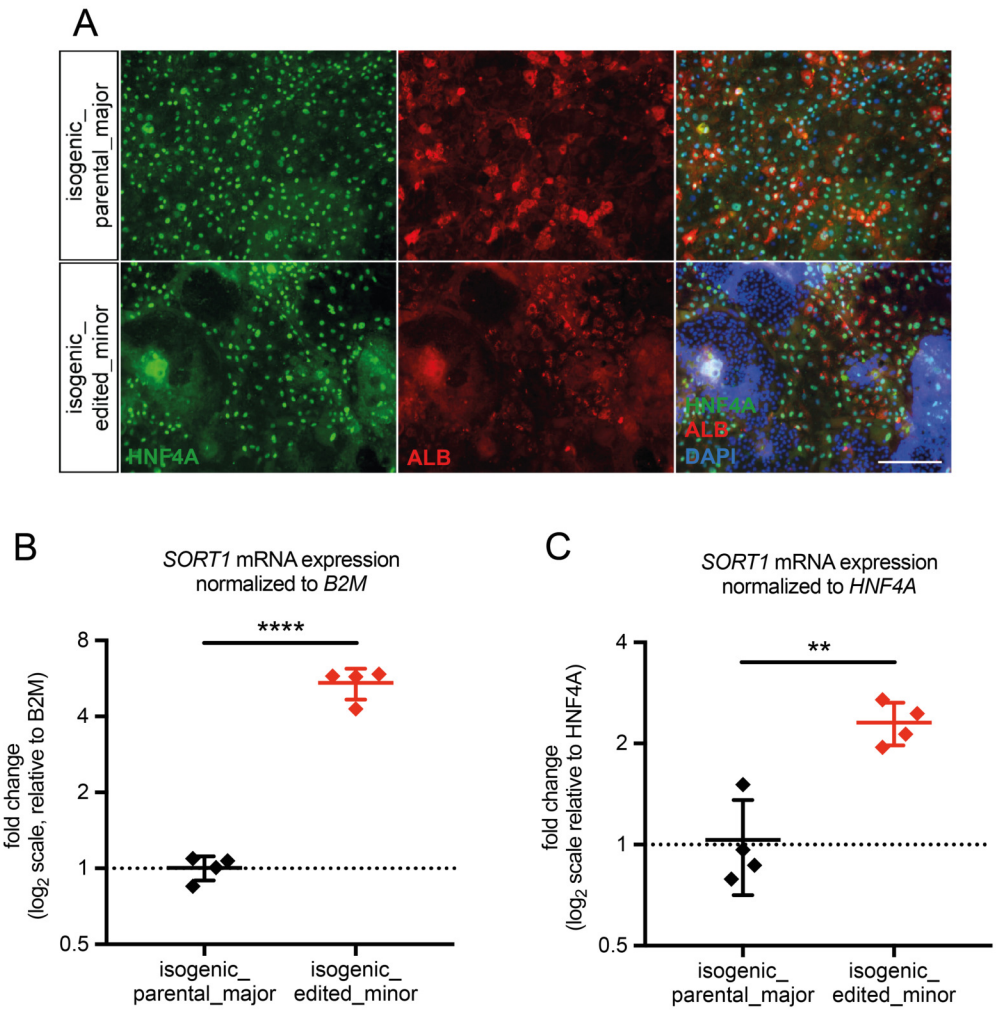

Figure 4-15: Genome-edited iPSC-derived hepatocytes carrying minor variant *SORT1* SNP rs12740374 show higher *SORT1* expression than their isogenic major variant control. (A) Genome-edited (minor variant) and parental (major variant) iPSC lines were differentiated for 30 days into hepatocytes and analyzed for expression of mature hepatocyte markers HNF4A and albumin (ALB) using immunofluorescence microscopy. Cell nuclei were counterstained with DAPI. Scale bar, 200 µm. (B, C) *SORT1* mRNA levels were determined using quantitative real-time (qRT) PCR, normalized to *B2M* (B) or *HNF4A* (C), and depicted as relative fold change. Data are shown as mean ± SD (n=1 experiment with 3 biological replicates; t test; **, p<0.01; ****, p<0.0001).

While the parental major variant carrying iPSC line uniformly differentiated into HNF4α- and albumin-positive hepatocytes, the genome-edited minor variant carrying iPSC line differentiated less efficiently, displaying clusters of HNF4α- and albumin-negative cells (Figure 4-15A).
Still, in this experiment *SORT1* mRNA expression was significantly increased in the minor variant carrying hepatocytes compared to the isogenic major control, both when normalized to *B2M* and to *HNF4α* (Figure 4-15B-C), suggesting that rs12740374 indeed regulates *SORT1* expression in hepatocytes.

4.1.7 C*/EBPα* is significtly higher expressed in iPSC-derived hepatocytes compared to iPSC-derived cortical neurons

My data suggested that rs12740374 predicts *SORT1* expression in hepatocytes, but not in neurons. As the minor variant of rs12740374 was proposed to generate a recognition site for the transcription factor C/EBPα (Musunuru *et al.*, 2010), I analyzed *C/EBPα* mRNA expression levels in iPSCs, iPSC-derived cortical neurons, and iPSC-derived hepatocytes (Figure 4-16).

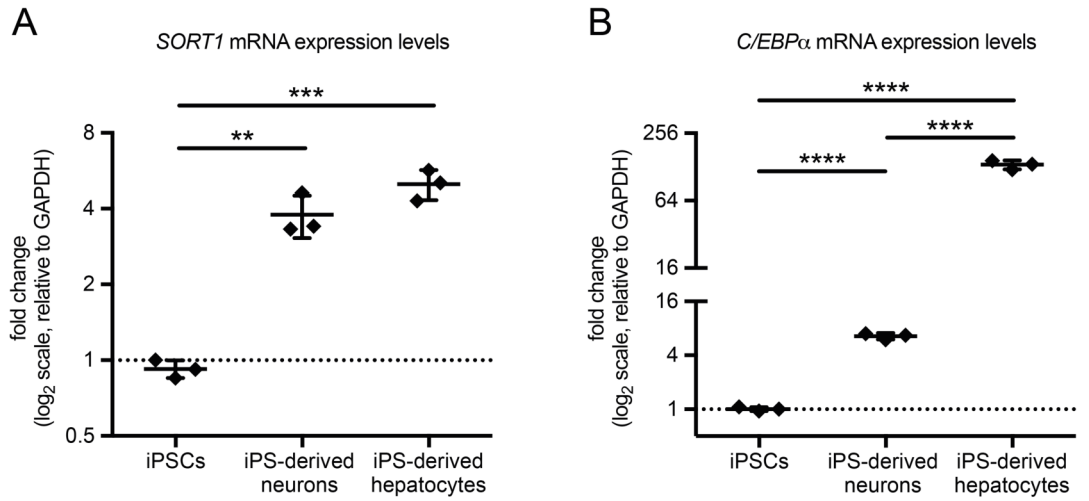

Figure 4-16: *SORT1* and *C/EBPα* mRNA levels in human iPSCs, neurons, and hepatocytes. (A, B) Human iPSCs were differentiated into cortical neurons or hepatocytes. *SORT1* (A) and *C/EBPα* (B) mRNA levels were determined using quantitative real-time (qRT) PCR, normalized to *GAPDH,* and depicted as fold change relative to iPSC levels. Data are shown as mean ± SD (n=1 experiment with 3 biological replicates; one-way ANOVA; **, p<0.01; ***, p<0.001; ****, p<0.0001).

While *SORT1* expression levels were similar between iPSC-derived neurons and iPSC-derived hepatocytes (approximately 4-fold increased as compared to iPSCs), *C/EBPα* expression was 130-fold elevated in iPSC-derived hepatocytes but only 7-fold increased in iPSC-derived neurons as compared to iPSCs, possibly explaining why rs12740374 regulates *SORT1* expression only in hepatocytes.

In conclusion, the *SORT1* risk locus predicted *SORT1* expression in iPSC-derived hepatocytes, but not in iPSC-derived neurons, which may be explained by differences in *C/EBPα* expression levels. Analysis of isogenic iPSC lines suggested that indeed rs12740374, and not rs646776, determines *SORT1* expression in hepatocytes.

4.2 Functional validation of coding *SORL1* mutations associated with early-onset Alzheimer's disease

Mutations in *APP* or *PSEN1/2* cause the severe early-onset form of Alzheimer's disease (EOAD) with symptoms typically appearing before 65 years of age (Guerreiro *et al.*, 2012). However, these gene mutations only account for approximately 30-50 % of the reported EOAD cases (Zou *et al.*, 2014), indicating the existence of mutations in additional genes that cause this aggressive form of the disease. Whole exome sequencing of EOAD patients with neither *APP* nor *PSEN1/2* mutations revealed *SORL1* as a top candidate gene. In affected individuals, seven previously unknown mutations were identified in *SORL1*, that were not retrieved in healthy individuals (Pottier *et al.*, 2012). *In silico* analysis predicted damaging effects of these newly identified mutations on SORLA expression and/or function. While two of the mutations caused a premature stop codon, the other five mutations were protein coding missense mutations (Figure 4-17A). Understanding their potentially damaging impact on SORLA function would not only validate them as novel EOAD-associated mutations, but also contribute to our understanding of SORLA's functional domains in the context of Alzheimer's disease. In line with this assumption, the G511R mutation was demonstrated to disrupt SORLA's ability to bind Aβ and to direct the peptide to lysosomes for catabolism (Caglayan *et al.*, 2014). Still, the functional significance of the N924S, N1358S and G1681D mutations remained elusive. Specifically, the N1358S mutation deemed an interesting candidate for me as it localizes to the APP binding domain of SORLA (Andersen *et al.*, 2006).

4.2.1 EOAD-associated *SORL1* mutations do not impact protein stability

To investigate the impact of the EOAD mutations on SORLA function, I introduced the N924S, N1358S and G1681D mutations into *SORL1* expression vectors using site-directed mutagenesis. Overexpression of the mutant constructs in SH-SY5Y cells demonstrated that all mutant receptor variants were expressed at similar levels as the wildtype protein, suggesting that reduced SORLA protein expression or stability is not the cause for their potential pathogenicity (Figure 4-17B).

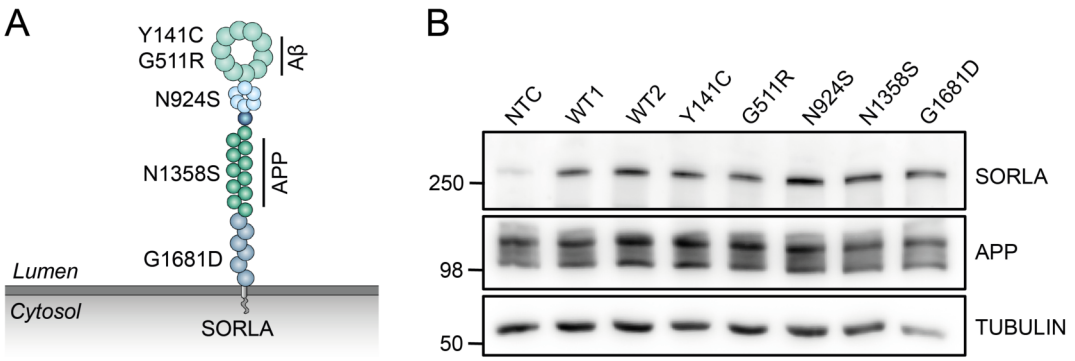

Figure 4-17: *SORL1* mutations associated with familial Alzheimer's disease do not impact protein stability. (A) The structural domains of SORLA, its interaction sites with Aβ and APP, and the localization of the disease -associated mutations in the receptor polypeptide are indicated in this schematic. (B) The familial Alzheimer's disease-associated *SORL1* mutations were introduced into a plasmid carrying the *SORL1* cDNA using site-directed mutagenesis. Wildtype (WT) and mutant variants of the receptor were transiently overexpressed in SH-SY5Y cells (stably overexpressing APP). Cells were harvested 48 h after transfection and analyzed for SORLA and APP levels using Western Blot. Detection of tubulin served as loading control. Molecular weights are given on the left in kilodaltons (kDa). NTC: non-transfected control.

4.2.2 The N1358S mutation affects SORLA's ability to reduce APP processing products

After verifying that all mutant *SORL1* constructs were expressed to the same extent as the wildtype receptor, I assessed SORLA receptor function in SH-SY5Y cell lines stably carrying either the mutant or the wildtype *SORL1* expression constructs.

Stable SH-SY5Y cells were generated by transfecting the respective expression construct encoding wildtype or mutant *SORL1* cDNA and selecting cells with integration of the expression construct into their genome by the respective antibiotic treatment. All stable SH-SY5Y cell lines also overexpressed APP to increase the level of the substrate and facilitate the detection of APP processing products in the conditioned medium. Stable cell line clones were compared for their levels of APP and SORLA using Western blot. Three clones per mutation, with APP and SORLA levels similar to the WT clone, were selected for further analysis (Figure 4-18A).

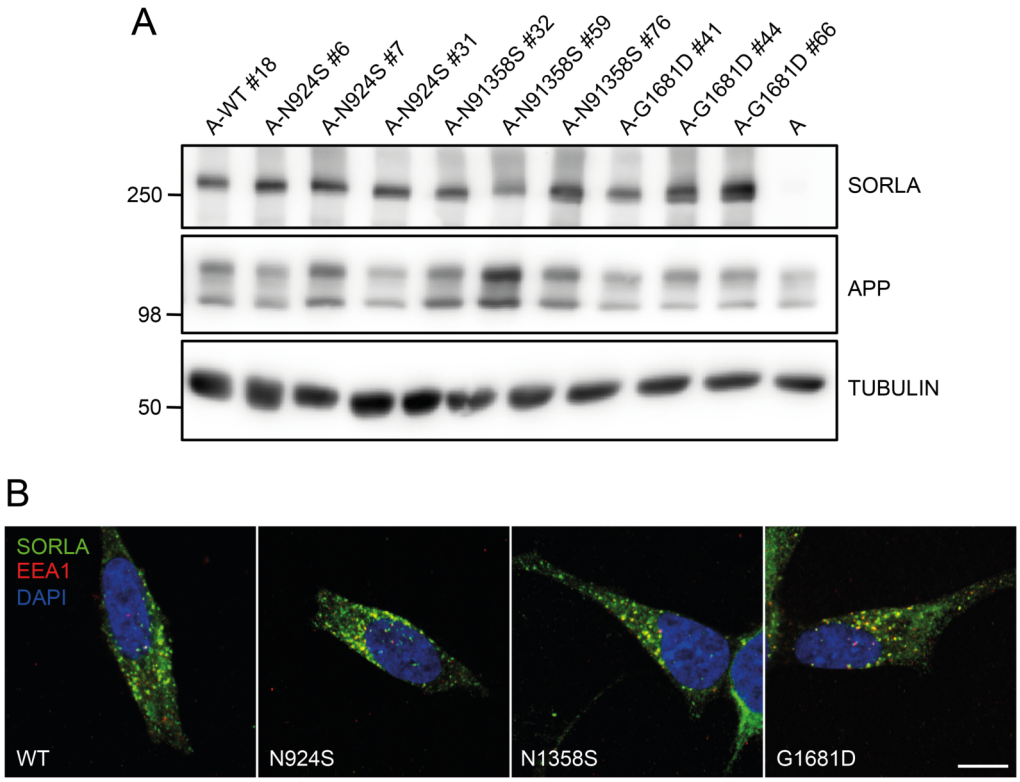

Figure 4-18: Generating SH-SY5Y cell lines stably overexpressing APP and wildtype or mutant SORLA variants. SH-SY5Y cells stably overexpressing APP were transfected with mutated *SORL1* cDNA plasmids, selected for transfected cells by Zeocin treatment, and picked as single colonies. Expanded colonies were screened by immunofluorescence staining for homogenous overexpression of APP and SORLA. (A) Levels of APP and SORLA were analyzed by Western Blot analysis. Three clones for each mutation with SORLA and APP levels similar to that of the wildtype (WT) clone were chosen for further analysis. Detection of tubulin served as loading control. Molecular weights are given on the left in kilodaltons (kDa). A, APP only overexpressing cell line. (B) Representative immunofluorescence images of SH-SY5Y cell lines stably overexpressing wildtype or the indicated mutant SORLA variants. Colocalization of the receptors with the early endosomal marker EEA1 is shown. Cell nuclei were counterstained with DAPI. Scale bar, 20 µm.

Besides impaired protein expression or stability, the EOAD-associated mutations may affect SORLA function by causing subcellular mislocalization of the receptor. SORLA carries an acidic cluster-dileucine-like motif in its cytoplasmatic tail that facilitates rapid internaliziation from the cell surface to endosomal and TGN compartments (Jacobsen *et al.*, 2001; Nielsen *et al.*, 2007). To determine whether the mutant SORLA variants are sorted to endosomal compartments, I performed immunofluorescence stainings of SORLA and the early endosomal marker EEA1 (Figure 4-18B). All receptor variants colocalized with EEA1, similar to wildtype SORLA,

suggesting that the potential pathogenic effect of these mutations is not caused by severe milocalization of the receptor.

Having established that the stable SH-SY5Y cell lines overexpressing wildtype or mutant variants of SORLA expressed SORLA and APP at silimar levels and did not demonstrate severe mislocalization of SORLA, I analyzed if SORLA function was affected by the EOAD-associated mutations by measuring APP processing products. Overexpression of wildtype SORLA reduces levels of APP processing products by two distinct mechanisms. SORLA interacts with APP and shuttles it to the TGN, where less APP is processed by both α- and β-secretases (Andersen *et al.*, 2005). Also, SORLA sorts newly produced Aβ for lysosomal degration and therefore further reduces Aβ levels (Caglayan *et al.*, 2014).

To evaluate the ability of mutant SORLA variants to impact amyloidogenic processes, I measured the amount of the APP processing products Aβ40, Aβ42, sAPPα and sAPPβ in the conditioned medium of two stable SH-SY5Y clones per mutations and compared them to the cell line expressing the wildtype receptor (Figure 4-19). I also included an SH-SY5Y cell line overexpressing only APP as a negative control for absence of SORLA activity. In line with previous reports, levels of all APP processing products in the medium decreased upon overexpression of $SORLA^{WT}$ compared to the APP only expressing cell line (Andersen *et al.*, 2005). Overexpression of $SORLA^{N924S}$ and $SORLA^{G1681D}$ resulted in a similar amount of APP processing products as observed for $SORLA^{WT}$, suggesting normal receptor activity. However, the two clones overexpressing $SORLA^{N1358S}$ showed increased Aβ40 and Aβ42 levels resembling the cell line that did not express SORLA at all (Figure 4-19A-B). Levels of sAPPα were also increased in the $SORLA^{N1358S}$ overexpressing cell line compared to the wildtype receptor condition (Figure 4-19C). Surprisingly, sAPPβ levels were not different in $SORLA^{WT}$ and $SORLA^{N1358S}$ overexpressing cells (Figure 4-19D).

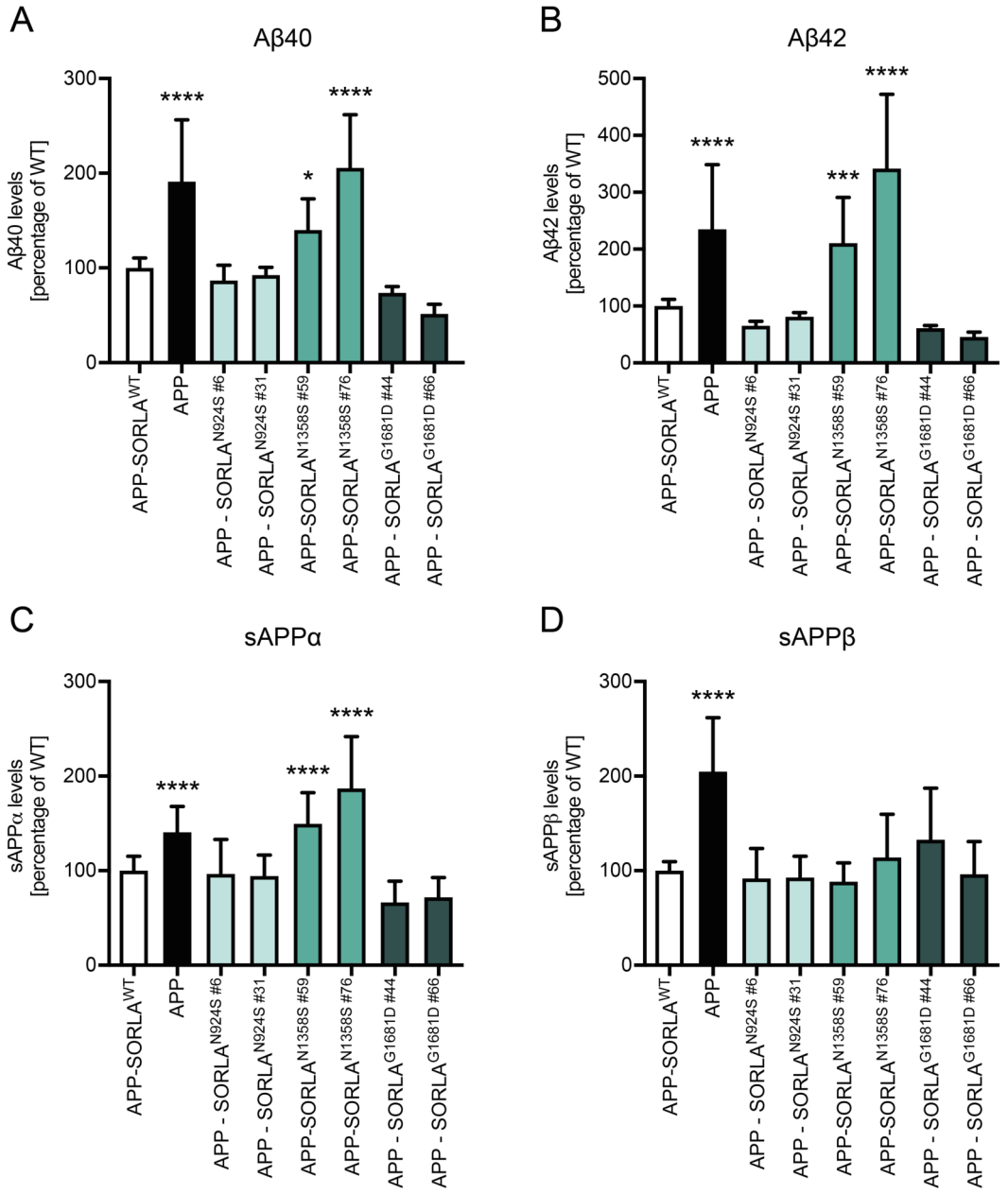

Figure 4-19: The N1358S mutation affects SORLA's ability to reduce APP processing products. (A-D) APP processing products were scored in SH-SY5Y cells stably overexpressing APP in the absence or presence of the indicated SORLA variants when cultured for 24 h at 90 % confluence. Aβ40 (A), Aβ42 (B), sAPPα (C), and sAPPβ (D) were measured in the conditioned media by ELISA and normalized to APP levels in the cell lysate. Data are shown as mean percentage of the WT ± SD levels (n=3 experiments with 2-3 biological replicates/experiment; one-way ANOVA compared to APP-SORLA^{WT}; *, p<0.05; ***, p<0.001; ****, p<0.0001).

In conclusion, the two EOAD-associated mutations N924S and G1681D did not affect SORLA expression levels, protein stability, or SORLA's ability to protect APP from being processed into the neurotoxic Aβ

peptide. However, the N1358S mutation, while also not affecting SORLA expression levels or protein stability, lead to a significant increase in both amyloidogenic and non-amyloidogenic processing products as compared to the wildtype receptor expression condition.

4.2.3 The N1358S mutation does not affect the interaction between SORLA and APP

Out of the three studied EOAD-associated *SORL1* mutations, N1358S demonstrated a loss of SORLA function as indicated by the increase in APP processing products. Interestingly, this mutation is located in the complement-type repeats domain of SORLA that represents the site for interaction with APP (Andersen *et al.*, 2006). As SORLA's ability to protect APP from being processed into the neurotoxic Aβ is dependent on SORLA interacting with APP and trafficking it to the TGN, I hypothesized that the N1358S mutation affects the interaction between SORLA and APP.

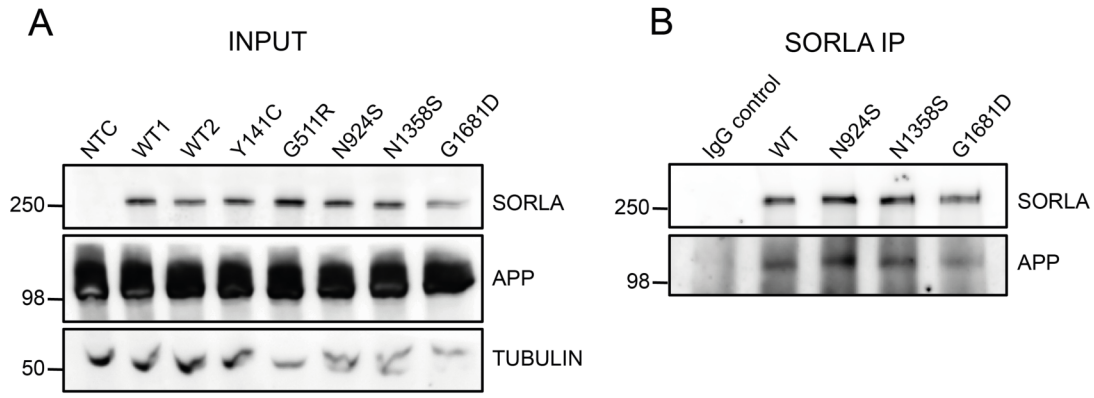

Figure 4-20: SORLA mutant variants co-immunoprecipitate with APP. (A) SORLA wildtype (WT) or mutant variants were transiently expressed in CHO cells stably overexpressing APP. Levels of SORLA and APP in the cell lysate (INPUT) were analyzed by Western Blot. Detection of tubulin served as loading control. (B) SORLA variants were immunoprecipitated (IP) with an antibody specific for the receptor and co-immunoprecipitation of APP was determined by Western Blot. Molecular weights are given on the left in kilodaltons (kDa). NTC: non-transfected control.

To test this hypothesis, I transfected the wildtype or mutant receptor variants into Chinese hamster ovary (CHO) cells stably overexpressing APP. Then, I immunoprecipitated SORLA from the cell lysates using a SORLA-specific antibody and analyzed co-immunoprecipitation of APP by Western Blotting.

APP co-immunoprecipitation was observed at a similar for all mutant SORLA variants as for the wildtype receptor, suggesting that the EOAD-mutations do not impair SORLA's ability to interact with APP (Figure 4-20).

Even though all mutant SORLA variants were able to co-immunprecipitate APP, differences in binding affinity between SORLA and APP may still explain the impact of the N1358S mutation on APP processing product levels in the stable SH-SY5Y cell lines. To determine $SORLA^{WT}$ and $SORLA^{N1358S}$ binding affinities to APP, I overexpressed the extracellular domains $SORLA^{WT}$ and $SORLA^{N1358S}$ in HEK293-EBNA cells and purified them from the conditioned medium using Ni^{2+} affinity chromatography. The purified WT and N1358S ectodomains of SORLA were immobilized on a BIAcore sensor chip for surface plasmon resonance (SPR) anaylsis and incubated with a concentration series of the ectodomain of APP as a ligand. SPR allows the calculation of binding affinities by measuring small changes in the refractive index at the sensor surface upon ligand binding (Szabo *et al.*, 1995). SPR analysis was performed by Dr. Olav Andersen (Aarhus University, Denmark). Comparative analysis of $SORLA^{WT}$ and $SORLA^{N1358S}$ incubation with APP ligand revealed no significant impact on the binding affinity between SORLA and APP by the N1358S mutation (Figure 4-21). Both $SORLA^{WT}$ and $SORLA^{N1358S}$ displayed an estimated dissociation constant (K_d) of 10-15 nM for their interaction with APP.

Taken together, both co-immunoprecipitation experiments and SPR analysis suggested that $SORLA^{WT}$ and $SORLA^{N1358S}$ bind APP with similar binding affinity. However, the amount of actual protein-protein interaction that occurs inside the cell does not only depend on the physical ability of the two proteins to interact. Many modifying factors, such as the subcellular localization of the two proteins, the pH in the subcellular compartment, in which they interact, and the presence of other interaction partners competing for binding may affect complex formation between SORLA and APP.

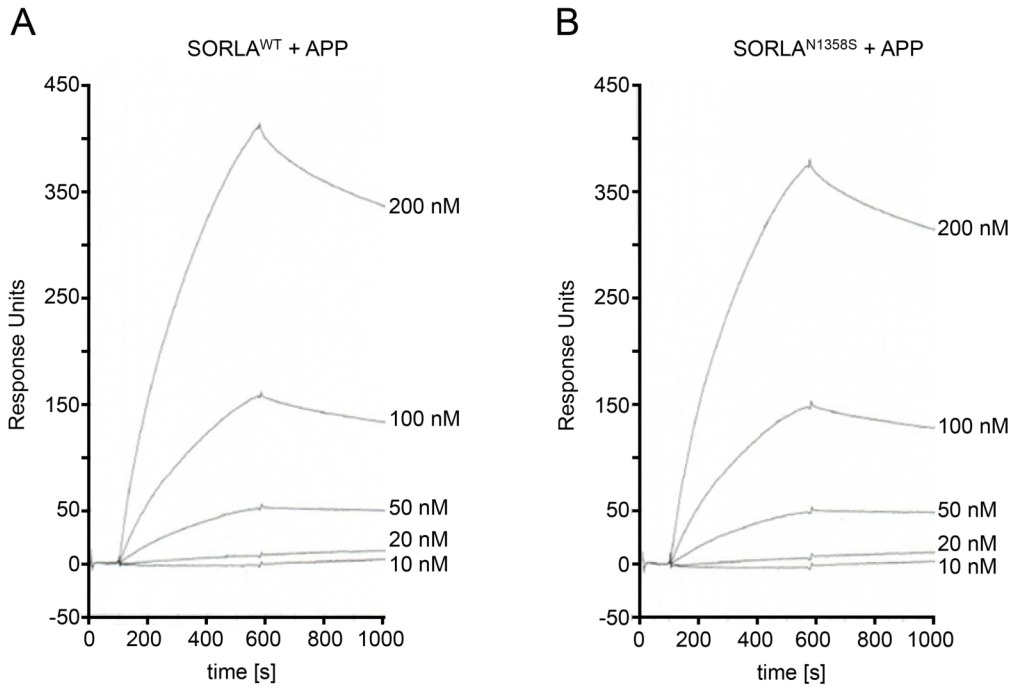

Figure 4-21: SORLA wildtype and SORLA^{N1358S} have similar binding affinities to APP. (A, B) The ectodomains of SORLA^{WT} and SORLA^{N1358S} were overexpressed in HEK 293 EBNA cells, purified from the conditioned media, and immobilized on the Biacore sensor chip for surface plasmon resonance (SPR). SPR analysis of SORLA^{WT} (A) and SORLA^{N1358S} (B) with a concentration series (10, 20, 50, 100 and 200 nM) of the ectodomain of APP as ligand revealed no significant difference in binding affinity.

To determine whether the interaction of SORLA and APP in the cellular environment was affected by the N1358S mutation, I used a fluorescence-lifetime imaging microscopy/fluorescence resonance energy transfer (FLIM/FRET) approach that is based on measuring the proximity of APP to SORLA^{WT} or SORLA^{N1358S} in intact cells (Figure 4-22). For this assay, I fused SORLA^{WT} and SORLA^{N1358S} to GFP to use them as the FRET donor fluorophore. As FRET acceptor fluorophore, I used an APP-RFP fusion construct. I transfected the GFP constructs into Cos7 cells, either alone or in combination with the APP-RFP construct. GFP molecules were excited with a laser and GFP fluorescence lifetime was recorded using a FLIM set-up. Lifetime of the GFP excitation is shortened if the donor fluorophore RFP is in close proximity (<10 nm), as the transfer of electrons to the donor is a faster process than the unaided emission of energy (Chen *et al.*, 2003). FLIM measurements and analysis were performed in collaboration with Dr. Anca Margineanu (Advanced Light Microscopy Technology Platform, MDC).

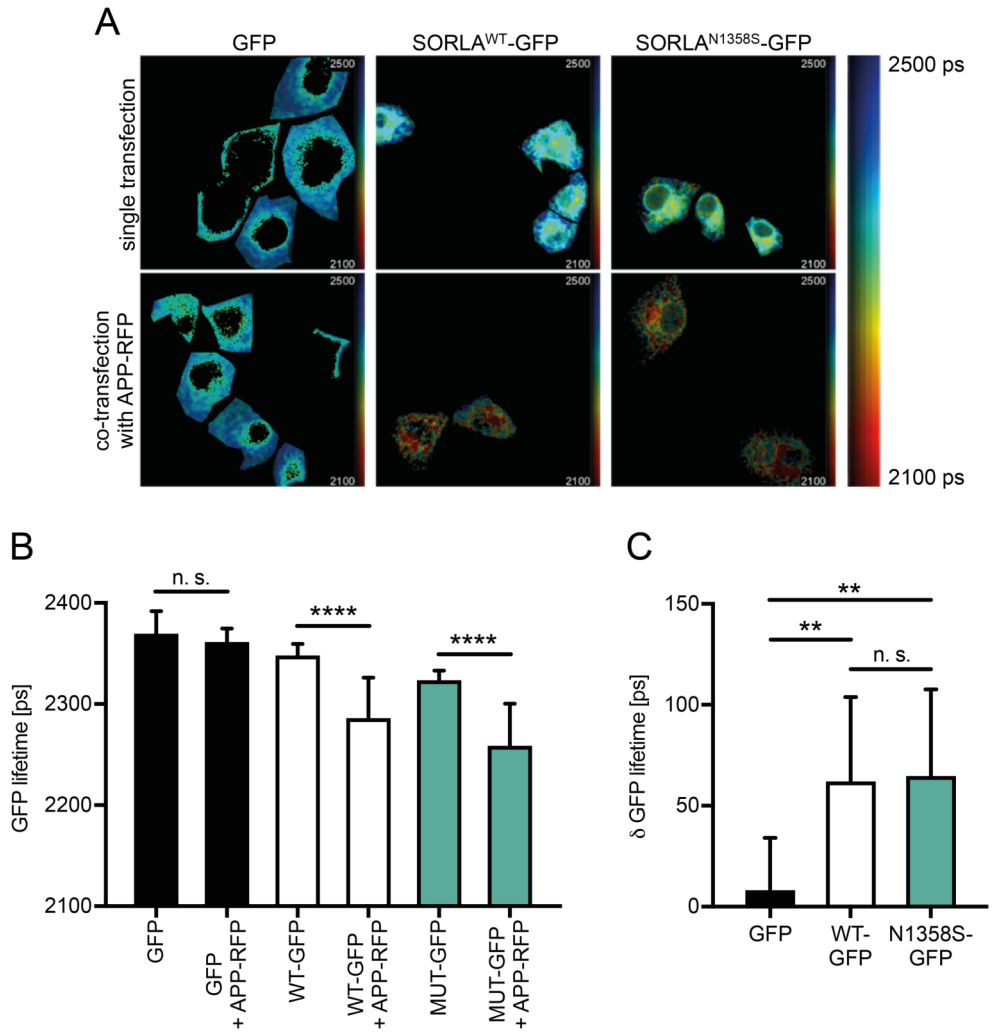

Figure 4-22: Fluorescence-lifetime imaging microscopy in intact cells shows no impact of the N1358S mutation on interaction of SORLA and APP. (A) Cos7 cells were transfected with green fluorescent protein (GFP, negative control), or SORLA wildtype or N1358S receptor fused to GFP (SORLAWT-GFP/ SORLAN1358S-GFP), either alone (first row) or in combination with APP fused to red fluorescent protein (APP-RFP) (second row). The GFP lifetime is overlayed with the fluorescence intensity microscope images. Legend for GFP lifetime (as color code) is given on the right in pico seconds (ps). GFP lifetime decreases when GFP and RFP are in close proximity to each other (< 10 nm) allowing fluorescence resonance energy transfer (FRET). (B) Quantification of the average GFP lifetime. (C) Quantification of the decrease in GFP lifetime when co-transfecting APP-RFP compared to transfecting the respective GFP construct alone. Data are shown as mean ± SD (n=1 experiment with 8-21 cells quantified per condition; one-way ANOVA; **, p<0.01; ****, p<0.0001).

In line with previous reports, APP and SORLA^{WT} formed complexes in the cell as indicated by the decrease in GFP lifetime upon co-transfection of APP-RFP (Andersen *et al.*, 2005). Quantitative comparison of the

decrease in GFP lifetime upon APP-RFP co-transfection revealed no difference between SORLA^{WT}-GFP and SORLA^{N1358S}-GFP, suggesting that, also in intact cells, the interaction between SORLA and APP is not affected by the N1358s mutation (Figure 4-22C).

4.2.4 The N1358S mutation does not block the ability of SORLA to target Aβ for lysosomal degradation

As discussed above, the impaired reduction of APP processing products in the SORLA^{N1358S} overexpressing SH-SY5Y cell lines compared to the wildtype cell line could not be explained by a loss of interaction between SORLA and APP.

Besides protecting APP from being processed by trafficking it to the TGN, SORLA reduces Aβ levels by directly binding Aβ and targeting it for lysosomal degradation (Caglayan *et al.*, 2014). To determine whether this function of SORLA is affected by the N1358S mutation, I studied Aβ degradation in SORLA^{WT} and SORLA^{N1358S} overexpressing SH-SY5Y cell lines for 3 h. To do so, I blocked de novo production of Aβ by DAPT treatment (Figure 4-23).

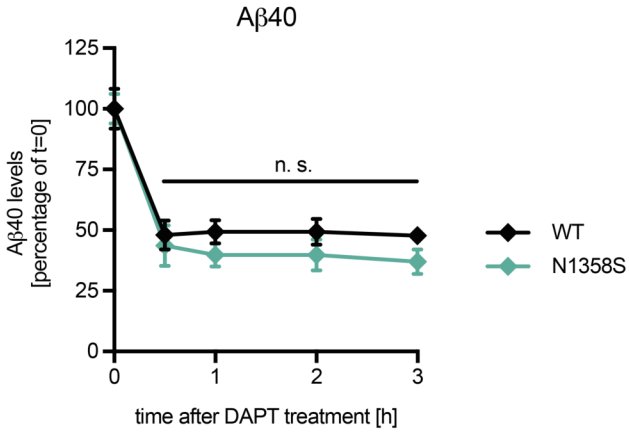

Figure 4-23: The ability of SORLA to mediate lysosomal degradation of Aβ40 is not affected by N1358S. SH-SY5Y cells stably overexpressing APP together with SORLA wildtype or N1358S (WT/N1358S) were treated with 5 µM of γ-secretase inhibitor DAPT that blocks Aβ40 production (t=0). Levels of intracellular Aβ40 were determined by ELISA at indicated time points and normalized to protein content. Data are shown as percentage of t=0 as mean ± SD (n=3-5 experiments with 3 replicates/experiment; 2way ANOVA; n. s., p>0.05).

DAPT is a γ-secretase inhibitor that blocks cellular production of Aβ. In line with previous reports, Aβ40 levels decreased around 50 % after 30 min of DAPT treatment in the $SORLA^{WT}$ overexpressing SH-SY5Y cell line due to lysosomal targeting of Aβ by SORLA (Caglayan *et al.*, 2014). Comparison of Aβ40 levels in the $SORLA^{WT}$ and $SORLA^{N1358S}$ overexpressing SH-SY5Y cell lines failed to reveal a difference in Aβ degradation rate, suggesting that the N1358S mutation does not affect SORLA's ability to target Aβ for lysosomal degradation.

4.2.5 The N1358S mutation alters subcellular trafficking of SORLA and APP

In summary, neither impaired binding of APP nor affected lysosomal targeting of Aβ could explain the increased levels of APP processing products observed in the $SORLA^{N1358S}$ overexpressing SH-SY5Y cell lines as compared to the $SORLA^{WT}$ overexpressing SH-SY5Y cell line. Thus, I assessed the subcellular distribution of $SORLA^{WT}$ and $SORLA^{N1358S}$ to determine whether the N1358S mutation altered intracellular trafficking of the receptor. Aberrant trafficking of $SORLA^{N1358S}$, which potentially leads to aberrant trafficking of APP, may explain the increase in APP processing products observed in the $SORLA^{N1358S}$ SH-SY5Y cell lines as compared the the $SORLA^{WT}$ overexpressing SH-SY5Y cell line. Conceptually, non-amyloidogenic processing into sAPPα occurs mainly at the cell surface while amyloidogenic processing into sAPPβ and the neurotoxic Aβ peptide takes place in endosomal compartments (Haass *et al.*, 2012).

To analyze intracellular trafficking of SORLA and APP in stable SH-SY5Y cell lines overexpressing $SORLA^{WT}$ or $SORLA^{N1358S}$, I co-immunostained SORLA or APP with either EEA1, which localizes to the membrane of early endosomes (Mu *et al.*, 1995), the late endosomal/TGN marker VTI1B (Kreykenbohm *et al.*, 2002), or GM130, which is mostly expressed in the *cis*-Golgi-network but also overlaps with *medial*- and *trans*-Golgi markers (Nakamura *et al.*, 1995) (Figure 4-24A). Subsequently, I analyzed the amount of colocalization as determined by the thresholded Manders' coefficient (tM1) calculating the fraction of SORLA and APP that overlaps with the cell compartment marker (Manders *et al.*, 1993).

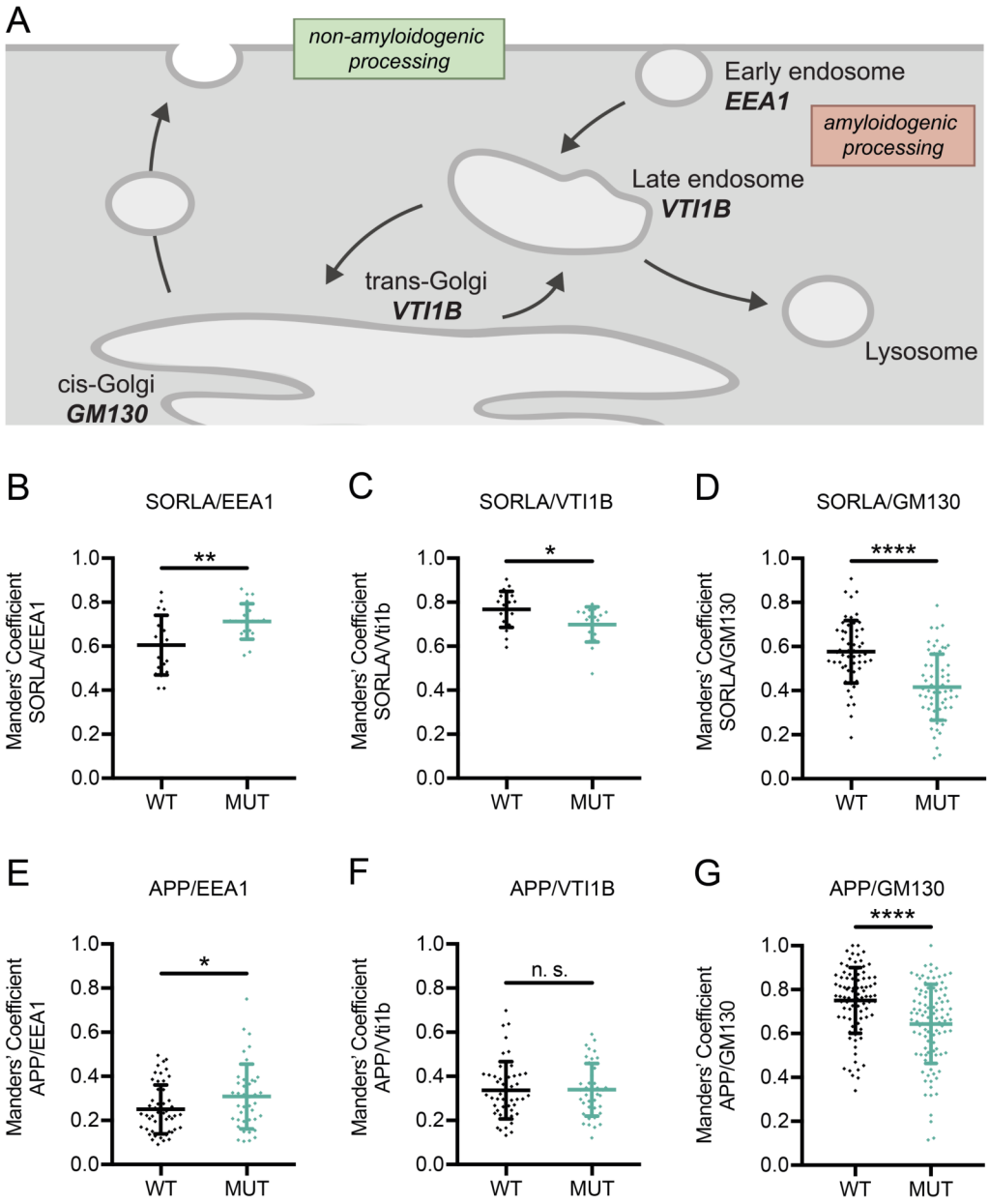

Figure 4-24: SORLA wildtype and SORLA^{N1358S} traffic differently along the endosomal pathway and Golgi complex. (A) Schematic depiction of the trafficking pathways and markers used for colocalization. EEA1 is a marker for early endosomes. VTI1B is mostly expressed in late endosomal and *trans*-Golgi compartments. GM130 is a *cis*-Golgi marker. Non-amyloidogenic processing takes place at the plasma membrane whereas amyloidogenic processing is located mainly to endosomal compartments. SORLA protects APP from processing by directing it to the *trans*-Golgi network (TGN). (B-G) Quantification of co-immunofluorescent signals for SORLA (B-D) or APP (E-G) with the indicated cell compartment marker in SH-SY5Y cells stably overexpressing APP and either SORLA wildtype (WT) or SORLA^{N1358S} (MUT). Data are shown as mean ± SD (each data point represents an immunofluorescent image containing 2-6 cells; t test; *, $p<0.05$; **, $p<0.01$; ****, $p<0.0001$).

Compared to SORLA^{WT}, SORLA^{N1358S} co-localized more with the early endosome marker EEA1 but less with the Golgi compartment markers VTI1B and GM130 (Figure 4-24B-D). APP localization showed a similar pattern, with less APP localized to the early endosome and more APP localized to the *cis*-Golgi compartment in the SORLA^{N1358S} overexpressing SH-SY5Y cell line (Figure 4-24E-G). In summary, both SORLA's and APP's subcellular localization were shifted upon overexpression of SORLA^{N1358S} instead of SORLA^{WT}, from Golgi compartments, where APP is protected from processing, to endosomal compartments, potentially explaining the increase in APP processing products observed in the SORLA^{N1358S} SH-SY5Y cell lines as compared the the SORLA^{WT} overexpressing SH-SY5Y cell line.

4.2.6 An unbiased interactome screen reveals novel interaction partners of SORLA binding differentially to SORLA^{WT} and SORLA^{N1358S}

In order to understand how the N1358S mutation may affect the subcellular localization of SORLA and, in turn, that of APP, I investigated if this mutation prevents SORLA from interacting with proteins other than APP. In collaboration with Katrina Meyer (Lab Selbach, MDC Berlin), I set up an unbiased mass spectrometry-based assay using stable isotope labeling by amino acids in cell culture (SILAC) to quantitatively compare the interactome of SORLA^{WT} and SORLA^{N1358S} (Figure 4-25).

Light or heavy isotope variants of L-arginine and L-lysine were added to amino acid deficient cell culture medium to be incorporated into newly synthesized proteins (Ong *et al.*, 2002). Stable SH-SY5Y cell lines overexpressing SORLA^{WT} or SORLA^{N1358S} were cultured in the respective isotope medium for three weeks to ensure that all proteins had been labeled. Next, SORLA and its interaction partners were immunoprecipitated (IP) from the cell lysates by coupling an antibody specific to SORLA to magnetic beads. Magnetic beads from the SORLA^{WT} IP including SORLA-interacting proteins labeled with heavy amino acids and magnetic beads from the SORLA^{N1358S} IP with interacting proteins labeled with light amino acids were combined and eluted together. The eluate was analyzed by mass spectrometry. The same approach was also performed *vice versa* - magnetic beads from the SORLA^{WT} IP with interacting proteins labeled with light amino

acids were combined with magnetic beads from the SORLA^{N1358S} IP with interacting proteins labeled with heavy amino acids - to control for labeling-specific differences such as incomplete isoptope labeling (Park *et al.*, 2012).

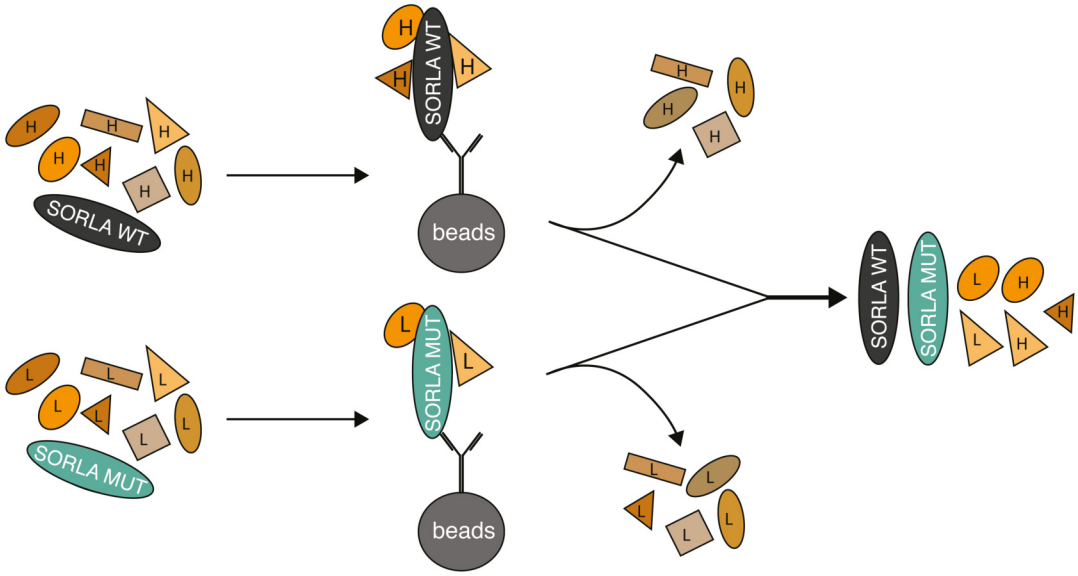

Figure 4-25: Stable isotope labeling by amino acids in cell culture (SILAC)-based approach to identify interaction partners of SORLA wildtype that fail to bind to mutant SORLA^{N1358S}. SH-SY5Y cells stably overexpressing APP and either wildtype (WT) or N1358S (MUT) SORLA were labeled with heavy (H) or light (L) SILAC medium for 3 weeks. SORLA and interaction partners were immunoprecipitated (IP) by coupling an antibody specific to SORLA to magnetic beads. Magnetic beads from WT and MUT IPs were combined and eluted together. The eluate was analyzed by mass spectrometry. Note that the schematic representation shows WT lysates only labeled with heavy and MUT lysates only labeled with light SILAC. However, the experiment was also conducted with WT cells labeled light and MUT cells labeled heavy, and only proteins enriched in the WT/MUT fraction, independent of the SILAC labeling, were considered.

To verify the specificity of the SORLA interactors, the SORLA^{WT} IP was first compared to an IP with an unspecific IgG control antibody using the same labeling strategy (Figure 4-26). Analysis of protein hits that were 1.5-fold enriched in the SORLA^{WT} IP compared to the IgG control IP (upper right quadrant), revealed known interaction partners of SORLA such as APP and SORLA itself, providing a proof of concept for the validity of the SILAC-based interactome screen.

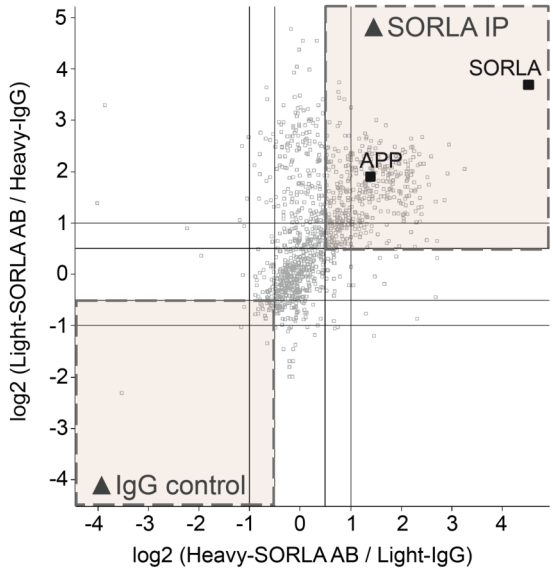

Figure 4-26: Protein hits enriched in SORLA antibody immunoprecipitation against IgG control as proof of concept of the SILAC-based interactome screen. Fold change of Heavy/Light and Light/Heavy SORLA immunoprecipitation (IP) against the non-specific IgG negative control. Enrichment is presented as $\log_2$ values. The line at 1/-1 indicates a 2-fold, the line at 0.5/-0.5 a 1.5-fold change in binding. Protein hits in the upper right quadrant are enriched in the SORLA IP compared to the IgG negative control in both SILAC-labeling set-ups. Among the hits are SORLA and its known interaction partner APP.

Subsequently, proteins enriched either in the $SORLA^{WT}$ or in the $SORLA^{N1358S}$ IP were analyzed using a 1.5-fold enrichment cutoff (Figure 4-27A). As the N1358S mutation affected SORLA trafficking along the endosome-Golgi route, novel interaction partners of SORLA with higher binding affinities to either $SORLA^{WT}$ or $SORLA^{N1358S}$ were screened for their known subcellular localization or reported influence on intracellular trafficking. In line with my hypothesis, I identified trafficking-related interaction partners binding stronger to $SORLA^{WT}$, suggesting that N1358S disrupts this interaction of the wildtype receptor. However, I also identified trafficking-related interaction partners binding stronger to $SORLA^{N1358S}$, suggesting a possible gain of function by the N1358S mutation as an alternative explanation for the observed phenoytpes (Figure 4-27B).

A

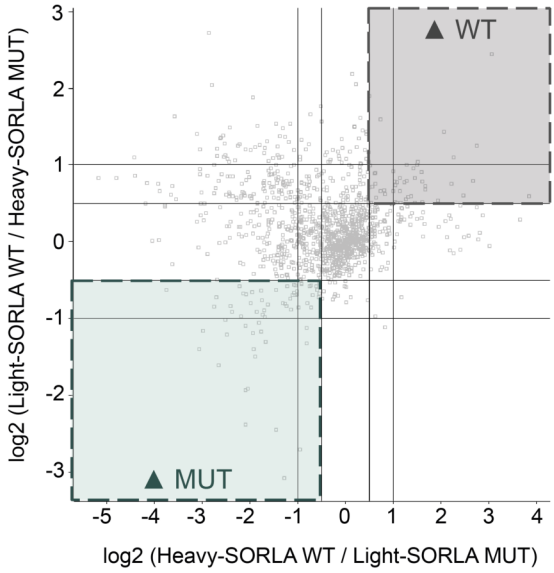

B

Enriched in WT IP	Enriched in MUT IP
Liprin-beta-1	ADAMTS19
Neuromodulin	ADAM22
Ras-related protein Rab-14	Kinectin
Semaphorin-3A	Ras-related protein Rab-5C
Thy-1 membrane glycoprotein	Synaptotagmin-4
	V-type proton ATPase subunit B2

Figure 4-27: SILAC-based interactome screen reveals novel interaction partners of SORLA binding more efficiently to SORLA wildtype or SORLA^{N1358S}. (A) Fold change of the SORLA wildtype (WT) immunoprecipitation (IP) compared to the SORLA^{N1358S} (MUT) IP. Enrichment is presented as $\log_2$ values. The line at 1/-1 therefore indicates a 2-fold, the line at 0.5/-0.5 a 1.5-fold change in binding. Protein hits in the upper right quadrant are enriched in the WT IP while protein hits in the lower left quadrant are enriched in the MUT IP in both SILAC-labeling set-ups. (B) Protein hits enriched at least 1.5-fold either in the WT or in the MUT IP and related to trafficking processes along the endosomal pathway are shown.

4.2.7 MFG-E8 is a novel interaction partner of SORLA that fails to bind SORLA^{N1358S} and is strongly increased in SORLA^{N1358S} exosomes

One of the most striking hits emerging from the SILAC-based interactome screen was the secreted glycoprotein MFG-E8 (milk fat globule epidermal growth factor 8, also known as lactadherin or SED1) (Raymond *et al.*, 2009). MFG-E8 was increased 4.0-fold in the SORLA^{WT} IP as compared to the SORLA^{N1358S} IP, suggesting a strong impairment of the interaction between SORLA and MFG-E8 by the N1358S mutation (Figure 4-28B). Furthermore, MFG-E8 was enriched 3.6-fold in the SORLA^{WT} IP compared to the IgG negative control IP, indicating that SORLA binds MFG-E8 with similarly high affinity as APP, which was enriched 3.1-fold (Figure 4-28A).

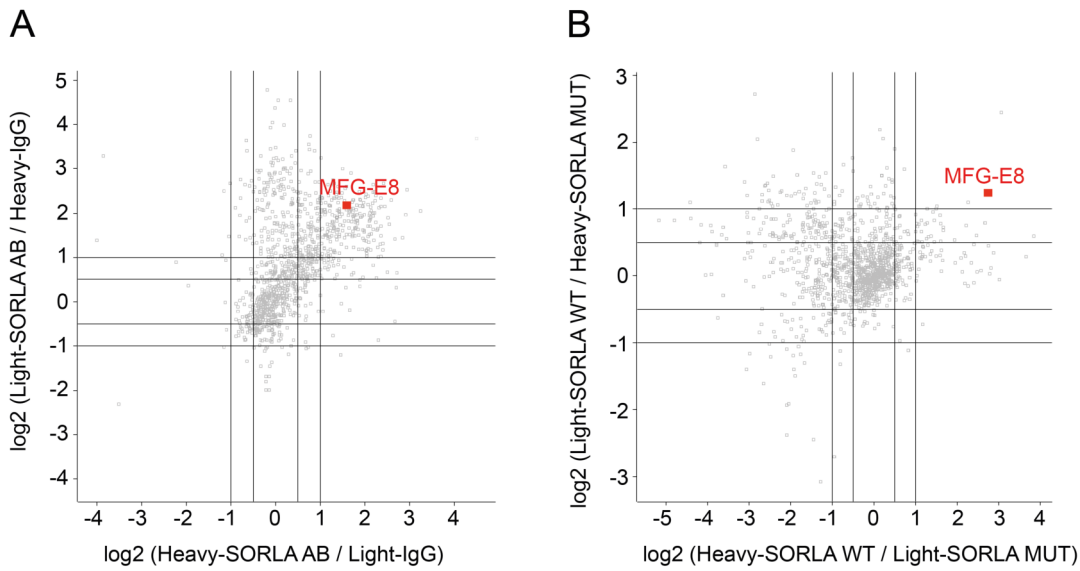

Figure 4-28: MFG-E8 is a novel interaction partner of SORLA that fails to bind SORLA^{N1358S}. (A) Enrichment plot of the SORLA immunoprecipitation (IP) against the non-specific IgG control reveals MFG-E8 as a strong interaction partner of SORLA (mean enrichment: 3.6-fold). (B) Enrichment plot of the SORLA wildtype IP against the SORLA^{N1358S} IP shows that MFG-E8 binds stronger to the wildtype (mean enrichment: 4.0-fold). This finding was replicated using a second stable SORLA^{N1358S} SH-SY5Y clone (mean enrichment: 3.1-fold, data not shown).

While MFG-E8 was first identified as a key regulator in facilitating phagocytosis of apoptotic cells (Hanayama *et al.*, 2002), it has since been implicated in a variety of cellular functions (reviewed in (Raymond *et al.*, 2009) and (Li *et al.*, 2013)). Interestingly, MFG-E8 can directly bind Aβ and mediate its clearance (Boddaert *et al.*, 2007). Also, *MFG-E8* mRNA levels are reduced in the brains of AD patients compared to healthy individuals. The loss of *MFG-E8* expression is mainly observed in glial cells in close proximity to senile plagues (Boddaert *et al.*, 2007).

To assess the functional relevance of the newly identified interaction between SORLA and MFG-E8, I measured MFG-E8 levels in the cell lysate and in the conditioned medium of primary mouse glia prepared from newborn *Sorl1*$^{+/+}$ and *Sorl1*$^{-/-}$ mice. While MFG-E8 levels in the cell lysate were not altered in the absence of SORLA, MFG-E8 levels were significantly reduced in the conditioned medium of *Sorl1*$^{-/-}$ primary mouse glia compared the wildtype condition (Figure 4-29), suggesting a potential role for SORLA as a release factor for MFG-E8.

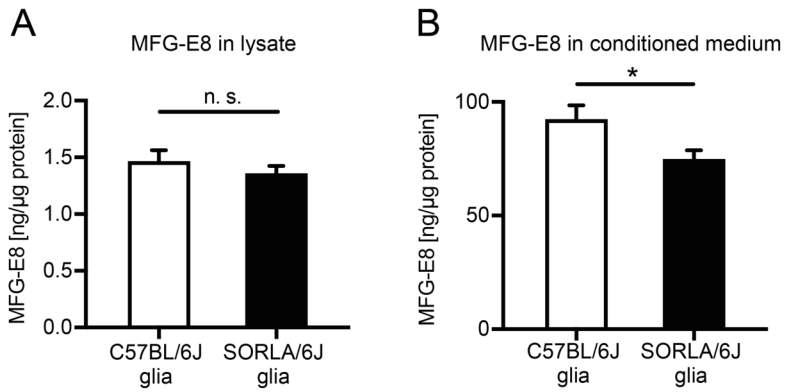

Figure 4-29: MFG-E8 levels are decreased in the conditioned medium of *Sorl1*$^{-/-}$ primary mouse glia. (A, B) Primary glia were prepared from P1 mouse cortices and seeded for conditioning of the medium after one week of culture. MFG-E8 was measured by ELISA in the cell lysate (A) and the medium conditioned for 48 h (B) and normalized to protein content in the cell lysate. Data are shown as mean ± SD (n=1 experiment with 3 biological replicates shown; representative for a total of 3 independent experiments performed; t test; *, $p<0.05$; n. s., $p>0.05$).

MFG-E8 is secreted in association with small membrane vesicles, called exosomes, and the number of secreted exosomes is determined by *MFG-E8* expression levels (Oshima *et al.*, 2002). As Aβ can also be secreted in exosomes (Rajendran *et al.*, 2006), I determined if *Sorl1*$^{-/-}$ deficiency affected the specific release of MFG-E8 or had a more global effect on exosomes secretion. For this purpose, I used ultracentrifugation to isolate exosomes from the conditioned medium of stable SH-SY5Y cell lines overexpressing APP alone or together with SORLA^{WT} or SORLA^{N1358S}. Western Blot analysis of the exosomal preparations for ALIX, a common exosome marker (Théry *et al.*, 2006), suggested that the overall number of secreted exosomes was not changed upon overexpression of SORLA^{WT} or SORLA^{N1358S} (Figure 4-30A). However, the amount of MFG-E8 was strongly increased in the exosomal fraction of SORLA^{N1358S} compared to SORLA^{WT} overexpressing cells. To verify the identity of the MFG-E8 band observed by Western Blot analysis, I also measured the amount of MFG-E8 in the exosomal preparations by ELISA. MFG-E8 levels in exosomes of SORLA^{N1358S} overexpressing cells were twice as high as in SORLA^{WT} exosomes, confirming the specific increase of MFG-E8 in SORLA^{N1358S} exosomes as compared to SORLA^{WT} exosomes (Figure 4-30B).

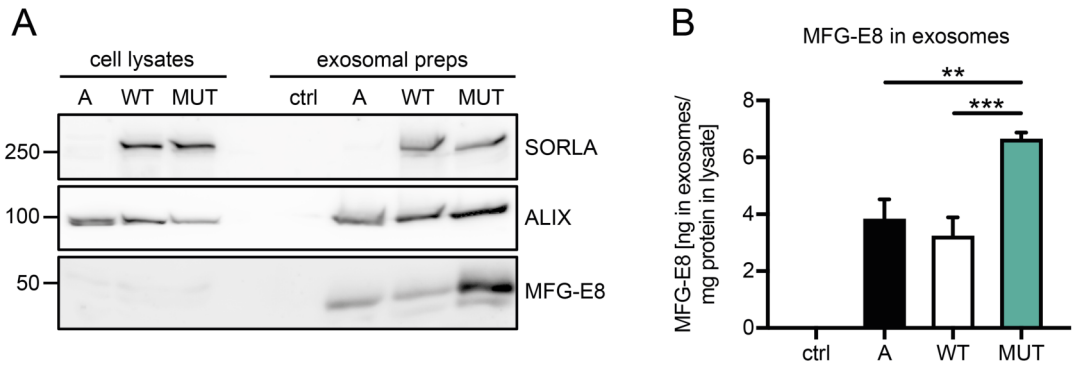

Figure 4-30: MFG-E8 levels are strongly increased in SORLA^{N1358S} exosomes. (A) SH-SY5Y cells stably overexpressing APP in the absence or presence of SORLA wildtype or SORLA^{N1358S} were cultured for 4 days. Exosomes were purified from the cleared conditioned media by ultracentrifugation, lysed, and analyzed for levels of SORLA, MFG-E8, and exosome marker ALIX. Molecular weights are given on the left in kilodaltons (kDa). Results are representative of three independent experiments. (B) Exosomal preparations were also analyzed by MFG-E8 ELISA. Data are shown as mean ± SD (n=1 experiment with 3 biological replicates given; representative for a total of 3 independent experiments; one-way ANOVA; **, $p<0.01$; ***, $p<0.001$).

In conclusion, MFG-E8 is a previously unknown interaction partner of SORLA and the interaction is affected by the EOAD-associated N1358S mutation in *SORL1*. Although more experiments are needed to further elucidate the interaction between SORLA and MFG-E8, my data suggest a novel role of SORLA in sorting MFG-E8 for exosome secretion. As both SORLA and MFG-E8 directly interact with Aβ (Boddaert *et al.*, 2007; Caglayan *et al.*, 2014), the newly identified interaction between SORLA and MFG-E8 may also indicate another mechanism by which SORLA reduces Aβ levels in the brain that is impaired by the N1358S mutation.

5 DISCUSSION

Almost 80 % of Alzheimer's disease risk is determined by genetic factors (Gatz *et al.*, 2006). Identifying the involved genes and causative mutations for EOAD and LOAD will not only fundamentally improve our knowledge of these diseases but also allow for an early genetic risk assessment of individuals. As the pathogenic mechanisms of Alzheimer's disease, such as the accumulation of Aβ peptides, start decades before patients experience first symptoms of memory loss, an early risk assessment is crucial for developing successful preventive treatment (Selkoe and Hardy, 2016).

The recent technological advances in DNA sequencing have greatly facilitated the identification of genetic variants that correlate with the occurrence of complex diseases including LOAD. Particularly, the implementation of GWAS has produced thousands of genetic variants that are associated with complex human diseases (Gallagher and Chen-Plotkin, 2018). However, due to the abundance of novel associations, so far only few genetic variants have actually been validated in their functional relevance. Analyzing the genetic variants found in GWAS is often difficult due to their relatively small effect sizes. Also, SNPs may be clustered in genetically linked haplotypes and GWAS often lack the statistical power to reliably determine the causal variant (Cooper and Shendure, 2011).

In contrast, EOAD-causing mutations conceptually have large effect sizes as they lead to a more severe form of the disease. However, due to their rarity, they cannot be identified by GWAS (Auer and Lettre, 2015). Instead, the identification of these rare EOAD-causing mutations requires exome or whole genome sequencing of affected individuals and their

families, and comparison to a pool of healthy individuals. Obviously, not every rare mutation in affected individuals is causative of the disease, so functional validation of the found mutations is crucial as well.

Both GWAS and exome sequencing studies have implicated members of the VPS10P domain receptor family in a range of neurological and metabolic disorders. However, most of these associated genetic variants had not been functionally validated in cell or mouse models. I was particularly interested in the proposed transcriptional regulation of *SORT1* by a non-coding SNP, and in the newly identified EOAD-associated missense mutations in *SORL1*. While coding non-sense or frame-shift mutations are presumed to cause a loss of protein expression, the effect of non-coding or coding missense mutations is more difficult to evaluate. *In silico* predictions can indicate if a genetic variant might have a damaging effect on protein function, but does not replace the functional analysis in a cellular context. In the end, the functional analyses of non-coding and coding missense variants is very important as they inform us about the transcriptional control and the functional domains of the protein of interest.

How to approach the functional characterization of an associated genetic variant depends on its predicted effect size in the relevant cell type. The EOAD-associated mutations in *SORL1* are suspected to have rather high effect sizes if they confer a high penetrance of EOAD. While it is possible that coding missense mutations affect the regulation of transcription, splicing processes or translation efficiency (Cartegni *et al.*, 2002; Caglayan *et al.*, 2012), they likely alter the conformation of SORLA's structural domains and the binding of interaction partners. These mechanisms can be assessed by overexpressing mutant *SORL1* constructs in the established neuronal cell line SH-SY5Y.

In contrast, to assess whether the *SORT1* risk variant regulates *SORT1* transcription in hepatocytes and/or neurons, I needed fully differentiated cell to recapitulate the endogenous machinery of transcription factors in both cell types. As a further complication, the proposed C/EBP recognition site, which is created by the minor variant, is absent in the mouse genome, limiting the functional analysis of this SNP to human cells. Finally, as minor variant carriers of the proposed functional SNP also harbor the

minor variants of all genetically linked SNPs, the use of gene-editing tools was necessary to unambiguously identify rs12740374 as the functional SNP. Modeling endogenous or genome-edited human genetic variants in fully differentiated human cell types has only recently become feasible by the progress made in the fields of human iPSCs technologies and genome-editing techniques.

5.1 *SORT1* risk variants in neurons and hepatocytes

5.1.1 Human iPSCs as a model to study cardiovascular and neurodegenerative diseases

The groundbreaking discovery that adult somatic cells can be reprogrammed into a pluripotent state by forced overexpression of the four transcription factors *OCT4*, *SOX2*, *c-MYC*, and *KLF4* has revolutionized the way we can model human genetic variants *in vitro* (Takahashi *et al.*, 2007; Yu *et al.*, 2007). While this relatively new technology still comes with some caveats, including cell line variability and genomic instability (Hockemeyer and Jaenisch, 2016; Yoshihara *et al.*, 2017), it provides a unique set of advantages compared to traditional models such as transgenic animals, immortalized cell lines, or primary human tissue. These advantages particularly apply to human disease modeling that depends on cell types that cannot be easily isolated and maintained in culture such as mature neurons or pancreatic β-cells (Ghaffari *et al.*, 2018).

While overexpression studies in transgenic mouse models and established cell culture systems studies offer valuable clues concerning protein function, genetic variants associated with complex diseases mostly have subtle effects that are highly cell type dependent. Human iPSCs are primary cell lines and therefore carry all genetic variants and express all genes at endogenous levels. As such, they provide insights into the effects of one genetic variant against an entire endogenous genetic background for disease-relevant phenotypes. In addition, iPSCs have the capacity to self-renew and can be propagated under maintenance conditions for many passages, making them an ideal target for genome-editing techniques such as TALENs or CRISPR-Cas9. Patient-derived or edited cell lines can then be subjected to differentiation into the desired disease-relevant cell type. In the

recent years, hundreds of differentiation protocols have been published, including but not limited to neural stem cells, several neuronal subtypes, cardiomyocytes, hepatocytes, cardiomyocytes, and pancreatic β-cells (Shi *et al.*, 2017).

To analyze *SORT1* risk loci in neurons and hepatocytes, I established iPSC culture, TALENs and CRISPR gene-editing tools, and differentiation into mature cortical neurons and hepatocytes using published protocols. Human iPSC-derived cortical neurons and hepatocytes expressed mature cell specific markers (Figure 4-2 and Figure 4-13) and upregulated *SORT1* expression as compared to iPSCs (Figure 4-16). To validate sortilin receptor function in my model system, I generated a *SORT1* deficient iPSC line (Figure 4-3) and analyzed PGRN metabolism in iPSC-derived cortical neurons with or without *SORT1* expression. Sortilin is an endocytic receptor for PGRN that rapidly delivers PGRN to the lysosomes for degradation (Hu *et al.*, 2010). Extracellular PGRN levels were increased about 4-fold in *SORT1* KO as compared to *SORT1* WT iPSC-derived cortical neurons (Figure 4-5). This is consistent with the results of a recent study aiming at inhibiting *SORT1* expression in order to rescue the reduced extracellular PGRN levels in a FTLD patient-derived iPSC line (Lee *et al.*, 2014). Suppression of *SORT1* gene expression in iPSC-derived neurons through treatment with the small molecule MPEP lead to a 5-fold increase in extracellular PGRN levels, similar to my observations in *SORT1* deficient iPSC-derived neurons. These data substantiate the value of iPSC-derived neurons as a model to study neuronal activities of sortilin.

5.1.2 *SORT1* expression levels in human hepatocytes are determined by the risk variant rs12740374

Several genome-wide associations studies have confirmed the association of a risk locus upstream of the *SORT1* gene (rs646776) with hypercholesterolemia and risk of myocardial infarction (Samani *et al.*, 2007; Kathiresan *et al.*, 2008, 2009; Teslovich *et al.*, 2010). Using expression quantitative trait locus (eQTL) analysis, the minor variant of this SNP was correlated with an increased *SORT1* expression in the liver (Musunuru *et al.*, 2010). However, rs646776 is highly linked to several neighboring SNPs, some of which were also associated with hypercholesterolemia. Whether one

of the SNPs in this haplotype block directly induces the change in *SORT1* gene expression seen in mature hepatocytes remained unclear. The rs12740374 SNP deemed a promising candidate as its minor variant creates a C/EBP consensus site (Musunuru *et al.*, 2010). However, finding the right model system to functionally validate this SNP was challenging. First, rs12740374 is not present in the mouse genome, limiting the functional analysis to human cell types. Established human hepatoma cell lines exhibit karyotype abnormalities and often do not reliably represent mature hepatocyte biology (Guguen-Guillouzo and Guillouzo, 2010). Primary human hepatocytes can be isolated, but only cultured for a few days (Guguen-Guillouzo and Guillouzo, 2010). Also, they carry all genetic variants linked of rs646776. In contrast, the ability of human iPSCs to self-renew in culture allows the use of genome-editing tools to introduce and thus unambiguously identify the causal genetic variant.

Here, I analyzed *SORT1* gene expression using minor or major donor iPSC lines as well as genome-edited iPSC lines to assess both whether the risk locus predicts *SORT1* expression levels in hepatocytes in general and whether rs12740374 is indeed the causal variant. All iPSC lines gave rise to mature hepatocytes expressing the hepatocyte-specific markers HNF4A, CYP3A and APOA2 at similar levels as primary human hepatocytes (Figure 4-13). Albumin levels in the differentiated iPSC-derived hepatocytes were slightly lower than in primary human hepatocytes. Also, the immature hepatocyte marker *AFP* (*α-fetoprotein*) was strongly expressed after 30 days of hepatic differentiation, suggesting that the culture still contained some immature hepatocytes. Longer differentiation times did not lead to a downregulation of *AFP* expression in my hands. The remaining immaturity of iPSC-derived hepatocytes as indicated by high *AFP* expression levels was also reported by other studies and seems to be a common problem of current hepatocyte differentiation protocols (Si-Tayeb *et al.*, 2010; Touboul *et al.*, 2010; Schwartz *et al.*, 2014). The hepatocyte differentiation efficiency also varied between the iPSC lines (Figure 4-15), a problem that may be solved by FACS sorting for hepatocyte-specific markers as done in a recent study (Warren *et al.*, 2017). Due to the difficulties in reliably differentiating all iPSC lines into mature hepatocytes, the *SORT1* expression analysis is so far

based on one preliminary experiment each and needs further verification. Still, in these experiments, *SORT1* expression was increased in minor variant carriers for both the donor and the genome-edited lines as compared to controls carrying the major SNP variant. These initial findings not only suggest this risk locus as a major regulator of *SORT1* expression in hepatocytes, but more specifically also indicates that rs12740374 is indeed the causal genetic variant.

While my work was in progress, other studies also investigated the functionality of the *SORT1* risk locus in hepatocytes. Two independent studies found that donor iPSC-derived hepatocytes carrying the minor SNP variant expressed higher levels of *SORT1*. However, both studies observed an increase in transcript levels that was significantly lower (1.3-fold and 1.7-fold) as compared to the increase predicted by the eQTL data (4-fold increase) (Musunuru *et al.*, 2010; Warren *et al.*, 2017; Wang *et al.*, 2018). The weak increase in *SORT1* expression in minor variant carriers was attributed to the immaturity of the iPSC-derived hepatocyte cultures. In one of the studies, CRISPR-Cas9 was used to delete rs12740374 in homozygous minor variant carriers using NHEJ which lead to a subtle decrease in *SORT1* expression (Warren *et al.*, 2017). In my hands, iPSC-derived hepatocytes showed a 3.3-fold *SORT1* induction for the minor variant in the donor cells and 5.4-fold in genome-edited cells when normalized to *B2M* (Figure 4-14 and Figure 4-15), recapitulating the eQTL prediction.

While hepatocyte differentiation protocols clearly need further optimization to generate homogenous, mature iPSC-derived hepatocyte cultures (Schwartz *et al.*, 2014), they provide a useful model system to functionally analyze genetic variants found in association studies. Specifically, I could confirm that the *SORT1* risk locus predicts *SORT1* expression levels in mature hepatocytes. Also, the minor variant of rs12740374, which creates a C/EBP consensus site, indeed induces hepatic *SORT1* expression. The association of rs646776 with hypercholesterolemia and risk of myocardial infarction likely resulted from the genetic linkage of rs646776 and rs12740374, highlighting the importance to functionally validate genetic variants found in GWAS.

5.1.3 Cardiovascular *SORT1* risk locus does not affect sortilin levels in neurons

While sortilin fulfills important functions in regulating lipoprotein secretion in the liver, it is actually a predominantly neuronal receptor with *SORT1* mRNA expression levels 15-fold higher in the brain than in the liver (Fagerberg *et al.*, 2014). As the major neuronal receptor for APOE and as an endocytic receptor for PGRN, sortilin plays an important role in molecular mechanisms underlying both Alzheimer's disease and frontotemporal lobar degeneration (Hu *et al.*, 2010; Carlo *et al.*, 2013). Thus, genetic variants potentially regulating *SORT1* expression in the brain may have important implications for neuropathological processes.

To determine whether rs12740374 also predicts *SORT1* expression in the brain, I assessed the functional relevance of this SNP in human iPSC-derived neurons. Using donor iPSC lines with all linked SNPs as well as the genome-engineered and parental cell lines, I again was able to distinguish general functionality of the risk locus from the specific causality of rs12740374 in neurons. The neuronal differentiation protocol using forced overexpression of the neuronal transcription factor NGN2 efficiently and reliably generated mature cortical neurons from all iPSC lines. By selecting for NGN2-transduced cells by puromycin treatment, all cells in the cultures expressed the neuronal markers TUJ1 and MAP2 (Figure 4-2). For the analysis of neuronal *SORT1* gene expression I used human-specific qRT-PCR probes to prevent scoring of *Sort1* transcripts from mouse glia, which I seeded on the differentiating neurons to support of neurite outgrowth. Human *SORT1* mRNA expression levels were not significantly different between minor and major variant carrying iPSC-derived neurons using both donor and genome-edited cell lines (Figure 4-11 and Figure 4-12). I analyzed *C/EBPα* mRNA expression levels in both neurons and hepatocytes and found that, although *C/EBPα* is upregulated in both neurons and hepatocytes compared to iPSCs, the iPSC-derived neurons expressed significantly less *C/EBPα* as compared to hepatocytes (Figure 4-16). This difference may explain why the minor variant induces an increase in *SORT1* expression in hepatocytes but not in neurons.

C/EBPα is a transcription factor that is mostly studied in hepatocytes

but is also widely expressed in the brain (Zhang *et al.*, 2014). Furthermore, the consensus site produced by the minor variant of the *SORT1* SNP is not only recognized by C/EBPα, but also by five other members of the C/EBP gene family, most of which are also expressed in neurons (Osada *et al.*, 1996; Zhang *et al.*, 2014). While *SORT1* expression was not regulated by rs12740374 in the excitatory cortical neurons that I analyzed here, it is possible that the SNP predicts *SORT1* expression levels in a different neuronal subtype. Also, the induction of *SORT1* mRNA expression may only be observable upon activation of C/EBP expression. This mechanism was illustrated by a recent study analyzing SNPs in the *SORL1* gene associated with Alzheimer's disease (Young *et al.*, 2015). A difference in *SORL1* expression levels between minor and major variant carriers was only observed after upregulation of *SORL1* expression by BDNF treatment (Young *et al.*, 2015). Finally, members of the C/EBP family can act as heterodimers with other basic-region leucine zipper (bZIP) transcription factors (Nerlov, 2007). Consequently, the induction of *SORT1* expression in the liver may not only depend on C/EBPα but also on other transcription factors that may be absent in neurons. Potentially, proteomics of isolated chromatin segments (PICh) could identify endogenous cell type specific C/EBP interacting transcription factors that are involved in regulating *SORT1* mRNA expression. Further elucidating these mechanisms in iPSC-derived hepatocytes and neurons will help understanding how *SORT1* expression is regulated in the brain.

Finally, *SORT1* expression in the brain may be regulated by different genetic variants than in the liver. While no other SNP has been functionally characterized in neurons yet, rs649281, another non-coding SNP upstream of the *SORT1* gene, deems an interesting candidate, as eQTL data on frontal cortex and cerebellum associated this SNP with *SORT1* mRNA levels (Carrasquillo *et al.*, 2010).

5.2 EOAD-associated mutations in *SORL1*

After the initial discovery of EOAD-causing mutations in genes encoding for APP, PSEN1, and PSEN2 twenty years ago, no additional genes were identified that harbor EOAD-causative mutations. However, the described mutations in *APP*, *PSEN1,* and *PSEN2* only account for 30-50 % of EOAD cases (Zou *et al.*, 2014) arguing for the existence of additional familial EOAD gene.

Recently, several studies have found potentially damaging *SORL1* mutations in EOAD families consistent with autosomal-dominant inheritance (Pottier *et al.*, 2012; Nicolas *et al.*, 2016; Verheijen *et al.*, 2016; Thonberg *et al.*, 2017; Gómez-Tortosa *et al.*, 2018). However, many of these novel EOAD-associated *SORL1* mutations have not been functionally characterized in mouse or cell models yet. The majority of these associations were based merely on the fact that they were not found in healthy controls and that *in silico* analysis predicted damaging effects on SORLA protein function. Furthermore, co-segregation analysis of the EOAD-associated *SORL1* mutations was so far only confirmed for a few mutations (Pottier *et al.*, 2012; Verheijen *et al.*, 2016; Gómez-Tortosa *et al.*, 2018). Furthermore, sequencing of healthy individuals revealed that rare missense *SORL1* mutations were also observed in non-affected individuals, albeit at a lower frequency than in EOAD patients (Nicolas *et al.*, 2016; Verheijen *et al.*, 2016). Non-sense or frameshift mutations on the other hand have so far only been identified in EOAD patients (Verheijen *et al.*, 2016), indicating that *SORL1* haploinsufficiency is indeed causative of EOAD. Several studies have demonstrated that EOAD-associated non-sense and frameshift *SORL1* mutations lead to nonsense-mediated mRNA decay and therefore to a reduce in *SORL1* expression levels (Pottier *et al.*, 2012; Nicolas *et al.*, 2016; Verheijen *et al.*, 2016).

While only some of the numerous rare missense *SORL1* mutations identified in EOAD patients may be causative of EOAD, the ones that do affect SORLA protein function potentially shed more light on SORLA's role in Alzheimer's disease-related processes than the non-sense mutations. This is best exemplified by the functional characterization of the G511R mutation, which was found in the initial report of *SORL1* mutations in EOAD patients

and locates to the VPS10P domain of SORLA (Pottier *et al.*, 2012). For this mutation cosegregation with EOAD was confirmed in a second family member. The G511R mutation was demonstrated to disrupt SORLA's ability to bind newly synthesized Aβ peptides and sort them to the lysosomes for catabolism causing an increase in extracellular Aβ accumulation (Caglayan *et al.*, 2014).

The three additional EOAD-associated mutations that I analyzed in my thesis project were also identified in the initial report of *SORL1* mutations in EOAD patients, but lacked pedigree analysis as DNA samples from affected relatives were not available (Pottier *et al.*, 2012). The fact that two of the three mutations in my study did not affect SORLA protein function indicates that many false-positive *SORL1* mutations were identified in EOAD patients. Ultimately, distinguishing random *SORL1* variants found in EOAD patients from actual causative EOAD mutations will be essential but can only be accomplished by sequencing many more healthy individuals, especially non-affected relatives of EOAD patients to exclude non-causative variants, and by thorough functional characterization of the EOAD-associated *SORL1* mutations in vitro.

5.2.1 The N1358S mutation affects subcellular trafficking of SORLA and APP

To functionally characterize the N924S, N1358S, and G1681D mutations identified in EOAD families consistent with autosomal-dominant inheritance (Pottier *et al.*, 2012), I generated stable SH-SY5Y cell lines overexpressing APP and the mutant SORLA variants (Figure 4-18). All three mutant SORLA variants were expressed at similar levels as the wildtype receptor, indicating that these mutations neither cause a decrease in transcription or translation efficiency nor an increase of degradation due to misfolding of the receptor (Figure 4-17). Subsequently, I analyzed SORLA receptor functions by measuring APP processing products in the conditioned medium of the stable SH-SY5Y cell lines overexpressing APP and the mutant SORLA variants. Out of the three analyzed EOAD-associated *SORL1* mutations only N1358S demonstrated an increase in extracellular Aβ and sAPPα levels compared to cells expressing the wildtype receptor (Figure 4-19A-C). In contrast, sAPPβ levels secreted by the $SORLA^{N1358S}$ and $SORLA^{WT}$ overexpressing SH-SY5Y

cell lines were comparable (Figure 4-19D). This finding was unexpected as SORLA's ability to sort APP to the TGN protects APP from being processed by α, β, and γ-secretases and thus lowers the levels of all APP processing products (Andersen *et al.*, 2005). If SORLA function was to be impaired, one would therefore expect that also sAPPβ levels are increased in the $SORLA^{N1358S}$ compared to the $SORLA^{WT}$ overexpressing SH-SY5Y cell line. However, SORLA fulfills multiple functions relevant for amyloidogenic processes. It sorts APP retrogradely to the TGN, it directs Aβ to the lysosomes, and it inhibits dimerization of APP, the preferred substrate of secretases (Schmidt *et al.*, 2007, 2011; Caglayan *et al.*, 2014). It was therefore conceivable that a mechanism of SORLA action specifically relevant for Aβ accumulation was affected by the N1358S mutation.

After having determined that the N1358S mutation affects SORLA function as indicated by the increase in APP processing products, I next aimed on investigating how exactly this mutation alters the functionality of the sorting receptor. As N1358S is located in the cluster of complement-type repeats, which is SORLA's site of interaction with APP (Andersen *et al.*, 2006), my first hypothesis was that this mutation affects binding of APP. Thus, I compared the interaction of $SORLA^{WT}$ and $SORLA^{N1358S}$ with APP using several different methods, including Co-IP (Figure 4-20), BiaCore (Figure 4-21), and a FLIM/FRET-based proximity assay (Figure 4-22). In all assays, APP binding to $SORLA^{N1358S}$ appeared unaltered as compared to $SORLA^{WT}$. It still remains to be tested whether N1358S affects the pH dependency of the interaction of SORLA and APP as differences in binding affinities may, for instance, only be observable at the low pH present in endosomes. Also, so far little is known on how SORLA controls the dimerization of APP. It is possible that $SORLA^{N1358S}$ loses the ability to prevent dimerization of APP and thereby protects APP less efficiently from being catalytically processed.

An alternative explanation for the increase in Aβ levels in $SORLA^{N1358S}$ overexpressing cells was suggested by my data on the subcellular trafficking of SORLA and APP in $SORLA^{N1358S}$ and $SORLA^{WT}$ overexpressing SH-SY5Y cell lines. In these studies, I co-stained SORLA and APP in both cell lines with the early endosomal marker EEA1, the TGN

marker VTI1B, and the Golgi marker GM130, and analyzed the amount of colocalization to identify the subcellular localization of SORLA and APP in these cells. In the SORLA^{N1358S} overexpressing cell line, the localization of both SORLA and APP was shifted towards endosomal instead of TGN/Golgi compartments as compared to the SORLA^{WT} overexpressing cell line (Figure 4-24 and Figure 5-1).

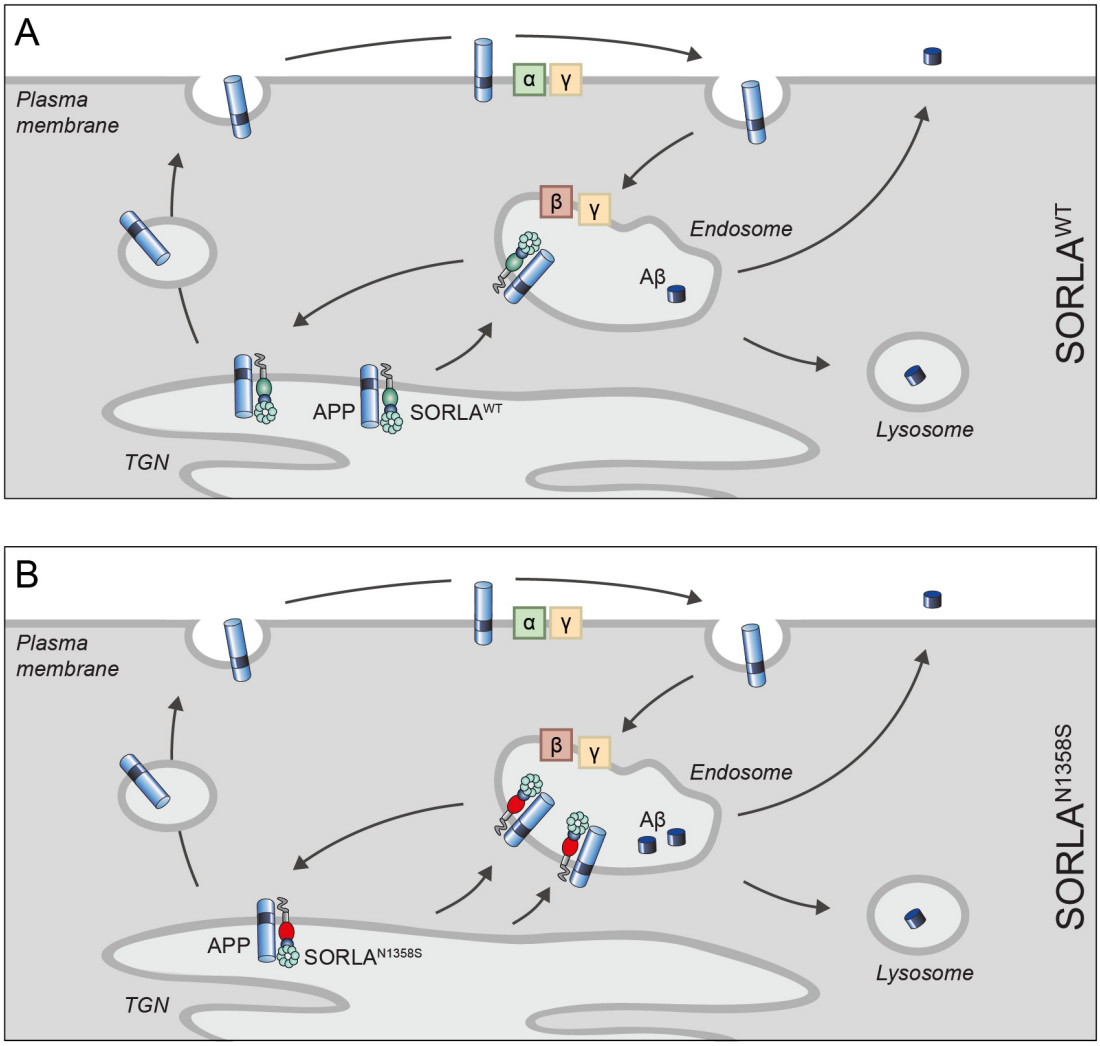

Figure 5-1: N1358S alters SORLA and APP trafficking. (A) When SORLA^{WT} is overexpressed, both SORLA and APP are mainly localized to the *trans*-Golgi-network (TGN). As secretases are localized to the plasma membrane and to endosomal compartments, APP in the TGN is largely protected from being processed. **(B)** Upon overexpression of SORLA^{N1358S}, SORLA and APP colocalized more with endosomal markers and less with Golgi markers. In the endosomes APP is subjected to catalytic processing by secretases, which may explain the increase in Aβ levels in the SORLA^{N1358S} expressing cell line compared to the SORLA^{WT} expressing cell line.

These data suggested that the interaction of SORLA and APP was not affected by N1358S, but rather that trafficking of SORLA^{N1358S}, and as a result also trafficking of APP, was altered as compared to the wildtype condition. The shift of SORLA^{N1358S} trafficking from TGN to endosomes closely resembles the subcellular localization of SORLA upon mutation of the FANSHY motif in SORLA's cytoplasmic tail (Fjorback *et al.*, 2012; Dumanis *et al.*, 2015). The VPS26 subunit of the retromer complex binds to the FANSHY motif and facilitates retrograde sorting of SORLA from the endosomes to the TGN (Fjorback *et al.*, 2012). Upon deletion of the retromer binding site, SORLA accumulates in endosomes. As a consequence, APP is not trafficked to the TGN and subjected to increased endosomal processing (Fjorback *et al.*, 2012; Dumanis *et al.*, 2015).

While alterations in SORLA trafficking caused by the N1358S mutation could explain the increase in APP processing products, the mechanism by which N1358S affects SORLA's subcellular localization still remains to be elucidated. My unbiased interactome screen revealed several differential binding partners of SORLA^{WT} and SORLA^{N1358S} related to trafficking processes along the endosomal pathway such as the Ras-related proteins Rab-5C and Rab-14 (Figure 4-27). Validating theses interactors in cell-based assays may determine which interaction partner influences SORLA trafficking and cause aberrant sorting of SORLA^{N1358S}. So far, all interaction partners that regulated trafficking of SORLA haven been shown to bind to the cytosolic tail of the receptor. Thus, it remains to be tested how mutations in its luminal domain (such as N1358S) may have an effect on receptor sorting. For example, these mutations may cause conformational changes or altered posttranslational modifications to indirectly affect receptor sorting.

5.2.2 The exosome marker MFG-E8 is a novel interaction partner for SORLA

Besides the differential interactions of SORLA^{WT} and SORLA^{N1358S} with proteins related to trafficking processes along the endosome-Golgi-pathway (Figure 4-27), one of the most intriguing hits from the SILAC-based interactome screen was MFG-E8. MFG-E8 had not been identified previously as an interaction partner of SORLA, but demonstrated a high binding affinity

in the SORLA^{WT} IP compared to the IgG negative control IP (Figure 4-28A). It was also one of the most significant hits enriched in the SORLA^{WT} IP as compared to the SORLA^{N1358S} IP, suggesting that the N1358S mutation strongly affects the interaction of SORLA with MFG-E8 (Figure 4-28B). Interestingly, MFG-E8 was also identified in another proteomics-based approach to identify novel receptor ligands sorted by SORLA to the neuronal cell surface conducted by Dr. Anna Malik in the lab. In this screen, MFG-E8 levels were decreased at the cell surface of *Sorl1*$^{-/-}$ as compared to *Sorl1*$^{+/+}$ primary mouse neurons (Dr. Anna Malik, personal communication), supporting the notion of MFG-E8 as a novel ligand for SORLA-dependent sorting to the cell surface.

MFG-E8 is a secreted glycoprotein that fulfills various cellular functions, particularly in cell-cell-interactions (Li *et al.*, 2013). It is most studied for its role in facilitating phagocytosis of apoptotic cells (Hanayama *et al.*, 2002). Interestingly, *MFG-E8* mRNA levels are reduced in the brains of Alzheimer's disease patients (Boddaert *et al.*, 2007). While the exact mechanism by which MFG-E8 influences Alzheimer's disease pathology is not fully understood, MFG-E8 was demonstrated to directly bind Aβ and mediate its cellular clearance (Boddaert *et al.*, 2007). Also, MFG-E8 is secreted in association with small membrane vesicles, called exosomes, and as such commonly used as an exosome marker (Théry *et al.*, 2006). Lately, the biology of exosome composition, secretion, and clearance has received increasing attention in the field of Alzheimer's disease due to the recent proposal of prion-like spreading of neuropathological lesions in Alzheimer's disease patients (Selkoe and Hardy, 2016; Watts and Prusiner, 2018). This hypothesis proposes that interneuronal spreading of misfolded Aβ and tau aggregates induce a cascade of protein misfolding that is similar to the pathogenic spreading of prion diseases and corresponds to the progressive nature of Alzheimer's disease (Watts and Prusiner, 2018). Exosomes, which serve as an alternative mechanism for cells to dispose of neurotoxic Aβ peptides are suggested as messengers in spreading the misfolded Aβ and tau proteins (Rajendran *et al.*, 2008; Xiao *et al.*, 2017). Furthermore, exosomes contain not only Aβ but also α- and β-secretases as well as APP suggesting that APP processing may also occur in exosomes (Sharples *et*

al., 2008). On the other hand, it has been suggested, that clearance of exosome-associated Aβ is more efficient than freely secreted Aβ through microglia-mediated endocytosis (Yuyama *et al.*, 2014). Thus, whether exosome secretion leads to Alzheimer's disease progression or may conversely prevent Aβ accumulation in the brain is still debated and requires a more detailed examination of exosome composition secreted by the different cell types in the brain.

To analyze whether the N1358S mutation alters the total number of secreted exosomes or affects the distribution of MFG-E8 in exosomes, I isolated exosomes from SORLA^{WT} and SORLA^{N1358S} overexpressing cells and analyzed levels of MFG.E8 levels and ALIX, another common exosome marker (Théry *et al.*, 2006). ALIX protein levels were unchanged comparing exosomes from SORLA^{WT} and SORLA^{N1358S} overexpressing cells, suggesting that the overall number of secreted exosomes was not affected by the N1358S mutation. However, exosomes from the SORLA^{N1358S} overexpressing cells showed a strong increase in MFG-E8 levels as compared to wildtype exosomes (Figure 4-30).

My above finding suggests a novel role of SORLA in regulating exosome composition that may also have implication for Aβ secretion and clearance in the brain as both SORLA and MFG-E8 directly interact with Aβ (Boddaert *et al.*, 2007; Caglayan *et al.*, 2014). Conceptually, two different modes of action of SORLA may explain the increase in MFG-E8 levels in exosomes isolated from SORLA^{N1358S} overexpressing cells. First, SORLA may be a sorting receptor for MFG-E8 that controls release of MFG-E8/Aβ complexes into exosomes by retaining them in endosomal compartments (Figure 5-2). SORLA would thereby balance the route of newly synthesized Aβ peptides between lysosomal degradation and exosomal release depending on the presence and binding of MFG-E8. This hypothesis would be consistent with the unaltered intracellular decay of Aβ levels in SORLA^{WT} and SORLA^{N1358S} overexpressing cells upon inhibition of Aβ production by DAPT treatment (Figure 4-23). The loss of MFG-E8 binding to SORLA^{N1358S} would cause a shift from lysosomal degradation to exosomal secretion of Aβ. As a consequence, intracellular Aβ levels would decrease at similar rates in

SORLA^{WT} and SORLA^{N1358S} overexpressing cells, while the increased exosomal sorting of Aβ and MFG-E8 in SORLA^{N1358S} overexpressing cells would lead to increased extracellular deposition of Aβ.

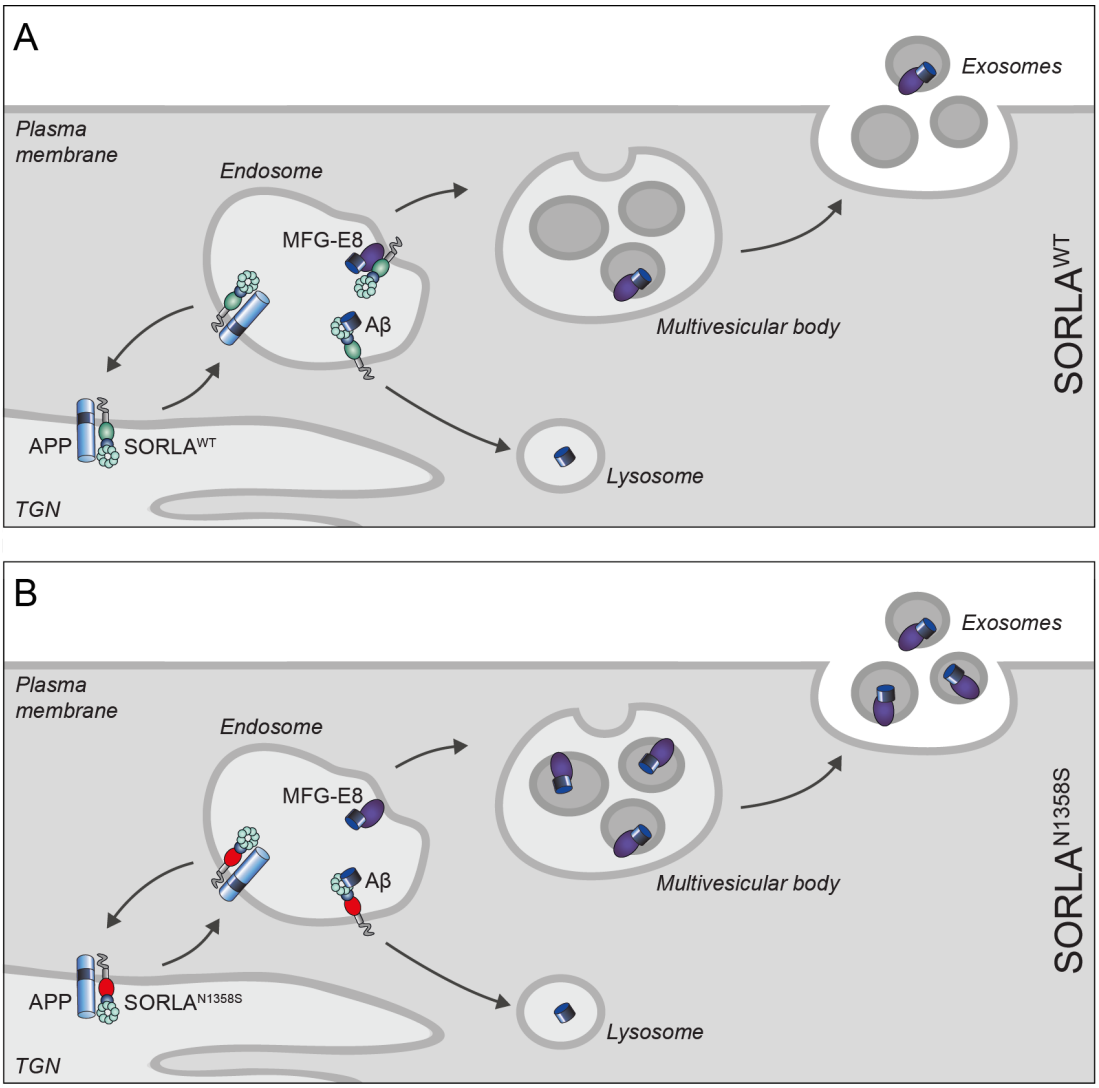

Figure 5-2: Hypothetical model of SORLA's role in controlling exosomal secretion of MFG-E8 and Aβ. (A) When SORLA^{WT} is overexpressed SORLA might bind to complexes of newly synthesized Aβ and MFG-E8 in endosomal compartments and prevent them from being sorted for exosomal secretion. Instead of secretion in exosomes, SORLA may facilitate MFG-E8 and Aβ degradation in the lysosomes. **(B)** SORLA^{N1358S} is not able to bind to MFG-E8 and therefore loses the ability to retain complexes of newly synthesized Aβ and MFG-E8 in endosomal compartments. As a result, more neurotoxic Aβ is secreted in the SORLA^{N1358S} expressing cell line compared to the SORLA^{WT} expressing cell line.

The second possible mechanism, by which SORLA's interaction with MFG-E8 may affect Alzheimer's disease-relevant processes, is clearance of MFG-E8 and Aβ containing exosomes. Clearance of Aβ containing exosomes has

been suggested to be mostly conducted by microglia, but also by neurons and astrocytes (Yuyama and Igarashi, 2017). Although SORLA's potential role in astrocytes and microglia has not been much investigated yet, transcriptome data on neurons, astrocytes and microglia demonstrate that SORLA is also expressed in astrocytes and microglia (Zhang *et al.*, 2014). Facilitating uptake and clearance of Aβ containing exosomes in microglia dependent on MFG-E8 could potentially be a separate mechanism by which SORLA prevent Aβ accumulation in the brain that is affected by the EOAD-associated N1358S mutation.

5.3 Outlook

The advances in DNA and RNA sequencing technologies have revealed genetic associations of VPS10P domain receptors with a variety of neurological and metabolic diseases. However, many of these genetic variants have not been functionally characterized to confirm their effect on receptor biology and disease-relevant phenotypes.

In my PhD thesis, I functionally analyzed the relevance of a non-coding risk SNP close to the *SORT1* gene locus and of three EOAD-associated coding *SORL1* mutations. The methods that I established for studying the *SORT1* SNP in human iPSCs, including genome-editing of single SNPs and the differentiation of cells into mature cortical neurons and hepatocytes, will be useful to validate additional genetic variants of VPS10P domain receptors. As exemplified by my studies, the characterization of disease-associated genetic variants potentially uncovers novel interaction partners of these receptors and sheds light on their transcriptional regulation. This data not only improve our knowledge of the VPS10P domain receptor biology, but also help to bridge the gap between genetic association studies and disease-relevant phenotypes.

6 REFERENCES

Al-Shawi, R., Hafner, A., Olson, J., Chun, S., Raza, S., Thrasivoulou, C., Lovestone, S., Killick, R., Simons, P., and Cowen, T. 2008. Neurotoxic and neurotrophic roles of proNGF and the receptor sortilin in the adult and ageing nervous system. *Eur. J. Neurosci.* **27**: 2103–2114.

Alemany, S., Ribasés, M., Vilor-Tejedor, N., Bustamante, M., Sánchez-Mora, C., Bosch, R., Richarte, V., Cormand, B., Casas, M., Ramos-Quiroga, J.A., et al. 2015. New suggestive genetic loci and biological pathways for attention function in adult attention-deficit/hyperactivity disorder. *Am. J. Med. Genet. Part B Neuropsychiatr. Genet.* **168**: 459–470.

Andersen, O.M., Reiche, J., Schmidt, V., Gotthardt, M., Spoelgen, R., Behlke, J., Arnim, C.A.F. von, Breiderhoff, T., Jansen, P., Wu, X., et al. 2005. Neuronal sorting protein-related receptor sorLA/LR11 regulates processing of the amyloid precursor protein. *Proc. Natl. Acad. Sci. U. S. A.* **102**: 13461–13466.

Andersen, O.M., Rudolph, I.-M., and Willnow, T.E. 2016. Risk factor SORL1: from genetic association to functional validation in Alzheimer's disease. *Acta Neuropathol.* **132**: 653–665.

Andersen, O.M., Schmidt, V., Spoelgen, R., Gliemann, J.J., Behlke, J., Galatis, D., McKinstry, W.J., Parker, M.W., Masters, C.L., Hyman, B.T., et al. 2006. Molecular dissection of the interaction between amyloid precursor protein and its neuronal trafficking receptor SorLA/LR11. *Biochemistry* **45**: 2618–2628.

Andersson, C.-H., Hansson, O., Minthon, L., Andreasen, N., Blennow, K., Zetterberg, H., Skoog, I., Wallin, A., Nilsson, S., and Kettunen, P. 2016. A Genetic Variant of the Sortilin 1 Gene is Associated with Reduced Risk of Alzheimer's Disease. *J. Alzheimer's Dis.* **53**: 1353–1363.

Andrew, R.J., Kellett, K.A.B., Thinakaran, G., and Hooper, N.M. 2016. A Greek Tragedy: The Growing Complexity of Alzheimer Amyloid Precursor Protein Proteolysis. *J. Biol. Chem.* **291**: 19235–19244.

Asplund, A., Pradip, A., Giezen, M. van, Aspegren, A., Choukair, H., Rehnström, M., Jacobsson, S., Ghosheh, N., Hajjam, D. El, Holmgren, S., et al. 2016. One Standardized Differentiation Procedure Robustly Generates Homogenous Hepatocyte Cultures Displaying Metabolic Diversity from a Large Panel of Human Pluripotent Stem Cells. *Stem Cell Rev. Reports* **12**: 90–104.

Auer, P.L., and Lettre, G. 2015. Rare variant association studies: considerations, challenges and opportunities. *Genome Med.* **7**: 16.

Baker, M., Mackenzie, I.R., Pickering-Brown, S.M., Gass, J., Rademakers, R., Lindholm, C., Snowden, J., Adamson, J., Sadovnick, A.D., Rollinson, S., et al. 2006. Mutations in progranulin cause tau-negative frontotemporal dementia linked to chromosome 17. *Nature* **442**: 916–919.

Baum, A.E., Akula, N., Cabanero, M., Cardona, I., Corona, W., Klemens, B., Schulze, T.G., Cichon, S., Rietschel, M., Nöthen, M.M., et al. 2008. A genome-wide association study implicates diacylglycerol kinase eta (DGKH) and several other genes in the etiology of bipolar disorder. *Mol. Psychiatry* **13**: 197–207.

Beher, D., Hesse, L., Masters, C.L., and Multhaup, G. 1996. Regulation of amyloid protein precursor (APP) binding to collagen and mapping of the binding sites on APP and collagen type I. *J. Biol. Chem.* **271**: 1613–20.

Bertram, L., Lill, C.M., and Tanzi, R.E. 2010. The Genetics of Alzheimer Disease: Back to the Future. *Neuron* **68**: 270–281.

Blennow, K., Leon, M.J. de, and Zetterberg, H. 2006. Alzheimer's disease. *Lancet* **368**: 387–403.

Boddaert, J., Kinugawa, K., Lambert, J., Boukhtouche, F., Blanc-brude, O., Mann, D., Berr, C., Journiac, N., Charue, D., Duyckaerts, C., et al. 2007. Evidence of a Role for Lactadherin in Alzheimer ' s Disease. **170**: 921–929.

Burgert, T., Schmidt, V., Caglayan, S., Lin, F., Füchtbauer, A., Füchtbauer, E.-M., Nykjaer, A., Carlo, A.-S.A.-S., Willnow, T.E., Fuchtbauer, A., et al. 2013. SORLA-dependent and -independent functions for PACS1 in control of amyloidogenic processes. *Mol. Cell. Biol.* **33**: 4308–20.

Caglayan, S., Bauerfeind, A., Schmidt, V., Carlo, A.-S., Prabakaran, T., Hübner, N., and Willnow, T.E. 2012. Identification of Alzheimer Disease Risk Genotype That Predicts Efficiency of SORL1 Expression in the Brain. *Arch. Neurol.* **69**: 373.

Caglayan, S., Takagi-Niidome, S., Liao, F., Carlo, A.-S.A.-S., Schmidt, V., Burgert, T., Kitago, Y.Y., Fuchtbauer, E.-M., Fuchtbauer, A., Holtzman, D.M., et al. 2014. Lysosomal sorting of amyloid-β by the SORLA receptor is impaired by a familial Alzheimer's disease mutation. *Sci. Transl. Med.* **6**: 223ra20.

Cai, X.D., Golde, T.E., and Younkin, S.G. 1993. Release of excess amyloid beta protein from a mutant amyloid beta protein precursor. *Science* **259**: 514–6.

Campion, D., Dumanchin, C., Hannequin, D., Dubois, B., Belliard, S., Puel, M., Thomas-Anterion, C., Michon, A., Martin, C., Charbonnier, F., et al. 1999. Early-Onset Autosomal Dominant Alzheimer Disease: Prevalence, Genetic Heterogeneity, and Mutation Spectrum. *Am. J. Hum. Genet.* **65**: 664–670.

Canuel, M., Lefrancois, S., Zeng, J., and Morales, C.R. 2008. AP-1 and retromer play opposite roles in the trafficking of sortilin between the Golgi apparatus and the lysosomes. *Biochem. Biophys. Res. Commun.* **366**: 724–730.

Caporaso, G.L., Takei, K., Gandy, S.E., Matteoli, M., Mundigl, O., Greengard, P., and Camilli, P. De 1994. Morphologic and biochemical analysis of the intracellular trafficking of the Alzheimer beta/A4 amyloid precursor protein. *J. Neurosci.* **14**: 3122–38.

Carlo, A.-S., Gustafsen, C., Mastrobuoni, G., Nielsen, M.S., Burgert, T., Hartl, D., Rohe, M., Nykjaer, A., Herz, J., Heeren, J., et al. 2013. The pro-neurotrophin receptor sortilin is a major neuronal apolipoprotein E receptor for catabolism of amyloid-β peptide in the brain. *J. Neurosci.* **33**: 358–70.

Carrasquillo, M.M., Nicholson, A.M., Finch, N., Gibbs, J.R., Baker, M., Rutherford, N.J., Hunter, T.A., Dejesus-Hernandez, M., Bisceglio, G.D., MacKenzie, I.R., et al. 2010. Genome-wide screen identifies rs646776 near sortilin as a regulator of progranulin levels in human plasma. *Am. J. Hum. Genet.* **87**: 890–897.

Cartegni, L., Chew, S.L., and Krainer, A.R. 2002. Listening to silence and understanding nonsense: exonic mutations that affect splicing. *Nat. Rev. Genet.* **3**: 285–298.

Castellano, J.M., Kim, J., Stewart, F.R., Jiang, H., DeMattos, R.B., Patterson, B.W., Fagan, A.M., Morris, J.C., Mawuenyega, K.G., Cruchaga, C., et al. 2011. Human apoE isoforms differentially regulate brain amyloid-β peptide clearance. *Sci. Transl. Med.* **3**: 89ra57.

Chen, Y., Mills, J.D., and Periasamy, A. 2003. Protein localization in living cells and tissues using FRET and FLIM. *Differentiation* **71**: 528–541.

Chen, Z.-Y., Ieraci, A., Teng, H., Dall, H., Meng, C.-X., Herrera, D.G., Nykjaer, A., Hempstead, B.L., and Lee, F.S. 2005. Sortilin Controls Intracellular Sorting of Brain-Derived Neurotrophic Factor to the Regulated Secretory Pathway. *J. Neurosci.* **25**: 6156–6166.

Christoforou, A., McGhee, K.A., Morris, S.W., Thomson, P.A., Anderson, S., McLean, A., Torrance, H.S., Hellard, S. Le, Pickard, B.S., StClair, D., et al. 2011. Convergence of linkage, association and GWAS findings for a candidate region for bipolar disorder and schizophrenia on chromosome 4p. *Mol. Psychiatry* **16**: 240–242.

Citron, M., Oltersdorf, T., Haass, C., McConlogue, L., Hung, A.Y., Seubert, P., Vigo-Pelfrey, C., Lieberburg, I., and Selkoe, D.J. 1992. Mutation of the β-amyloid precursor protein in familial Alzheimer's disease increases β-protein production. *Nature* **360**: 672–674.

Clee, S.M., Yandell, B.S., Schueler, K.M., Rabaglia, M.E., Richards, O.C., Raines, S.M., Kabara, E.A., Klass, D.M., Mui, E.T.-K., Stapleton, D.S., et al. 2006. Positional cloning of Sorcs1, a type 2 diabetes quantitative trait locus. *Nat. Genet.* **38**: 688–693.

Cole, G.M., Bell, L., Truong, Q.B., and Saitoh, T. 1992. An endosomal-lysosomal pathway for degradation of amyloid precursor protein. *Ann. N. Y. Acad. Sci.* **674**: 103–17.

Cooper, G.M., and Shendure, J. 2011. Needles in stacks of needles: finding disease-causal variants in a wealth of genomic data. *Nat. Rev. Genet.* **12**: 628–640.

Corder, E., Saunders, A., Strittmatter, W., Schmechel, D., Gaskell, P., Small, G., Roses, A., Haines, J., and Pericak-Vance, M. 1993. Gene dose of apolipoprotein E type 4 allele and the risk of Alzheimer's disease in late onset families. *Science* **261**: 921–923.

Cruts, M., Gijselinck, I., Zee, J. van der, Engelborghs, S., Wils, H., Pirici, D., Rademakers, R., Vandenberghe, R., Dermaut, B., Martin, J.-J., et al. 2006. Null mutations in progranulin cause ubiquitin-positive frontotemporal dementia linked to chromosome 17q21. *Nature* **442**: 920–924.

Damme, P. Van, Hoecke, A. Van, Lambrechts, D., Vanacker, P., Bogaert, E., Swieten, J. van, Carmeliet, P., Bosch, L. Van Den, and Robberecht, W. 2008. Progranulin functions as a neurotrophic factor to regulate neurite outgrowth and enhance neuronal survival. *J. Cell Biol.* **181**: 37–41.

Das, U., Scott, D.A., Ganguly, A., Koo, E.H., Tang, Y., and Roy, S. 2013. Activity-Induced Convergence of APP and BACE-1 in Acidic Microdomains via an Endocytosis-Dependent Pathway. *Neuron* **79**: 447–460.

Ding, Q., Lee, Y.K., Schaefer, E.A.K., Peters, D.T., Veres, A., Kim, K., Kuperwasser, N., Motola, D.L., Meissner, T.B., Hendriks, W.T., et al. 2013. A TALEN genome-editing system for generating human stem cell-based disease models. *Cell Stem Cell* **12**: 238–251.

Dodson, S.E., Andersen, O.M., Karmali, V., Fritz, J.J., Cheng, D., Peng, J., Levey, A.I., Willnow, T.E., and Lah, J.J. 2008. Loss of LR11/SORLA enhances early pathology in a mouse model of amyloidosis: evidence for a proximal role in Alzheimer's disease. *J. Neurosci.* **28**: 12877–86.

Dulin, F., Léveillé, F., Ortega, J.B., Mornon, J.-P., Buisson, A., Callebaut, I., and Colloc'h, N. 2008. p3 peptide, a truncated form of Aβ devoid of synaptotoxic effect, does not assemble into soluble oligomers. *FEBS Lett.* **582**: 1865–1870.

Dumanis, S.B., Burgert, T., Caglayan, S., Fuchtbauer, A., Fuchtbauer, E.-M., Schmidt, V., and Willnow, T.E. 2015. Distinct Functions for Anterograde and Retrograde Sorting of SORLA in Amyloidogenic Processes in the Brain. *J. Neurosci.* **35**: 12703–12713.

Eggert, S., Thomas, C., Kins, S., and Hermey, G. 2018. Trafficking in Alzheimer's Disease: Modulation of APP Transport and Processing by the Transmembrane Proteins LRP1, SorLA, SorCS1c, Sortilin, and Calsyntenin. *Mol. Neurobiol.* **55**: 5809–5829.

Esch, F.S., Keim, P.S., Beattie, E.C., Blacher, R.W., Culwell, A.R., Oltersdorf, T., McClure, D., and Ward, P.J. 1990. Cleavage of amyloid beta peptide during constitutive processing of its precursor. *Science* **248**: 1122–4.

Fagerberg, L., Hallström, B.M., Oksvold, P., Kampf, C., Djureinovic, D., Odeberg, J., Habuka, M., Tahmasebpoor, S., Danielsson, A., Edlund, K., et al. 2014. Analysis of the Human Tissue-specific Expression by Genome-wide Integration of Transcriptomics and Antibody-based Proteomics. *Mol. Cell. Proteomics* **13**: 397–406.

Fahnestock, M., Michalski, B., Xu, B., and Coughlin, M.D. 2001. The Precursor Pro-Nerve Growth Factor Is the Predominant Form of Nerve Growth Factor in Brain and Is Increased in Alzheimer's Disease. *Mol. Cell. Neurosci.* **18**: 210–220.

Farrer, L.A., Cupples, L.A., Haines, J.L., Hyman, B., Kukull, W.A., Mayeux, R., Myers, R.H., Pericak-Vance, M.A., Risch, N., and Duijn, C.M. van 1997. Effects of age, sex, and ethnicity on the association between apolipoprotein E genotype and Alzheimer disease. A meta-analysis. APOE and Alzheimer Disease Meta Analysis Consortium. *JAMA* **278**: 1349–56.

Fillat, C., Carrio, M., Cascante, A., and Sangro, B. 2003. Suicide Gene Therapy Mediated by the Herpes Simplex Virus Thymidine Kinase Gene / Ganciclovir System: Fifteen Years of Application. *Curr. Gene Ther.* **3**: 13–26.

Finan, G.M., Okada, H., and Kim, T.-W. 2011. BACE1 Retrograde Trafficking Is Uniquely Regulated by the Cytoplasmic Domain of Sortilin. *J. Biol. Chem.* **286**: 12602–12616.

Fjorback, A.W., Seaman, M., Gustafsen, C., Mehmedbasic, A., Gokool, S., Wu, C., Militz, D., Schmidt, V., Madsen, P., Nyengaard, J.R., et al. 2012. Retromer Binds the FANSHY Sorting Motif in SorLA to Regulate Amyloid Precursor Protein Sorting and Processing. *J. Neurosci.* **32**: 1467–1480.

Franke, B., Figiel, M., and Engele, J. 1998. CNS glia are targets for GDNF and neurturin. *Histochem. Cell Biol.* **110**: 595–601.

Frisardi, V., Solfrizzi, V., Seripa, D., Capurso, C., Santamato, A., Sancarlo, D., Vendemiale, G., Pilotto, A., and Panza, F. 2010. Metabolic-cognitive syndrome: A cross-talk between metabolic syndrome and Alzheimer's disease. *Ageing Res. Rev.* **9**: 399–417.

Gaj, T., Gersbach, C.A., Barbas, C.F., and III 2013. ZFN, TALEN, and CRISPR/Cas-based methods for genome engineering. *Trends Biotechnol.* **31**: 397–405.

Gallagher, M.D., and Chen-Plotkin, A.S. 2018. The Post-GWAS Era: From Association to Function. *Am. J. Hum. Genet.* **102**: 717–730.

Gass, J., Cannon, A., Mackenzie, I.R., Boeve, B., Baker, M., Adamson, J., Crook, R., Melquist, S., Kuntz, K., Petersen, R., et al. 2006. Mutations in progranulin are a major cause of ubiquitin-positive frontotemporal lobar degeneration. *Hum. Mol. Genet.* **15**: 2988–3001.

Gass, J., Prudencio, M., Stetler, C., and Petrucelli, L. 2012. Progranulin: An emerging target for FTLD therapies. *Brain Res.* **1462**: 118–128.

Gatz, M., Reynolds, C.A., Fratiglioni, L., Johansson, B., Mortimer, J.A., Berg, S., Fiske, A., and Pedersen, N.L. 2006. Role of Genes and Environments for Explaining Alzheimer Disease. *Arch. Gen. Psychiatry* **63**: 168.

Ghaffari, L.T., Starr, A., Nelson, A.T., and Sattler, R. 2018. Representing Diversity in the Dish: Using Patient-Derived in Vitro Models to Recreate the Heterogeneity of Neurological Disease. *Front. Neurosci.* **12**: 56.

Goate, A., Chartier-Harlin, M.-C.C., Mullan, M., Brown, J., Crawford, F., Fidani, L., Giuffra, L., Haynes, A., Irving, N., James, L., et al. 1991. Segregation of a missense mutation in the amyloid precursor protein gene with familial Alzheimer's disease. *Nature* **349**: 704–706.

Golde, T., Estus, S., Younkin, L., Selkoe, D., and Younkin, S. 1992. Processing of the amyloid protein precursor to potentially amyloidogenic derivatives. *Science* **255**: 728–730.

Goldgaber, D., Lerman, M.I., McBride, O.W., Saffiotti, U., and Gajdusek, D.C. 1987. Characterization and chromosomal localization of a cDNA encoding brain amyloid of Alzheimer's disease. *Science* **235**: 877–80.

Gómez-Isla, T., Price, J.L., McKeel, D.W., Morris, J.C., Growdon, J.H., and Hyman, B.T. 1996. Profound loss of layer II entorhinal cortex neurons occurs in very mild Alzheimer's disease. *J. Neurosci.* **16**: 4491–500.

Gómez-Tortosa, E., Ruggiero, M., Sainz, M.J., Villarejo-Galende, A., Prieto-Jurczynska, C., Venegas Pérez, B., Ordás, C., Agüero, P., Guerrero-López, R., and Pérez-Pérez, J. 2018. SORL1 Variants in Familial Alzheimer's Disease. *J. Alzheimer's Dis.* **61**: 1275–1281.

Graham, W.V., Bonito-Oliva, A., and Sakmar, T.P. 2017. Update on Alzheimer's Disease Therapy and Prevention Strategies. *Annu. Rev. Med.* **68**: 413–430.

Granhall, C., Park, H.-B., Fakhrai-Rad, H., and Luthman, H. 2006. High-Resolution Quantitative Trait Locus Analysis Reveals Multiple Diabetes Susceptibility Loci Mapped to Intervals <800 kb in the Species-Conserved *Niddm1i* of the GK Rat. *Genetics* **174**: 1565–1572.

Grear, K.E., Ling, I.-F., Simpson, J.F., Furman, J.L., Simmons, C.R., Peterson, S.L., Schmitt, F.A., Markesbery, W.R., Liu, Q., Crook, J.E., et al. 2009. Expression of SORL1 and a novel SORL1 splice variant in normal and Alzheimers disease brain. *Mol. Neurodegener.* **4**: 46.

Grupe, A., Li, Y., Rowland, C., Nowotny, P., Hinrichs, A.L., Smemo, S., Kauwe, J.S.K., Maxwell, T.J., Cherny, S., Doil, L., et al. 2006. A Scan of Chromosome 10 Identifies a Novel Locus Showing Strong Association with Late-Onset Alzheimer Disease. *Am. J. Hum. Genet.* **78**: 78–88.

Guerreiro, R.J., Gustafson, D.R., and Hardy, J. 2012. The genetic architecture of Alzheimer's disease: beyond APP, PSENs and APOE. *Neurobiol. Aging* **33**: 437–56.

Guguen-Guillouzo, C., and Guillouzo, A. 2010. General Review on In Vitro Hepatocyte Models and Their Applications In: Methods in Molecular Biology (Clifton, N.J.). pp. 1–40.

Guo, Q., Li, H., Gaddam, S.S.K., Justice, N.J., Robertson, C.S., and Zheng, H. 2012. Amyloid Precursor Protein Revisited. *J. Biol. Chem.* **287**: 2437–2445.

Gustafsen, C., Glerup, S., Pallesen, L.T., Olsen, D., Andersen, O.M., Nykjær, A., Madsen, P., Petersen, C.M., Nykjaer, A., Madsen, P., et al. 2013. Sortilin and SorLA display distinct roles in processing and trafficking of amyloid precursor protein. *J. Neurosci.* **33**: 64–71.

Haass, C., Kaether, C., Thinakaran, G., and Sisodia, S. 2012. Trafficking and proteolytic processing of APP. *Cold Spring Harb. Perspect. Med.* **2**: a006270.

Haass, C., Schlossmacher, M.G., Hung, A.Y., Vigo-Pelfrey, C., Mellon, A., Ostaszewski, B.L., Lieberburg, I., Koo, E.H., Schenk, D., Teplow, D.B., et al. 1992. Amyloid β-peptide is produced by cultured cells during normal metabolism. *Nature* **359**: 322–325.

Haass, C., and Selkoe, D.J. 2007. Soluble protein oligomers in neurodegeneration: lessons from the Alzheimer's amyloid beta-peptide. *Nat. Rev. Mol. Cell Biol.* **8**: 101–112.

Hampe, W., Rezgaoui, M., Hermans-Borgmeyer, I., and Schaller, C.H. 2001. The genes for the human VPS10 domain-containing receptors are large and contain many small exons. *Hum. Genet.* **108**: 529–536.

Hampe, W., Riedel, I.B., Lintzel, J., Bader, C.O., Franke, I., and Schaller, H.C. 2000. Ectodomain shedding, translocation and synthesis of SorLA are stimulated by its ligand head activator. *J. Cell Sci.* **113 Pt 24**: 4475–85.

Hampe, W., Urny, J., Franke, I., Hoffmeister-Ullerich, S.A., Herrmann, D., Petersen, C.M., Lohmann, J., and Schaller, H.C. 1999. A head-activator binding protein is present in hydra in a soluble and a membrane-anchored form. *Development* **126**: 4077–86.

Hanayama, R., Tanaka, M., Miwa, K., Shinohara, A., Iwamatsu, A., and Nagata, S. 2002. Identification of a factor that links apoptotic cells to phagocytes. *Nature* **417**: 182–187.

Hardy, J., and Higgins, G. 1992. Alzheimer's disease: the amyloid cascade hypothesis. *Science* **256**: 184–185.

Hardy, J., and Selkoe, D.J. 2002. The amyloid hypothesis of Alzheimer's disease: progress and problems on the road to therapeutics. *Science* **297**: 353–356.

He, Z., Ong, C.H.P., Halper, J., and Bateman, A. 2003. Progranulin is a mediator of the wound response. *Nat. Med.* **9**: 225–229.

Heller, D.A., Faire, U. de, Pedersen, N.L., Dahlen, G., and McClearn, G.E. 1993. Genetic and Environmental Influences on Serum Lipid Levels in Twins. *N. Engl. J. Med.* **328**: 1150–1156.

Hendriks, L., Duijn, C.M. van, Cras, P., Cruts, M., Hul, W. Van, Harskamp, F. van, Warren, A., McInnis, M.G., Antonarakis, S.E., Martin, J.-J., et al. 1992. Presenile dementia and cerebral haemorrhage linked to a mutation at codon 692 of the β–amyloid precursor protein gene. *Nat. Genet.* **1**: 218–221.

Hermey, G., Riedel, I.B., Hampe, W., Schaller, H.C., and Hermans-Borgmeyer, I. 1999. Identification and Characterization of SorCS, a Third Member of a Novel Receptor Family. *Biochem. Biophys. Res. Commun.* **266**: 347–351.

Hermey, G., Sjøgaard, S.S., Petersen, C.M., Nykjær, A., and Gliemann, J. 2006. Tumour necrosis factor α-converting enzyme mediates ectodomain shedding of Vps10p-domain receptor family members. *Biochem. J.* **395**: 285–293.

Herskowitz, J.H., Offe, K., Deshpande, A., Kahn, R.A., Levey, A.I., and Lah, J.J. 2012. GGA1-mediated endocytic traffic of LR11/SorLA alters APP intracellular distribution and amyloid-β production. *Mol. Biol. Cell* **23**: 2645–2657.

Hockemeyer, D., and Jaenisch, R. 2016. Induced Pluripotent Stem Cells Meet Genome Editing. *Cell Stem Cell* **18**: 573–586.

Holtzman, D.M., Herz, J., and Bu, G. 2012. Apolipoprotein E and apolipoprotein E receptors: normal biology and roles in Alzheimer disease. *Cold Spring Harb. Perspect. Med.* **2**: a006312.

Hu, F., Padukkavidana, T., Vægter, C.B., Brady, O.A., Zheng, Y., Mackenzie, I.R., Feldman, H.H., Nykjaer, A., and Strittmatter, S.M. 2010. Sortilin-mediated endocytosis determines levels of the frontotemporal dementia protein, progranulin. *Neuron* **68**: 654–667.

Huang, Y., and Mucke, L. 2012. Alzheimer mechanisms and therapeutic strategies. *Cell* **148**: 1204–1222.

Jacobsen, L., Madsen, P., Jacobsen, C., Nielsen, M.S., Gliemann, J., and Petersen, C.M. 2001. Activation and functional characterization of the mosaic receptor SorLA/LR11. *J. Biol. Chem.* **276**: 22788–96.

Jacobsen, L., Madsen, P., Moestrup, S.K., Lund, A.H., Tommerup, N., Nykjær, A., Sottrup-Jensen, L., Gliemann, J., and Petersen, C.M. 1996. Molecular Characterization of a Novel Human Hybrid-type Receptor That Binds the α_2-Macroglobulin Receptor-associated Protein. *J. Biol. Chem.* **271**: 31379–31383.

Jacobsen, L., Madsen, P., Nielsen, M.S., Geraerts, W.P.M., Gliemann, J., Smit, A.B., and Petersen, C.M. 2002. The sorLA cytoplasmic domain interacts with GGA1 and -2 and defines minimum requirements for GGA binding. *FEBS Lett.* **511**: 155–158.

Jansen, P., Giehl, K., Nyengaard, J.R., Teng, K., Lioubinski, O., Sjoegaard, S.S., Breiderhoff, T., Gotthardt, M., Lin, F., Eilers, A., et al. 2007. Roles for the pro-neurotrophin receptor sortilin in neuronal development, aging and brain injury. *Nat. Neurosci.* **10**: 1449–1457.

Jellinger, K.A. 2004. Head injury and dementia. *Curr. Opin. Neurol.* **17**: 719–23.

Jin, C., Liu, X., Zhang, F., Wu, Y., Yuan, J., Zhu, J., Zhang, F., Wang, G., and Cheng, Z. 2013. An updated meta-analysis of the association between SORL1 variants and the risk for sporadic Alzheimer's disease. *J. Alzheimers. Dis.* **37**: 429–37.

Kamenetz, F., Tomita, T., Hsieh, H., Seabrook, G., Borchelt, D., Iwatsubo, T., Sisodia, S., and Malinow, R. 2003. APP processing and synaptic function. *Neuron* **37**: 925–37.

Kanekiyo, T., Zhang, J., Liu, Q., Liu, C.-C., Zhang, L., and Bu, G. 2011. Heparan Sulphate Proteoglycan and the Low-Density Lipoprotein Receptor-Related Protein 1 Constitute Major Pathways for Neuronal Amyloid- Uptake. *J. Neurosci.* **31**: 1644–1651.

Kang, J., Lemaire, H.-G., Unterbeck, A., Salbaum, J.M., Masters, C.L., Grzeschik, K.-H., Multhaup, G., Beyreuther, K., and Müller-Hill, B. 1987. The precursor of Alzheimer's disease amyloid A4 protein resembles a cell-surface receptor. *Nature* **325**: 733–736.

Kathiresan, S., Melander, O., Guiducci, C., Surti, A., Burtt, N.P., Rieder, M.J., Cooper, G.M., Roos, C., Voight, B.F., Havulinna, A.S., et al. 2008. Six new loci associated with blood low-density lipoprotein cholesterol, high-density lipoprotein cholesterol or triglycerides in humans. *Nat. Genet.* **40**: 189–97.

Kathiresan, S., Voight, B.F., Purcell, S., Musunuru, K., Ardissino, D., Mannucci, P.M., Anand, S., Engert, J.C., Samani, N.J., Schunkert, H., et al. 2009. Genome-wide association of early-onset myocardial infarction with single nucleotide polymorphisms and copy number variants. *Nat. Genet.* **41**: 334–341.

Khachaturian, Z.S. 1985. Diagnosis of Alzheimer's Disease. *Arch. Neurol.* **42**: 1097–1105.

Kibbey, M.C., Jucker, M., Weeks, B.S., Neve, R.L., Nostrand, W.E. Van, and Kleinman, H.K. 1993. beta-Amyloid precursor protein binds to the neurite-promoting IKVAV site of laminin. *Proc. Natl. Acad. Sci. U. S. A.* **90**: 10150–3.

Kim, J., Castellano, J.M., Jiang, H., Basak, J.M., Parsadanian, M., Pham, V., Mason, S.M., Paul, S.M., and Holtzman, D.M. 2009. Overexpression of Low-Density Lipoprotein Receptor in the Brain Markedly Inhibits Amyloid Deposition and Increases Extracellular Aβ Clearance. *Neuron* **64**: 632–644.

Kimberly, W.T., LaVoie, M.J., Ostaszewski, B.L., Ye, W., Wolfe, M.S., and Selkoe, D.J. 2003. Gamma-secretase is a membrane protein complex comprised of presenilin, nicastrin, Aph-1, and Pen-2. *Proc. Natl. Acad. Sci. U. S. A.* **100**: 6382–7.

King, G.D., and Scott Turner, R. 2004. Adaptor protein interactions: modulators of amyloid precursor protein metabolism and Alzheimer's disease risk? *Exp. Neurol.* **185**: 208–219.

Kitago, Y., Nagae, M., Nakata, Z., Yagi-Utsumi, M., Takagi-Niidome, S., Mihara, E., Nogi, T., Kato, K., and Takagi, J. 2015. Structural basis for amyloidogenic peptide recognition by sorLA. *Nat. Struct. Mol. Biol.* **22**: 199–206.

Kjolby, M., Andersen, O.M., Breiderhoff, T., Fjorback, A.W., Pedersen, K.M., Madsen, P., Jansen, P., Heeren, J., Willnow, T.E., and Nykjaer, A. 2010. Sort1, encoded by the cardiovascular risk locus 1p13.3, is a regulator of hepatic lipoprotein export. *Cell Metab.* **12**: 213–223.

Kölsch, H., Jessen, F., Wiltfang, J., Lewczuk, P., Dichgans, M., Teipel, S.J., Kornhuber, J., Frölich, L., Heuser, I., Peters, O., et al. 2009. Association of SORL1 gene variants with Alzheimer's disease. *Brain Res.* **1264**: 1–6.

Kreykenbohm, V., Wenzel, D., Antonin, W., Atlachkine, V., and Fischer von Mollard, G. 2002. The SNAREs vti1a and vti1b have distinct localization and SNARE complex partners. *Eur. J. Cell Biol.* **81**: 273–280.

Kuhn, P.-H., Wang, H., Dislich, B., Colombo, A., Zeitschel, U., Ellwart, J.W., Kremmer, E., Roßner, S., and Lichtenthaler, S.F. 2010. ADAM10 is the physiologically relevant, constitutive α-secretase of the amyloid precursor protein in primary neurons. *EMBO J.* **29**: 3020–3032.

Kumar-Singh, S. 2011. Progranulin and TDP-43: Mechanistic Links and Future Directions. *J. Mol. Neurosci.* **45**: 561–573.

Kumar-Singh, S., and Broeckhoven, C. Van 2007. Frontotemporal Lobar Degeneration: Current Concepts in the Light of Recent Advances. *Brain Pathol.* **17**: 104–114.

LaDu, M.J., Falduto, M.T., Manelli, A.M., Reardon, C.A., Getz, G.S., and Frail, D.E. 1994. Isoform-specific binding of apolipoprotein E to beta-amyloid. *J. Biol. Chem.* **269**: 23403–6.

Lai, A., Sisodia, S.S., and Trowbridge, I.S. 1995. Characterization of sorting signals in the beta-amyloid precursor protein cytoplasmic domain. *J. Biol. Chem.* **270**: 3565–73.

Lambert, J.-C.C., Ibrahim-Verbaas, C.A., Harold, D., Naj, A.C., Sims, R., Bellenguez, C., Jun, G., DeStefano, A.L., Bis, J.C., Beecham, G.W., et al. 2013. Meta-analysis of 74,046 individuals identifies 11 new susceptibility loci for Alzheimer's disease. *Nat. Genet.* **45**: 1452–8.

Lammich, S., Kojro, E., Postina, R., Gilbert, S., Pfeiffer, R., Jasionowski, M., Haass, C., and Fahrenholz, F. 1999. Constitutive and regulated alpha-secretase cleavage of Alzheimer's amyloid precursor protein by a disintegrin metalloprotease. *Proc. Natl. Acad. Sci. U. S. A.* **96**: 3922–7.

Lee, D., Walsh, J.D., Migliorini, M., Yu, P., Cai, T., Schwieters, C.D., Krueger, S., Strickland, D.K., and Wang, Y.-X. 2007. The structure of receptor-associated protein (RAP). *Protein Sci.* **16**: 1628–40.

Lee, W.C., Almeida, S., Prudencio, M., Caulfield, T.R., Zhang, Y.J., Tay, W.M., Bauer, P.O., Chew, J., Sasaguri, H., Jansen-west, K.R., et al. 2014. Targeted manipulation of the sortilin-progranulin axis rescues progranulin haploinsufficiency. *Hum. Mol. Genet.* **23**: 1467–1478.

Levy-Lahad, E., Wasco, W., Poorkaj, P., Romano, D.M., Oshima, J., Pettingell, W.H., Yu, C.E., Jondro, P.D., Schmidt, S.D., and Wang, K. 1995. Candidate gene for the chromosome 1 familial Alzheimer's disease locus. *Science* **269**: 973–7.

Li, B.-Z., Zhang, H.-Y., Pan, H.-F., and Ye, D.-Q. 2013. Identification of MFG-E8 as a novel therapeutic target for diseases. *Expert Opin. Ther. Targets* **17**: 1275–85.

Linsel-Nitschke, P., Heeren, J., Aherrahrou, Z., Bruse, P., Gieger, C., Illig, T., Prokisch, H., Heim, K., Doering, A., Peters, A., et al. 2010. Genetic variation at chromosome 1p13.3 affects sortilin mRNA expression, cellular LDL-uptake and serum LDL levels which translates to the risk of coronary artery disease. *Atherosclerosis* **208**: 183–189.

Lionel, A.C., Crosbie, J., Barbosa, N., Goodale, T., Thiruvahindrapuram, B., Rickaby, J., Gazzellone, M., Carson, A.R., Howe, J.L., Wang, Z., et al. 2011. Rare copy number variation discovery and cross-disorder comparisons identify risk genes for ADHD. *Sci. Transl. Med.* **3**: 95ra75.

Liu, C.-C., Kanekiyo, T., Xu, H., Bu, G., and Bu, G. 2013. Apolipoprotein E and Alzheimer disease: risk, mechanisms and therapy. *Nat. Rev. Neurol.* **9**: 106–118.

Lu, T., Pan, Y., Kao, S.-Y., Li, C., Kohane, I., Chan, J., and Yankner, B.A. 2004. Gene regulation and DNA damage in the ageing human brain. *Nature* **429**: 883–891.

Mackenzie, I.R.A., Baker, M., Pickering-Brown, S., Hsiung, G.-Y.R., Lindholm, C., Dwosh, E., Gass, J., Cannon, A., Rademakers, R., Hutton, M., et al. 2006. The neuropathology of frontotemporal lobar degeneration caused by mutations in the progranulin gene. *Brain* **129**: 3081–3090.

Manders, E.M.M., Verbeek, F.J., and Aten, J.A. 1993. Measurement of co-localization of objects in dual-colour confocal images. *J. Microsc.* **169**: 375–382.

Mari, M., Bujny, M. V., Zeuschner, D., Geerts, W.J.C., Griffith, J., Petersen, C.M., Cullen, P.J., Klumperman, J., and Geuze, H.J. 2008. SNX1 Defines an Early Endosomal Recycling Exit for Sortilin and Mannose 6-Phosphate Receptors. *Traffic* **9**: 380–393.

Mayeux, R. 2003. Epidemiology of neurodegeneration. *Annu. Rev. Neurosci.* **26**: 81–104.

McCarthy, J.J., Saith, S., Linnertz, C., Burke, J.R., Hulette, C.M., Welsh-Bohmer, K.A., and Chiba-Falek, O. 2012. The Alzheimer's associated 5' region of the SORL1 gene cis regulates SORL1 transcripts expression. *Neurobiol. Aging* **33**: 1485.e1-8.

Meckler, X., and Checler, F. 2016. Presenilin 1 and Presenilin 2 Target γ-Secretase Complexes to Distinct Cellular Compartments. *J. Biol. Chem.* **291**: 12821–12837.

Mehmedbasic, A., Christensen, S.K., Nilsson, J., Rüetschi, U., Gustafsen, C., Poulsen, A.S.A., Rasmussen, R.W., Fjorback, A.N., Larson, G., and Andersen, O.M. 2015. SorLA Complement-type Repeat Domains Protect the Amyloid Precursor Protein against Processing. *J. Biol. Chem.* **290**: 3359–3376.

Miyashita, A., Koike, A., Jun, G., Wang, L.-S.S., Takahashi, S., Matsubara, E., Kawarabayashi, T., Shoji, M., Tomita, N., Arai, H., et al. 2013. SORL1 Is Genetically Associated with Late-Onset Alzheimer's Disease in Japanese, Koreans and Caucasians. *PLoS One* **8**: e58618.

Mortimer, J.A., Snowdon, D.A., and Markesbery, W.R. 2003. Head circumference, education and risk of dementia: findings from the Nun Study. *J. Clin. Exp. Neuropsychol.* **25**: 671–9.

Motoi, Y., Aizawa, T., Haga, S., Nakamura, S., Namba, Y., and Ikeda, K. 1999. Neuronal localization of a novel mosaic apolipoprotein E receptor, LR11, in rat and human brain. *Brain Res.* **833**: 209–215.

Mu, F.T., Callaghan, J.M., Steele-Mortimer, O., Stenmark, H., Parton, R.G., Campbell, P.L., McCluskey, J., Yeo, J.P., Tock, E.P., and Toh, B.H. 1995. EEA1, an early endosome-associated protein. EEA1 is a conserved alpha-helical peripheral membrane protein flanked by cysteine fingers and contains a calmodulin-binding IQ motif. *J. Biol. Chem.* **270**: 13503–11.

Mukherjee, O., Pastor, P., Cairns, N.J., Chakraverty, S., Kauwe, J.S.K., Shears, S., Behrens, M.I., Budde, J., Hinrichs, A.L., Norton, J., et al. 2006. HDDD2 is a familial frontotemporal lobar degeneration with ubiquitin-positive, tau-negative inclusions caused by a missense mutation in the signal peptide of progranulin. *Ann. Neurol.* **60**: 314–322.

Mullan, M., Crawford, F., Axelman, K., Houlden, H., Lilius, L., Winblad, B., and Lannfelt, L. 1992. A pathogenic mutation for probable Alzheimer's disease in the APP gene at the N–terminus of β–amyloid. *Nat. Genet.* **1**: 345–347.

Musunuru, K., Strong, A., Frank-Kamenetsky, M., Lee, N.E., Ahfeldt, T., Sachs, K. V, Li, X., Li, H., Kuperwasser, N., Ruda, V.M., et al. 2010. From noncoding variant to phenotype via SORT1 at the 1p13 cholesterol locus. *Nature* **466**: 714–9.

Nakamura, N., Rabouille, C., Watson, R., Nilsson, T., Hui, N., Slusarewicz, P., Kreis, T.E., and Warren, G. 1995. Characterization of a cis-Golgi matrix protein, GM130. *J. Cell Biol.* **131**: 1715–26.

Navarro, V., Vincent, J.-P., and Mazella, J. 2002. Shedding of the luminal domain of the neurotensin receptor-3/sortilin in the HT29 cell line. *Biochem. Biophys. Res. Commun.* **298**: 760–4.

Neary, D., Snowden, J.S., Gustafson, L., Passant, U., Stuss, D., Black, S., Freedman, M., Kertesz, A., Robert, P.H., Albert, M., et al. 1998. Frontotemporal lobar degeneration: a consensus on clinical diagnostic criteria. *Neurology* **51**: 1546–54.

Nerlov, C. 2007. The C/EBP family of transcription factors: a paradigm for interaction between gene expression and proliferation control. *Trends Cell Biol.* **17**: 318–324.

Nicolas, G., Charbonnier, C., Wallon, D., Quenez, O., Bellenguez, C., Grenier-Boley, B., Rousseau, S., Richard, A.-C., Rovelet-Lecrux, A., Guennec, K. Le, et al. 2016. SORL1 rare variants: a major risk factor for familial early-onset Alzheimer's disease. *Mol. Psychiatry* **21**: 831–836.

Nielsen, M.S. 2001. The sortilin cytoplasmic tail conveys Golgi-endosome transport and binds the VHS domain of the GGA2 sorting protein. *EMBO J.* **20**: 2180–2190.

Nielsen, M.S., Gustafsen, C., Madsen, P., Nyengaard, J.R., Hermey, G., Bakke, O., Mari, M., Schu, P., Pohlmann, R., Dennes, A., et al. 2007. Sorting by the cytoplasmic domain of the amyloid precursor protein binding receptor SorLA. *Mol. Cell. Biol.* **27**: 6842–51.

Nykjaer, A., Lee, R., Teng, K.K., and Jansen, P. 2004. Sortilin is essential for proNGF- induced neuronal cell death. *Nature* **427**: 15–20.

Offe, K., Dodson, S.E., Shoemaker, J.T., Fritz, J.J., Gearing, M., Levey, A.I., and Lah, J.J. 2006. The Lipoprotein Receptor LR11 Regulates Amyloid beta Production and Amyloid Precursor Protein Traffic in Endosomal Compartments. *J. Neurosci.* **26**: 1596–1603.

Olson, M.I., and Shaw, C.M. 1969. Presenile dementia and Alzheimer's disease in mongolism. *Brain* **92**: 147–56.

Ong, S.-E., Blagoev, B., Kratchmarova, I., Kristensen, D.B., Steen, H., Pandey, A., and Mann, M. 2002. Stable isotope labeling by amino acids in cell culture, SILAC, as a simple and accurate approach to expression proteomics. *Mol. Cell. Proteomics* **1**: 376–86.

Osada, S., Yamamoto, H., Nishihara, T., and Imagawa, M. 1996. DNA binding specificity of the CCAAT/enhancer-binding protein transcription factor family. *J. Biol. Chem.* **271**: 3891–6.

Oshima, K., Aoki, N., Kato, T., Kitajima, K., and Matsuda, T. 2002. Secretion of a peripheral membrane protein, MFG-E8, as a complex with membrane vesicles. *Eur. J. Biochem.* **269**: 1209–18.

Palacios, G., Palacios, J.M., Mengod, G., and Frey, P. 1992. Beta-amyloid precursor protein localization in the Golgi apparatus in neurons and oligodendrocytes. An immunocytochemical structural and ultrastructural study in normal and axotomized neurons. *Brain Res. Mol. Brain Res.* **15**: 195–206.

Palop, J.J., Chin, J., and Mucke, L. 2006. A network dysfunction perspective on neurodegenerative diseases. *Nature* **443**: 768–773.

Park, S.-S., Wu, W.W., Zhou, Y., Shen, R.-F., Martin, B., and Maudsley, S. 2012. Effective correction of experimental errors in quantitative proteomics using stable isotope labeling by amino acids in cell culture (SILAC). *J. Proteomics* **75**: 3720–3732.

Parks, B.W., Nam, E., Org, E., Kostem, E., Norheim, F., Hui, S.T., Pan, C., Civelek, M., Rau, C.D., Bennett, B.J., et al. 2013. Genetic Control of Obesity and Gut Microbiota Composition in Response to High-Fat, High-Sucrose Diet in Mice. *Cell Metab.* **17**: 141–152.

Pearson, H.A., and Peers, C. 2006. Physiological roles for amyloid beta peptides. *J. Physiol.* **575**: 5–10.

Peters, D. 2014. Genome editing in human pluripotent stem cells. *StemBook* https://doi.org/10.3824/stembook.1.94.1.

Petersen, C.M., Nielsen, M.S., Jacobsen, C., Tauris, J., Jacobsen, L., Gliemann, J., Moestrup, S.K., and Madsen, P. 1999. Propeptide cleavage conditions sortilin/neurotensin receptor-3 for ligand binding. *EMBO J.* **18**: 595–604.

Petersen, C.M., Nielsen, M.S., Nykjær, A., Jacobsen, L., Tommerup, N., Rasmussen, H.H., Røigaard, H., Gliemann, J., Madsen, P., and Moestrup, S.K. 1997. Molecular Identification of a Novel Candidate Sorting Receptor Purified from Human Brain by Receptor-associated Protein Affinity Chromatography. *J. Biol. Chem.* **272**: 3599–3605.

Petkau, T.L., Neal, S.J., Orban, P.C., MacDonald, J.L., Hill, A.M., Lu, G., Feldman, H.H., Mackenzie, I.R.A., and Leavitt, B.R. 2010. Progranulin expression in the developing and adult murine brain. *J. Comp. Neurol.* **518**: 3931–3947.

Pottier, C., Hannequin, D., Coutant, S., Rovelet-Lecrux, a, Wallon, D., Rousseau, S., Legallic, S., Paquet, C., Bombois, S., Pariente, J., et al. 2012. High frequency of potentially pathogenic SORL1 mutations in autosomal dominant early-onset Alzheimer disease. *Mol. Psychiatry* **17**: 875–879.

Quistgaard, E.M., Madsen, P., Grøftehauge, M.K., Nissen, P., Petersen, C.M., and Thirup, S.S. 2009. Ligands bind to Sortilin in the tunnel of a ten-bladed β-propeller domain. *Nat. Struct. Mol. Biol.* **16**: 96–98.

Rader, D.J., Cohen, J., and Hobbs, H.H. 2003. Monogenic hypercholesterolemia: new insights in pathogenesis and treatment. *J. Clin. Invest.* **111**: 1795–803.

Rajendran, L., Honsho, M., Zahn, T.R., Keller, P., Geiger, K.D., Verkade, P., and Simons, K. 2006. Alzheimer's disease beta-amyloid peptides are released in association with exosomes. *Proc. Natl. Acad. Sci.* **103**: 11172–11177.

Rajendran, L., Schneider, A., Schlechtingen, G., Weidlich, S., Ries, J., Braxmeier, T., Schwille, P., Schulz, J.B., Schroeder, C., Simons, M., et al. 2008. Efficient Inhibition of the Alzheimer's Disease -Secretase by Membrane Targeting. *Science* **320**: 520–523.

Ratnavalli, E., Brayne, C., Dawson, K., and Hodges, J.R. 2002. The prevalence of frontotemporal dementia. *Neurology* **58**: 1615–21.

Raymond, A., Ensslin, M.A., and Shur, B.D. 2009. SED1/MFG-E8: A Bi-motif protein that orchestrates diverse cellular interactions. *J. Cell. Biochem.* **106**: 957–966.

Reitz, C., and Mayeux, R. 2014. Alzheimer disease: Epidemiology, diagnostic criteria, risk factors and biomarkers. *Biochem. Pharmacol.* **88**: 640–651.

Reitz, C., Prince, J.A., Maier, W., Riemenschneider, M., Cellini, E., Sorbi, S., and Nacmias, B. 2011a. Meta-analysis of the Association Between Variants in SORL1 and Alzheimer Disease. *Arch. Neurol.* **68**.

Reitz, C., Tokuhiro, S., Clark, L.N., Conrad, C., Vonsattel, J.-P., Hazrati, L.-N., Palotás, A., Lantigua, R., Medrano, M., Z. Jiménez -Velázquez, I., et al. 2011b. SORCS1 alters amyloid precursor protein processing and variants may increase Alzheimer's disease risk. *Ann. Neurol.* **69**: 47–64.

Reitz, C., Tosto, G., Vardarajan, B., Rogaeva, E., Ghani, M., Rogers, R.S., Conrad, C., Haines, J.L., Pericak-Vance, M.A., Fallin, M.D., et al. 2013. Independent and epistatic effects of variants in VPS10-d receptors on Alzheimer disease risk and processing of the amyloid precursor protein (APP). *Transl. Psychiatry* **3**: e256.

Rezgaoui, M., Hermey, G., Riedel, I.B., Hampe, W., Schaller, H.C., and Hermans-Borgmeyer, I. 2001. Identification of SorCS2, a novel member of the VPS10 domain containing receptor family, prominently expressed in the developing mouse brain. *Mech. Dev.* **100**: 335–8.

Rogaeva, E., Meng, Y., Lee, J.H., Gu, Y., Kawarai, T., Zou, F., Katayama, T., Baldwin, C.T., Cheng, R., Hasegawa, H., et al. 2007. The neuronal sortilin-related receptor SORL1 is genetically associated with Alzheimer's Disease. *Nat. Genet.* **39**: 168–177.

Rohe, M., Carlo, A.-S.S., Breyhan, H., Sporbert, A., Militz, D., Schmidt, V., Wozny, C., Harmeier, A., Erdmann, B., Bales, K.R., et al. 2008. Sortilin-related receptor with A-type repeats (SORLA) affects the amyloid precursor protein-dependent stimulation of ERK signaling and adult neurogenesis. *J. Biol. Chem.* **283**: 14826–14834.

Rohe, M., Synowitz, M., Glass, R., Paul, S.M., Nykjaer, A., and Willnow, T.E. 2009. Brain-Derived Neurotrophic Factor Reduces Amyloidogenic Processing through Control of SORLA Gene Expression. *J. Neurosci.* **29**: 15472–15478.

Saido, T., and Leissring, M.A. 2012. Proteolytic degradation of amyloid β-protein. *Cold Spring Harb. Perspect. Med.* **2**: a006379.

Samani, N.J., Erdmann, J., Hall, A.S., Hengstenberg, C., Mangino, M., Mayer, B., Dixon, R.J., Meitinger, T., Braund, P., Wichmann, H.-E., et al. 2007. Genomewide Association Analysis of Coronary Artery Disease. *N. Engl. J. Med.* **357**: 443–453.

Sampathu, D.M., Neumann, M., Kwong, L.K., Chou, T.T., Micsenyi, M., Truax, A., Bruce, J., Grossman, M., Trojanowski, J.Q., and Lee, V.M.-Y. 2006. Pathological heterogeneity of frontotemporal lobar degeneration with ubiquitin-positive inclusions delineated by ubiquitin immunohistochemistry and novel monoclonal antibodies. *Am. J. Pathol.* **169**: 1343–52.

Sannerud, R., Declerck, I., Peric, A., Raemaekers, T., Menendez, G., Zhou, L., Veerle, B., Coen, K., Munck, S., Strooper, B. De, et al. 2011. ADP ribosylation factor 6 (ARF6) controls amyloid precursor protein (APP) processing by mediating the endosomal sorting of BACE1. *Proc. Natl. Acad. Sci.* **108**: E559–E568.

Sannerud, R., Esselens, C., Ejsmont, P., Mattera, R., Rochin, L., Tharkeshwar, A.K., De Baets, G., De Wever, V., Habets, R., Baert, V., et al. 2016. Restricted Location of PSEN2/γ-Secretase Determines Substrate Specificity and Generates an Intracellular Aβ Pool. *Cell* **166**: 193–208.

Sarret, P., Krzywkowski, P., Segal, L., Nielsen, M.S., Petersen, C.M., Mazella, J., Stroh, T., and Beaudet, A. 2003. Distribution of NTS3 receptor/sortilin mRNA and protein in the rat central nervous system. *J. Comp. Neurol.* **461**: 483–505.

Scherzer, C., Offe, K., and Lah, J.J. 2004. Loss of Apolipoprotein E Receptor. *Arch. Neurol.* **61**: 1200–5.

Scheuner, D., Eckman, C., Jensen, M., Song, X., Citron, M., Suzuki, N., Bird, T.D., Hardy, J., Hutton, M., Kukull, W., et al. 1996. Secreted amyloid β–protein similar to that in the senile plaques of Alzheimer's disease is increased in vivo by the presenilin 1 and 2 and APP mutations linked to familial Alzheimer's disease. *Nat. Med.* **2**: 864–870.

Schmidt, V., Baum, K., Lao, A., Rateitschak, K., Schmitz, Y., Teichmann, A., Wiesner, B., Petersen, C.M., Nykjaer, A., Wolf, J., et al. 2011. Quantitative modelling of amyloidogenic processing and its influence by SORLA in Alzheimer's disease. *EMBO J.* **31**: 187–200.

Schmidt, V., Schulz, N., Yan, X., Schürmann, A., Kempa, S., Kern, M., Blüher, M., Poy, M.N., Olivecrona, G., and Willnow, T.E. 2016. SORLA facilitates insulin receptor signaling in adipocytes and exacerbates obesity. *J. Clin. Invest.* **126**: 2706–2720.

Schmidt, V., Sporbert, A., Rohe, M., Reimer, T., Rehm, A., Andersen, O.M., and Willnow, T.E. 2007. SorLA/LR11 regulates processing of amyloid precursor protein via interaction with adaptors GGA and PACS-1. *J. Biol. Chem.* **282**: 32956–32964.

Schmittgen, T.D., and Livak, K.J. 2008. Analyzing real-time PCR data by the comparative C(T) method. *Nat. Protoc.* **3**: 1101–8.

Schwartz, R.E., Fleming, H.E., Khetani, S.R., and Bhatia, S.N. 2014. Pluripotent stem cell-derived hepatocyte-like cells. *Biotechnol. Adv.* **32**: 504–513.

Seaman, M.N.J. 2004. Cargo-selective endosomal sorting for retrieval to the Golgi requires retromer. *J. Cell Biol.* **165**: 111–122.

Seaman, M.N.J. 2007. Identification of a novel conserved sorting motif required for retromer-mediated endosome-to-TGN retrieval. *J. Cell Sci.* **120**: 2378–2389.

Selkoe, D.J. 1991. The molecular pathology of Alzheimer's disease. *Neuron* **6**: 487–498.

Selkoe, D.J., and Hardy, J. 2016. The amyloid hypothesis of Alzheimer's disease at 25 years. *EMBO Mol. Med.* **8**: 595–608.

Sharples, R.A., Vella, L.J., Nisbet, R.M., Naylor, R., Perez, K., Barnham, K.J., Masters, C.L., and Hill, A.F. 2008. Inhibition of γ-secretase causes increased secretion of amyloid precursor protein C-terminal fragments in association with exosomes. *FASEB J.* **22**: 1469–1478.

Sherrington, R., Rogaev, E.I., Liang, Y., Rogaeva, E.A., Levesque, G., Ikeda, M., Chi, H., Lin, C., Li, G., Holman, K., et al. 1995. Cloning of a gene bearing missense mutations in early-onset familial Alzheimer's disease. *Nature* **375**: 754–760.

Shi, Y., Inoue, H., Wu, J.C., and Yamanaka, S. 2017. Induced pluripotent stem cell technology: a decade of progress. *Nat. Rev. Drug Discov.* **16**: 115–130.

Si-Tayeb, K., Noto, F.K., Nagaoka, M., Li, J., Battle, M.A., Duris, C., North, P.E., Dalton, S., and Duncan, S.A. 2010. Highly efficient generation of human hepatocyte-like cells from induced pluripotent stem cells. *Hepatology* **51**: 297–305.

Sisodia, S.S., Koo, E.H., Beyreuther, K., Unterbeck, A., and Price, D.L. 1990. Evidence that beta-amyloid protein in Alzheimer's disease is not derived by normal processing. *Science* **248**: 492–5.

Small, D.H., Clarris, H.L., Williamson, T.G., Reed, G., Key, B., Mok, S.S., Beyreuther, K., Masters, C.L., and Nurcombe, V. 1999. Neurite-Outgrowth Regulating Functions of the Amyloid Protein Precursor of Alzheimer's Disease*. *J. Alzheimer's Dis.* **1**: 275–285.

Small, D.H., Nurcombe, V., Reed, G., Clarris, H., Moir, R., Beyreuther, K., and Masters, C.L. 1994. A heparin-binding domain in the amyloid protein precursor of Alzheimer's disease is involved in the regulation of neurite outgrowth. *J. Neurosci.* **14**: 2117–27.

Smith, E.N., Chen, W., Kähönen, M., Kettunen, J., Lehtimäki, T., Peltonen, L., Raitakari, O.T., Salem, R.M., Schork, N.J., Shaw, M., et al. 2010. Longitudinal Genome-Wide Association of Cardiovascular Disease Risk Factors in the Bogalusa Heart Study. *PLoS Genet.* **6**: e1001094.

Snowden, J.S., Pickering-Brown, S.M., Mackenzie, I.R., Richardson, A.M.T., Varma, A., Neary, D., and Mann, D.M.A. 2006. Progranulin gene mutations associated with frontotemporal dementia and progressive non-fluent aphasia. *Brain* **129**: 3091–3102.

Steiner, H., Fluhrer, R., and Haass, C. 2008. Intramembrane proteolysis by gamma-secretase. *J. Biol. Chem.* **283**: 29627–31.

Strong, A., Ding, Q., Edmondson, A.C., Millar, J.S., Sachs, K. V, Li, X., Kumaravel, A., Wang, M.Y., Ai, D., Guo, L., et al. 2012. Hepatic sortilin regulates both apolipoprotein B secretion and LDL catabolism. *J. Clin. Invest.* **122**: 2807–16.

Suzuki, N., Cheung, T.T., Cai, X.D., Odaka, A., Otvos, L., Eckman, C., Golde, T.E., and Younkin, S.G. 1994. An increased percentage of long amyloid beta protein secreted by familial amyloid beta protein precursor (beta APP717) mutants. *Science* **264**: 1336–40.

Szabo, A., Stolz, L., and Granzow, R. 1995. Surface plasmon resonance and its use in biomolecular interaction analysis (BIA). *Curr. Opin. Struct. Biol.* **5**: 699–705.

Takahashi, K., Tanabe, K., Ohnuki, M., Narita, M., Ichisaka, T., Tomoda, K., and Yamanaka, S. 2007. Induction of Pluripotent Stem Cells from Adult Human Fibroblasts by Defined Factors. *Cell* **131**: 861–872.

Takahashi, K., and Yamanaka, S. 2006. Induction of Pluripotent Stem Cells from Mouse Embryonic and Adult Fibroblast Cultures by Defined Factors. *Cell* **126**: 663–676.

Tanzi, R., Gusella, J., Watkins, P., Bruns, G., St George-Hyslop, P., Keuren, M. Van, Patterson, D., Pagan, S., Kurnit, D., and Neve, R. 1987. Amyloid beta protein gene: cDNA, mRNA distribution, and genetic linkage near the Alzheimer locus. *Science* **235**: 880–884.

Terry, A. V., Kutiyanawalla, A., and Pillai, A. 2011. Age-dependent alterations in nerve growth factor (NGF)-related proteins, sortilin, and learning and memory in rats. *Physiol. Behav.* **102**: 149–157.

Teslovich, T.M., Musunuru, K., Smith, A. V., Edmondson, A.C., Stylianou, I.M., Koseki, M., Pirruccello, J.P., Ripatti, S., Chasman, D.I., Willer, C.J., et al. 2010. Biological, clinical and population relevance of 95 loci for blood lipids. *Nature* **466**: 707–713.

Théry, C., Amigorena, S., Raposo, G., and Clayton, A. 2006. Isolation and Characterization of Exosomes from Cell Culture Supernatants and Biological Fluids. *Curr. Protoc. Cell Biol.* **30**: 3.22.1-3.22.29.

Thonberg, H., Chiang, H.-H., Lilius, L., Forsell, C., Lindström, A.-K., Johansson, C., Björkström, J., Thordardottir, S., Sleegers, K., Broeckhoven, C. Van, et al. 2017. Identification and description of three families with familial Alzheimer disease that segregate variants in the SORL1 gene. *Acta Neuropathol. Commun.* **5**: 43.

Touboul, T., Hannan, N.R.F., Corbineau, S., Martinez, A., Martinet, C., Branchereau, S., Mainot, S., Strick-Marchand, H., Pedersen, R., Santo, J. Di, et al. 2010. Generation of functional hepatocytes from human embryonic stem cells under chemically defined conditions that recapitulate liver development. *Hepatology* **51**: 1754–1765.

Vaegter, C.B., Jansen, P., Fjorback, A.W., Glerup, S., Skeldal, S., Kjolby, M., Richner, M., Erdmann, B., Nyengaard, J.R., Tessarollo, L., et al. 2011. Sortilin associates with Trk receptors to enhance anterograde transport and neurotrophin signaling. *Nat. Neurosci.* **14**: 54–61.

Vassar, R., Bennett, B.D., Babu-Khan, S., Kahn, S., Mendiaz, E.A., Denis, P., Teplow, D.B., Ross, S., Amarante, P., Loeloff, R., et al. 1999. Beta-secretase cleavage of Alzheimer's amyloid precursor protein by the transmembrane aspartic protease BACE. *Science* **286**: 735–41.

Verheijen, J., Bossche, T. Van den, Zee, J. van der, Engelborghs, S., Sanchez-Valle, R., Lladó, A., Graff, C., Thonberg, H., Pastor, P., Ortega-Cubero, S., et al. 2016. A comprehensive study of the genetic impact of rare variants in SORL1 in European early-onset Alzheimer's disease. *Acta Neuropathol.* **132**: 213–224.

Wang, X., Raghavan, A., Peters, D.T., Pashos, E.E., Rader, D.J., and Musunuru, K. 2018. Interrogation of the Atherosclerosis-Associated *SORT1* (Sortilin 1) Locus With Primary Human Hepatocytes, Induced Pluripotent Stem Cell-Hepatocytes, and Locus-Humanized MiceHighlights. *Arterioscler. Thromb. Vasc. Biol.* **38**: 76–82.

Wang, Z., Lei, H., Zheng, M., Li, Y., Cui, Y., and Hao, F. 2016. Meta-analysis of the Association between Alzheimer Disease and Variants in GAB2, PICALM, and SORL1. *Mol. Neurobiol.* **53**: 6501–6510.

Warren, C.R., O'Sullivan, J.F., Friesen, M., Becker, C.E., Zhang, X., Liu, P., Wakabayashi, Y., Morningstar, J.E., Shi, X., Choi, J., et al. 2017. Induced Pluripotent Stem Cell Differentiation Enables Functional Validation of GWAS Variants in Metabolic Disease. *Cell Stem Cell* **20**: 547–557.e7.

Watts, J.C., and Prusiner, S.B. 2018. β-Amyloid Prions and the Pathobiology of Alzheimer's Disease. *Cold Spring Harb. Perspect. Med.* **8**: a023507.

Westergaard, U.B., Sørensen, E.S., Hermey, G., Nielsen, M.S., Nykjær, A., Kirkegaard, K., Jacobsen, C., Gliemann, J., Madsen, P., and Petersen, C.M. 2004. Functional Organization of the Sortilin Vps10p Domain. *J. Biol. Chem.* **279**: 50221–50229.

Whittle, A.J., Jiang, M., Peirce, V., Relat, J., Virtue, S., Ebinuma, H., Fukamachi, I., Yamaguchi, T., Takahashi, M., Murano, T., et al. 2015. Soluble LR11/SorLA represses thermogenesis in adipose tissue and correlates with BMI in humans. *Nat. Commun.* **6**: 8951.

Willnow, T.E., and Andersen, O.M. 2013. Sorting receptor SORLA – a trafficking path to avoid Alzheimer disease. *J. Cell Sci.* **126**: 2751–2760.

Willnow, T.E., Petersen, C.M., and Nykjaer, A. 2008. VPS10P-domain receptors — regulators of neuronal viability and function. *Nat. Rev. Neurosci.* **9**: 899–909.

Wolfe, M.S., Xia, W., Ostaszewski, B.L., Diehl, T.S., Kimberly, W.T., and Selkoe, D.J. 1999. Two transmembrane aspartates in presenilin-1 required for presenilin endoproteolysis and γ-secretase activity. *Nature* **398**: 513–517.

Xiao, T., Zhang, W., Jiao, B., Pan, C.-Z., Liu, X., and Shen, L. 2017. The role of exosomes in the pathogenesis of Alzheimer' disease. *Transl. Neurodegener.* **6**: 3.

Yoshihara, M., Hayashizaki, Y., and Murakawa, Y. 2017. Genomic Instability of iPSCs: Challenges Towards Their Clinical Applications. *Stem Cell Rev.* **13**: 7–16.

Young, J.E.E., Boulanger-Weill, J., Williams, D.A.A., Woodruff, G., Buen, F., Revilla, A.C.C., Herrera, C., Israel, M.A.A., Yuan, S.H.H., Edland, S.D.D., et al. 2015. Elucidating molecular phenotypes caused by the SORL1 Alzheimer's disease genetic risk factor using human induced pluripotent stem cells. *Cell Stem Cell* **16**: 373–385.

Yu, J., Vodyanik, M.A., Smuga-Otto, K., Antosiewicz-Bourget, J., Frane, J.L., Tian, S., Nie, J., Jonsdottir, G.A., Ruotti, V., Stewart, R., et al. 2007. Induced Pluripotent Stem Cell Lines Derived from Human Somatic Cells. *Science* **318**: 1917–1920.

Yusa, K. 2013. Seamless genome editing in human pluripotent stem cells using custom endonuclease-based gene targeting and the piggyBac transposon. *Nat. Protoc.* **8**: 2061–78.

Yuyama, K., and Igarashi, Y. 2017. Exosomes as Carriers of Alzheimer's Amyloid-ß. *Front. Neurosci.* **11**: 229.

Yuyama, K., Sun, H., Sakai, S., Mitsutake, S., Okada, M., Tahara, H., Furukawa, J.-I., Fujitani, N., Shinohara, Y., and Igarashi, Y. 2014. Decreased amyloid-β pathologies by intracerebral loading of glycosphingolipid-enriched exosomes in Alzheimer model mice. *J. Biol. Chem.* **289**: 24488–98.

Zhang, Y., Chen, K., Sloan, S.A., Bennett, M.L., Scholze, A.R., O'Keeffe, S., Phatnani, H.P., Guarnieri, P., Caneda, C., Ruderisch, N., et al. 2014. An RNA-sequencing transcriptome and splicing database of glia, neurons, and vascular cells of the cerebral cortex. *J. Neurosci.* **34**: 11929–47.

Zhang, Y., Pak, C., Han, Y., Ahlenius, H., Zhang, Z., Chanda, S., Marro, S., Patzke, C., Acuna, C., Covy, J., et al. 2013. Rapid single-step induction of functional neurons from human pluripotent stem cells. *Neuron* **78**: 785–798.

Zou, Z., Liu, C., Che, C., and Huang, H. 2014. Clinical genetics of Alzheimer's disease. *Biomed Res. Int.* **2014**: 291862.

7 APPENDICES

7.1 Supplementary data

7.1.1 Karyotyping of reprogrammed and gene-edited iPSC lines

Human iPSC lines were karyotyped using the Illumina platform and the OMNI-EXPRESS-8v1.4 Chip by the MDC stem cell core facility (in cooperation with the Hübner Lab). Karyotypes were analyzed using Karyostudio 1.4.

The virtual karyotype was analyzed for the reprogrammed iPSC line MDCH0003/BIH013-A (donor_minor_1), the *SORT1* KO line and the *SORT1* SNP edited cell line (isogenic_edited_minor) as well as their parental controls. Insertions are depicted in green, deletions in red and loss of heterozygosity in gray.

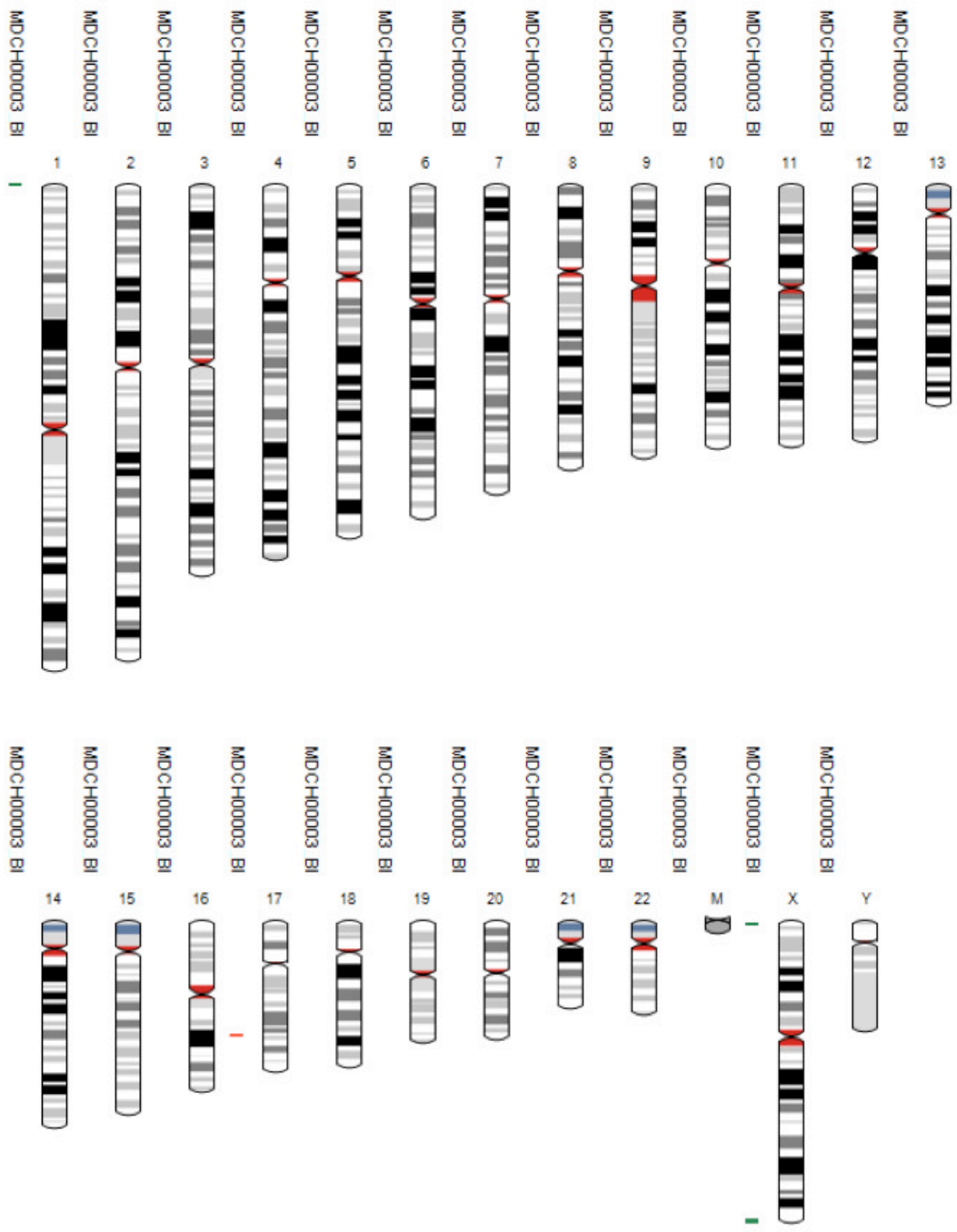

Figure 7-1: Virtual karyotype of the reprogrammed iPSC line MDCH0003/BIH013-A (donor_minor_1). MDCH0003/BIH013-A shows a normal karyotype without larger areas of insertions (green), deletions (red), or loss of heterozygosity (gray).

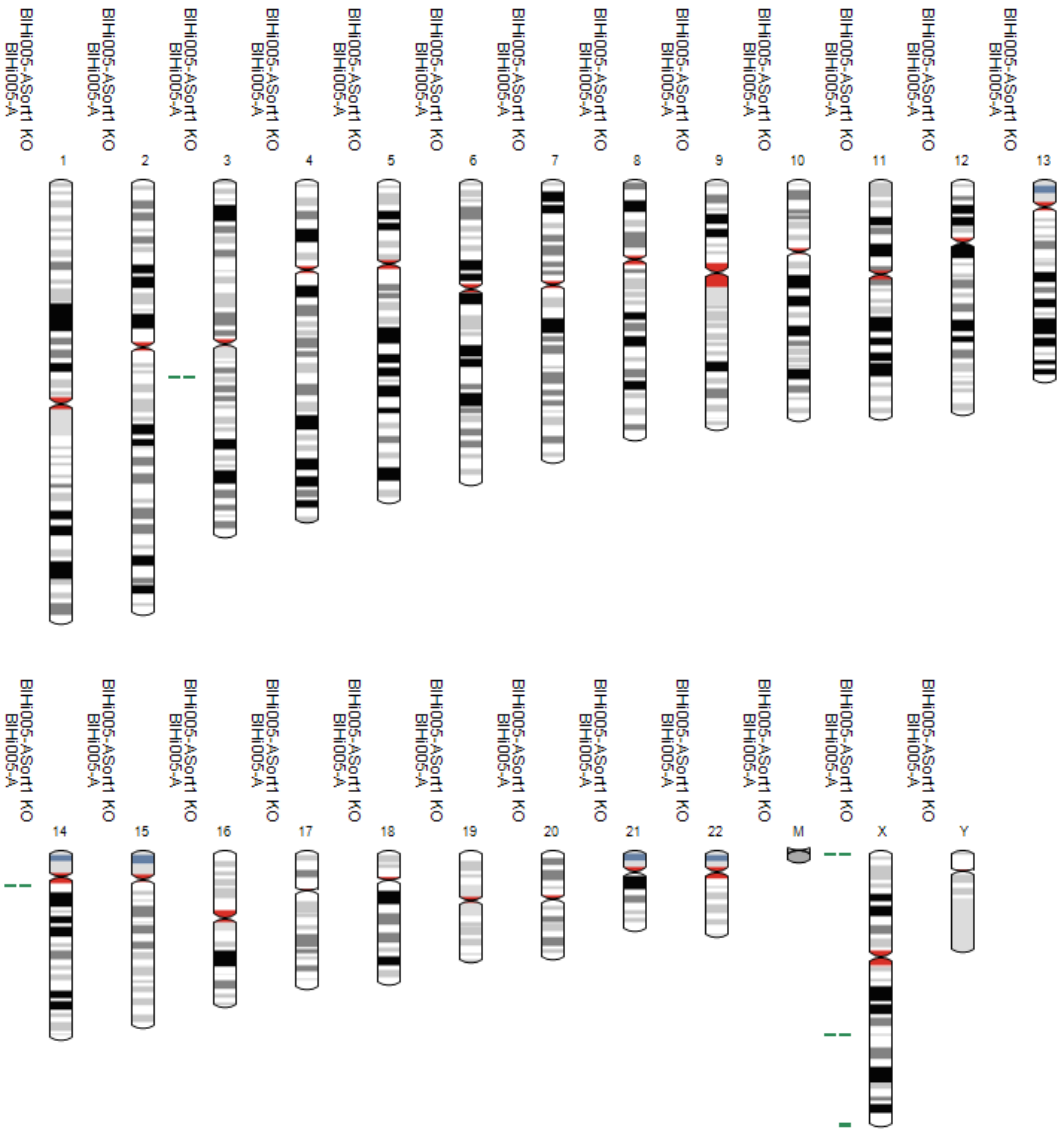

Figure 7-2: Virtual karyotype of the parental iPSC line BIH005-A (*SORT1* WT) and the generated *SORT1* KO iPSC line. Both cell lines show normal karyotypes without larger areas of insertions (green), deletions (red), or loss of heterozygosity (gray).

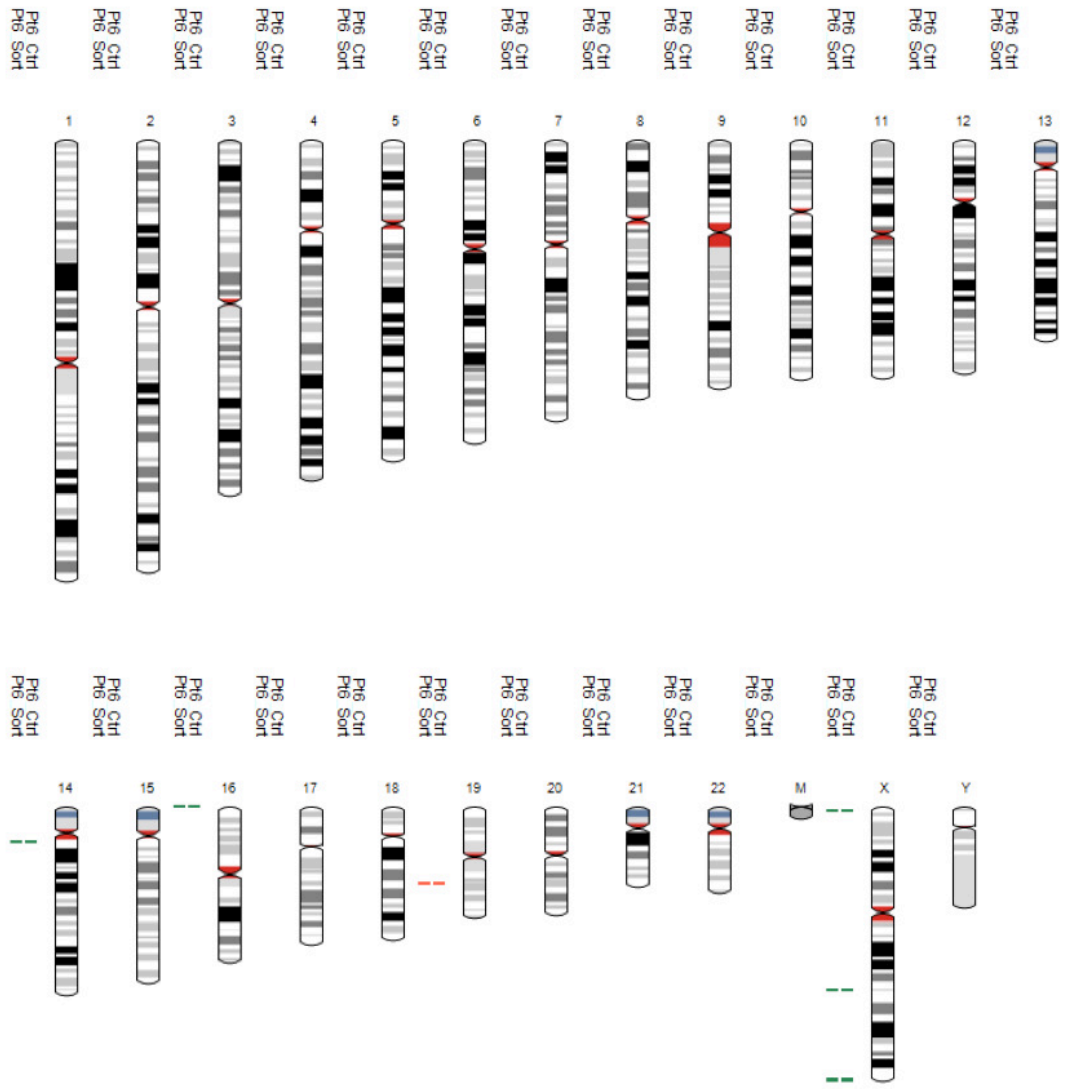

Figure 7-3: Virtual karyotype of the parental iPSC line BIH049-A (Pt6 Ctrl, isogenic_parental_major) and the *SORT1* risk SNP edited iPSC line (Pt6 Sort, isogenic_edited_minor). Both cell lines show normal karyotypes without larger areas of insertions (green), deletions (red), or loss of heterozygosity (gray).

7.2 Publications

Andersen, O.M., **Rudolph, I.-M.**, and Willnow, T.E. 2016. Risk factor SORL1: from genetic association to functional validation in Alzheimer's disease. *Acta Neuropathol.* 132: 653–665.

Meyer, K., Kirchner, M., Uyar, B., Cheng, J.-Y., Russo, G., Hernandez-Miranda, L.R., Szymborska, A., Zauber, H., **Rudolph, I.-M.**, Willnow, T.E., et al. 2018. Mutations in Disordered Regions Can Cause Disease by Creating Dileucine Motifs. *Cell* in press.

7.3 Selbstständigkeitserklärung

Hiermit erkläre ich, dass ich die vorliegende Arbeit mit dem Titel “Functional validation of Alzheimer’s disease risk genes using established and pluripotent human cell culture models” selbstständig und ohne Hilfe Dritter angefertigt habe. Sämtliche Hilfsmittel, Hilfen sowie Literaturquellen sind als solche kenntlich gemacht. Außerdem erkläre ich hiermit, dass ich mich nicht anderweitig um einen entsprechenden Doktorgrad beworben habe. Die Promotionsordnung des Fachbereichs Biologie, Chemie und Pharmazie der Freien Universität Berlin habe ich gelesen und akzeptiert.

Berlin, Oktober 2018

Ina-Maria Rudolph

7.4 Danksagung

Zu allererst möchte ich mich bei Prof. Dr. Thomas E. Willnow für die hervorragende Betreuung meines Projekts, die stetige Unterstützung und den ansteckenden wissenschaftlichen Enthusiasmus bedanken.

Ebenfalls bin ich Prof. Dr. Silke Rickert-Sperling sehr dankbar für die Bereitschaft meine Dissertation zu betreuen und zu begutachten.

Sehr dankbar bin ich außerdem Dr. Sebastian Diecke für seine großartige Unterstützung und Einarbeitung in iPSCs und Genomeditierung. Ich danke auch der gesamten Stem Cell Core Facility, insbesondere Polixeni Burazi und Anna Iwanska, für die Hilfe bei der Generierung der genomeditierten Zelllinien und der Etablierung der Differenzierungsprotokolle.

Ein riesiges Dankeschön gilt meinen Kolleginnen und Kollegen der AG Willnow für die tolle Arbeitsatmosphäre im Labor, die konstante Unterstützung bei neuen Experimenten und den wissenschaftlichen und persönlichen Austausch. Ich danke insbesondere Christine Kruse und Tatjana Pasternack für ihre technische Unterstützung und Dr. Annabel Christ für den stetigen Office-Support.

Weiterhin gilt mein Dank allen Kollaborationspartnern, die mir geholfen haben meine Projekte voranzubringen. Katrina Meyer danke ich für die fachliche Unterstützung bei der Durchführung des Interaktom-Screens. Ich danke außerdem Dr. Anca Margineanu für die Hilfe bei der Analyse der FLIM/FRET-Experimente sowie der Advanced Light Microscopy Technologie Plattform für die generelle technische Unterstützung. Silvia Ruzittu danke ich vielmals für die Charakterisierung der Hepatozyten-Differenzierung.

Für den bedingungslosen Rückhalt und das Verständnis in den letzten Jahren bin ich meinen Eltern, meinen Freunden und Julian zutiefst dankbar.

7.5 Curriculum vitae

Aus Datenschutzgründen wurde der Lebenslauf entfernt.